NTNU
Norwegian University of
Science and Technology

Elucidating glycan-mediated interactions at cell surfaces by optical tweezers

Katsiaryna Siarpilina

Biotechnology (5 year)
Submission date: July 2017
Supervisor: Marit Sletmoen, IBT

Norwegian University of Science and Technology
Department of Biotechnology and Food Science

Abstract

In this study, carbohydrate-interactions were investigated by using optical tweezers, which is an instrument for the measurement of forces ca. 0.1-100 pN. Carbohydrates are added to various biological polymers in a process called glycosylation: the covalent attachment of sugar-chains to proteins and lipids. The huge diversity makes these sugars well suited for cell-recognition. During carcinogenesis, the cells often express much shorter glycans on its surface molecules, which are known as as tumour-associated cancer antigens (TACAs). MUC1 is a surface protein that has an upregulated expression in cancer cells, with the appearance of TACAs like Tn, T, STn and ST. The functions of the antigens are unknown, but the expression of Tn and STn correlates with methastasis and poor prognosis.. This study aimed to investigate how all of the aforementioned antigens interact by using optical tweezers, to attempt to find out whether some of these glycans can be able to modulate the interactions at cell surfaces.

It was found MUC1-Tn, MUC1-STn and MUC1-ST all were able to bind to themselves and each other. The strength of the forces between MUC1-Tn - self and MUC1-STn - self antigens appeared to be of similar strength, but MUC1-STn bound slightly stronger and experienced interactions more frequently. x_β of the inner energy barrier for MUC1-Tn - self was found to be 0.33 nm, while MUC1-STn - self was 0.39 nm. MUC1-T was also able to self-interact, but was not found to bind the other mucins. This might be due to experimental difficulties. It was found that GalNAc, had a central role in the interactions. The N-acetyl group of the sugar appears to be important. A more heavily glycosylated mucin, TR-PSM H8, was investigated. It was found that, at the loading rates measured, the TR-PSM-H8 mucin exhibited unbinding forces about twice as high as those found for MUC1-Tn - self and MUC1-STn - self, and was found to have an x_β of 0.22 nm.

Lectins are proteins that can bind to sugar moieties and mediate a cell's response to them. Macrophage galactose-type C-type lectin (MGL) is a receptor-protein that can be found only on dendritic cells and macrophages, which are antigen-presenting cells. MGL has been of interest in the development of cancer vaccines, as it is believed that its efficient activation can create a response against TACAs. It was found that MGL was able to bind to MUC1-Tn, in the absense of calcium. It was not found to bind a polyacrylamide backbone with 80% Tn. Both of these results require further investigation.

Optical tweezers were used to investigate the interactions between a mycotoxin from *Fusarium moniliforme*: fumonicin B1, and the cell wall glycans on yeast cells. Fumonisin is a carcinogen that can contaminate wheat, oat, and corn. The *Saccharomyces cereviciae* yeast cell wall consists of an inner layer of chitin, a middle layer of β-glucan, and an outer coating of mannan. It was found that fumonisin interacted strongly with laminarin (hydrolyzed β-glucan) and chitosan (deacetylated chitin), but not with the mannan. The mannan seemed to protect whole yeast cells and mannan-deficient mutants from fumonsin. A yeast mutant with a poorly organized cell wall could potentially bind fumonisin better. Another possible option might be to use cell-fragments of yeast instead.

Sammendrag

I denne studien ble karbohydrat-interaksjoner undersøkt ved hjelp av optiske pinsetter, som er et instrument for måling av krefter ca. 0,1-100 pN. Karbohydrater festes på forskjellige biologiske polymerer i en prosess som kalles glykosylering: kovalent bindingen av sukkerkjeder til proteiner og lipider. Det store mangfoldet gjør disse sukkerene godt egnet for cellegenkjenning. Under karsinogenese uttrykker cellene ofte mye kortere glykaner på overflatemolekyler, som er kjent som tumorassosierte kreftantigener (TACAer). MUC1 er et overflateprotein som har et oppregulert uttrykk i kreftceller, med tilstedeværelse av TACA som Tn, T, STn og ST. Funksjonene til antigenene er ukjente, men uttrykket av Tn og STn korrelerer med metastase og dårlig prognose. Denne studien hadde som formål å undersøke hvordan alle de nevnte antigenene interagerer, ved hjelp av optiske pinsetter, for å forsøke å finne ut om noen av disse glykanene kan modulere interaksjoner på celleoverflater.

Det ble funnet at MUC1-Tn, MUC1-STn og MUC1-ST var i stand til å binde seg selv og hverandre. Styrken av kreftene mellom MUC1-Tn-self og MUC1-STn-selvantigener syntes å ha tilsvarende styrke, men at MUC1-STn bandt litt sterkere og interagerte oftere. x_{beta} av den indre energibarrieren for MUC1-Tn-selv ble funnet å være 0,33 nm, mens den mellom MUC1-STn-self var 0,39 nm. MUC1-T var også i stand til å selvinteragere, men ble ikke funnet å binde de andre mucins. Dette kan skyldes eksperimentelle vanskeligheter. Det ble funnet at GalNAc hadde en sentral rolle i samspillet. N-acetylgruppen av sukkeret ser ut til å være viktig. En mer tungt glykosylert mucin, TR-PSM H8, ble undersøkt. Det ble funnet at TR-PSM H8-mucinet hadde nesten dobbelt så høye bindingskrefter som MUC1-Tn - selv og MUC1-STn - self ved samme belastningshastigheter, og ble funnet å ha en x_{beta} på 0,22 nm.

Lektiner er proteiner som kan binde seg til sukkergrupper og formidle en celles respons på dem. Macrophage galactose-type C-type lectin (MGL) er et reseptorprotein som bare finnes på dendritiske celler og makrofager, som er antigenpresenterende celler. MGL har vært interessant i utviklingen av kreftvaksiner, da det antas at dens effektive aktivering kan utløse en immunrespons mot TACAer. Det ble funnet at MGL var i stand til å binde MUC1-Tn i fravær av kalsium. Det bandt ikkeen polyakrylamid-kjede med 80% Tn. Begge disse resultatene krever videre granskning.

Optiske pinsetter ble brukt til å undersøke samspillet mellom et mykotoksin fra *Fusarium moniliforme*: fumonisin B1 og cellevegg-glykaner på gjærceller. Fumonisin er et kreftfremkallende stoff som kan forurense hvete, havre og mais. Gjercelleveggen hos *Saccharomyces cereviciae* består av et indre lag av kitin, et mellomlag av β-glukan, og et ytre lag av mannan. Det ble funnet at fumonisin interagert sterkt med laminarin (hydrolysert β-glukan) og kitosan (deasetylert kitin), men ikke med mannan. Mannan syntes å beskytte hele gjærceller, og mutanter med mindre mannan på celleveggen, fra fumonsin. En gjærmutant med en dårlig organisert cellevegg kan potensielt binde fumonisin bedre. Et annet mulig alternativ kan være å bruke cellefragmenter av gjær i stedet.

1 Preface

This thesis is submitted to the department of Biotechnology at the Norwegian University of Science and Technology (Norges Teknisk-Naturvitenskapelige Universitet, NTNU) as a final part of the Integrated Master's Programme in Biotechnology. The work for this thesis was carried out between February 2016 and July 2017, with Professor Marit Sletmoen as the supervisor. I would like to thank Marit for evoking my interest in the field of research of carbohydrate-mediated cancer vaccines, inspiring me to investigate the different systems that have been studied during the work with this thesis, and finding time to discuss results that were hard to make sense of. I would also like to thank her for acquiring a computer that I could do most of my analysis on, which reduced the time it took to go through the countless files that had to be analyzed.

During this study, the results were analyzed using software made by Professor Bjørn Torger Stokke, at the Department of Physics. I would like to thank him for the maintnance of this software swiftly and on short notice. Thank you for answering questions and providing me with articles that made the work with the topics on hands easier.

A thank you goes to Gjertrud Maurstad, Head Engeneer at the faculty of Physics, for helpful discussions about some of the technical aspects of this work, and for keeping the lab stocked with equipment.

I would like to thank Mickaël Castelain and Hélène Martin-Yken from Laboratoire d'Ingénierie des Systèmes Biologiques et des Procédés (LISBP), who were both helpful in the work with fumonisin. Mickaël's contribution in understanding how to work with optical tweezers is appreciated, and Hélène's contribution in explaining the reasoning and research behind the work at hand greatly sped up the writing.

A big thank you goes to my husband, Sondre Andreas Engebråten, who supported me throughout all this time, cheered me up through long conversations during the working hours in the lab, and provided me with pizza in times of frustration. His help as teacher and tech-support person in Latex has been greatly appreciated during this work.

Katsiaryna Siarpilina
Trondheim, July 2017

Contents

2 Introduction

2.1 Why forces between molecules are of interest in molecular biology

In the field of molecular biology it is of interest to know what types of molecules are able to bind to each other. Interactions can mean creation of complexes, changes in conformation, signalling, aggregation of molecules and many other behaviours of that could induce important changes in a cell [1]. It has long been known that the properties of molecules at the cell surface are very important determinants for what kinds of cells stick together. Surface molecules are essential for such phenomena as the self-assembly of tissues [2]. The expression of different molecules at surfaces of cells can determine their localization and mobility [3, 4]. The strength and lifetime of interactions can be an important factor for how cells responds when many different ligands are available [5]. The strength of a ligand and its receptor is of high importance in pharmakinetics [6], where the strength and lifetime of the interaction can determine the effect of the drug. Understandably, data where strength is quantified can be very useful.

2.2 The mucin experiments

Mucins are big proteins that are normally heavily glycosylated. These proteins are the main part of mucus, but are also found both on the surface and on the inside of cells. Human epitelial mucins have since the 1980's been found to experience changes both in the level of expression and the degree of glycosylation. Changes in the glycosylation of some of these epithelial mucins is a marker of cancer onset and progression, but these changes also seem to be able to induce transformation of healthy cells. Much evidense exists that the change in glycosylation is an important factor for the cells' ability to migrate, invade other tissues and avoid the immune system. Interactions that lead to this have traditionally been believed to act either through lectins - glycosyl-binding proteins, or through protein-protein contact. Recently, it has also been hypothesized that interactions between glycosyl groups on the mucin-proteins might have the ability to increase or decrease the contact between cells, which in itself can induce a change in how the cells communicate and behave.

In this thesis, it was attempted to investigate whether there are differences in how mucins with different glycosylation intract, as this might give insight into what kind of changes might happen when such glycosylation accumulated on the cell surface. It was of interest to estimate the strength and lifetime of these interactions. Mucins that were found to have interactions were investigated further by trying to figure out what groups might be contributing to the interactions. Such an investigation is of interest because proteins are still regarded as the most important components in the membrane of a cell when it comes to the cell's interactions with its environment. Later, carbohydrates have been found important for the adhesive properties of a cell. It is already known that some carbohydrates are able to

concentrate various molecules and ions at the cell surface. It would be interesting to see whether carbohydrates could have functions beyond what is already known: whether they might have inter-carbohydrate interactions that could modulate cell-cell interaction additionally to proteins.

2.3 The fumonisin experiments

The original scope of this project was only work around the topic of mucins. Although the mucin and the fumonisin experiments deal with two different topics, their focus are interactions mediated by carbohydrates at cell surfaces, and ways these might be useful and interesting. Investigating the interactions between fumonisin and different carbohydrate components of the yeast cell wall resulted in more insight into interactions that involve carbohydrates.

Fumonisin is a mycotoxin from the mold *Fusarium moniliforme*. The mold can be found in crops like corn, oats and wheat [7], and its toxin has been found to induce cancer [8] and edema in animals [9, 10] and humans [11, 12]. In some cases, the removal of toxins from food can be challenging without affecting other characteristics of the product. Microorganisms is one option of removing toxins from food and feed [13]. Yeast cell wall components have been used in the detoxification of animal feed for almost two decades [14, 15]. These components are used in detoxofication by mixing them into the animal feed, where they bind strongly to the toxins, and prevent them from entering the blood stream of animals [14]. The yeast cell wall components with now inactvated mycotoxin pass through the digestive tract of the animal.

A yeast cell's cytoplasm is surrounded by a thick cell wall that consists of an outer mannan layer, a middle β-glucan layer and an inner chitosan layer. It would be of interest to know if any of these carbohydrate layers are able to efficiently bind the fumonisin toxin. This involves investigation into whether there are any interactions between fumonisin and any of the components of the yeast cell wall, and if so, whether any of these interactions are strong. If successful, the results may lead to knowledge about how to improve the efficiency of detoxification of animal feed, and possibly also other products that have been exposed to *Fusarium*.

3 Background

3.1 Glycosylation of proteins

Glycosylation is the attachment of glycans to a molecule, commonly protein or lipid, and can have many different functions. Glycans are polysacharides of varying lengths, which can be both linear and branched. Glycosylation proceeds in well-defined steps, which happen in the endoplasmatic reticulum (ER) and Golgi apparatus during the trafficking through the secretory pathway. In mammals, glycans are made up of nine different sugar moieties that are formed by glycosidases and glycosyltransferases [16]: β-D-glucose (Glc), β-D-mannose (Man), N-acetylglucosamine (GalNAc), N-acetylglucosamine (GlcNAc), N-acetylneuraminic acid (NANA)/sialic acid, , β-D-galactose (Gal), xylose (Xyl) [17], α-L-fucose (Fuc) [18] (Figure 1) and N-acetyllactosamine (LacNAc) [19].

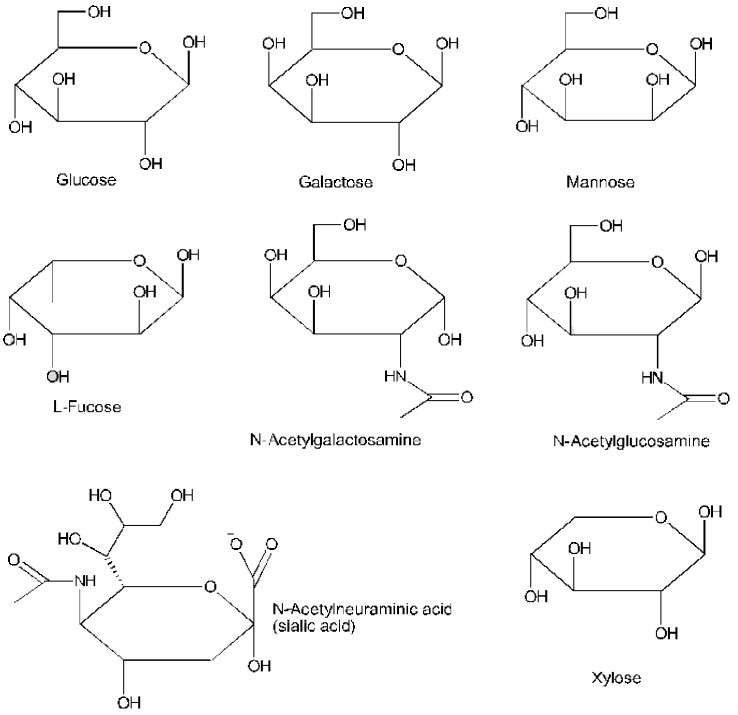

Figure 1: Different sugar moieties that can be found on glycosylated proteins in mammals.

Glycan structures on proteins can be divided into three major classes:

1) N-linked glycans: the glycans are bound to the nitrogen of an asparagine of a protein.

2) O-linked glycans: attached to serine or threonine residues of proteins.

3) Glucosaminoglycans (GAGs): attached to serine residues of proteoglycans (small protein part, very big glycan part).

The sugars of N- and O-linked glycans can be branched; N-glycans can have up to four antennae, and O-glycans can have up to two, and N-glycosylation is typically quite larger. While the sugar structures of N- and O-linked glycans can be branched, those on GAGs are linear. As the sugar moieties can be combined in many ways and attached at many sites, there is an enormous variety of possible structures. [16].

Glycans attached to proteins can function as mechanical protection, be protective from or bind certain chemicals, they can work as antigens that affect the behaviour of immune cells, modulate cell behaviour and cell-to-cell contact, and can be detrimental to the shape and functions of certain proteins. Some glycans can have binding points for other glycans and organize them in the extracellular matrix (ECM), or affect how proteins interact with each other, and there are many receptors that have glycans as their ligand. The effects of altered glycosylation can be variable: in some cases the change is undetectable, while in others it can be important. The same change in glycosylation in differnt cell types can give different outcomes [20]. Glycobiolody has for a long time had as a major focus to relate certain structures to specific diseases [16].

3.2 O-linked glycosylation in humans

O-linked glycosylation is when the glycans are bound to the oxygen of a hydroxyl group on serine or threonine, but can also appear on hydroxylysine and hydroxyproline. N-glycosylation begins already in the ER, where a precursor glycan, already assembled on a scaffold, is added to asparagine; this is called glycosylation en bloc. The precurson glycan is then modified further while on the target protein. O-linked glycosylation differs in that the sugar moieties are added one-by-one, and the end product is often smaller and thus more simple. Both N- and O-glucosylation can occur on the same protein [21, 22]. It is convenient to divide glycans into two domains: the core and the antennae. Although the core structures of N- and O-linked glycans are very different, the antennae can be common for both [17]. However, the N-linked glycans are often much bigger and more branched than the O-linked glycans. The higher the amount of attached sugars, the more hydrophlic the product will be [23].

A protein that is to be O-glycosylated is translated an cotranslocated from the ribosome into the ER lumen. O-linked glycosylation commonly starts in the Golgi apparatus, where a nucleotide sugar, uridyldiphosphate-N-acetylgalactosamine (UDP-GalNAc), is transferred onto a β-OH-group of either serine or threonine of polypeptde, by N-acetylgalactosamine (GalNAc) transferase. This glycosylation form is called the Tn-antigen, which is, in healthy tissue, modified further with other saccharides [17].

After the addition of a single GalNAc, the polypeptide is trafficked to the trans-Golgi network for further processing. The core structure is a small part of the glycosyl groups that is common for many of the possible saccharides created by

further processing. There are at least eight O-linked glycan core structures that can be made in mammals by adding more saccharides [24]. One of four core structures are commonly created (Figure 4) at this point, all of which involve either addition of galactose or N-glucosamine [17]. The additional structures created when the core is elongated are called antennae. The antennae for both N- and O-linked glycans are crated in a similar way, and some the same antennae can be found in both types of glycans [17].

From the trans-Golgi network, the proteins can be targeted to various organelles; some might be secreted outside the cells, some become components of the plasma membrane, and some are sent to lysosomes for degradation. This is determined by the protein's signal sequences, whether the processing on the protein has proceeded correctly, and various signals the cells receive.

3.3 Aberrant glycosylation in cancer cells

It has been known since early 1970s that the structure of glycans on the cell surfaces of eukaryotic cells changes with the onset of cancer [25], but also other diseases. Cancer cells often have a change in the level of expression of different glycans, or display glycan structures that are different from those on normal cells, or can express structures that are common in an earlier developmental stage of a cell (Figure 2). Cells from tumors and cells transformed *in vitro* have been shown to have a signifficant difference of glycosylation of surface proteins of many kinds and lipids (especially ceramides) [26].

Glycoylation is not a template-driven process, like the expression of proteins. Instead, the result depends on the amount, activity level and types of enzymes present in the compartments where glycosylation is carried out - the Golgi and the ER, and the amount and type of available sugar moieties. This is a dynamic process that is affected by the expression of genes in the cell, and the availability of different nutrients, which can be used as precursor-molecules for the glycosylases and glycosyltransferases [21]. The resulting glycosylation can, in turn, affect the behaviour of the cell and modify aspects of its interaction with the surroundings. The normal O-glycosylation of proteins often generates glycan-structures with six or more sugar moieties, and are often branched, the cancer-specific glycans are often much shorter - one to five sugar moieties. The glycosyl groups can appear both more [27] and less frequently [28] on the possible glycosylation sites than normal.

It has been found that diverse neoplastic lesions, like cancer of the colon, breast, cervix and skin express truncated O-linked glycans on plasma membrane glycoproteins and also on glycolipids. These tumor-associated carbohydrate antigens (TACAs) are not only markers of cancerous transformation, but can also be markers of tumor progression, and may be involved in cancer progression and metastasis [29]. One of the most common changes in cancerous cells is an increased number of terminal sites for sialic acid. Sialic acid is negatively charged. Charges are important because they can alter the concentration of ions, like for example calcium, at the cell membrane surface. These altered conditions, can, in turn lead to to other effects [30]. The sugar groups of different membrane molecules play an important

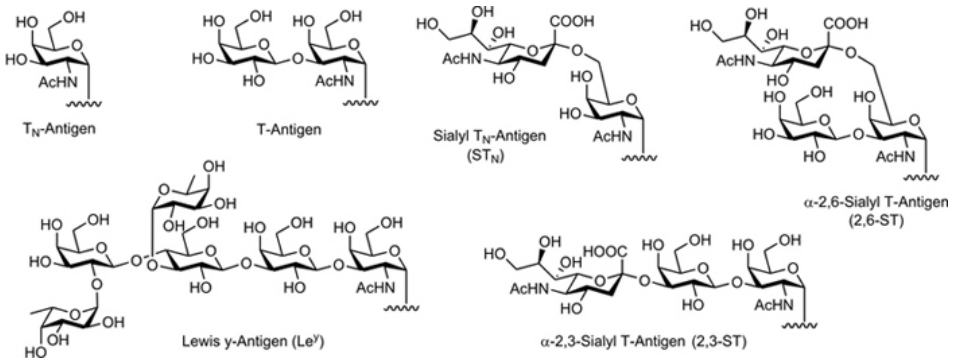

Figure 2: Some of the common tumor-associated carbohydrate antigens. From upper left to lower right: Tn, T - also called Thomsem-Friedenreich antigen, or TF, for short, Tn, ST, LewisY ans di-ST. The figure was adapted from Dr. Anne Hoffman Röder.

role in the interaction of the cell with its surroundings.

Some of these cancer structures are different enough from normal glycosylation of mucins that they are possible to detect using immunological methods. The changes in tumors can be characterized as one of two major categories: changes in glycolysation of glycolipids or glycoproteins. Glycoprotein changes can further be divided into three groups, one of which is a change in O-glycosylation is seen. The glycosyl chains are either incompletely synthesized, contain a higher than normal abundance of sialic acid or are are expressed on structures where they are not normally present [26]. Some antigens commonly found on cancerous cells include the Tn antigen (a single O-linked GalNAc), the STn-antigen, the T antigen (Gal-β1,3-GalNAc) [31], and the ST-antigen . The ST-antigen can be found on mucins on normal cells too, like blood cells, but it is in that case not found on the MUC1-protein [32] (Figure 3).

Some of the same glycan structures that are found on cancerous cells can also be found on normal cells, but they are then either expressed to a much lower degree [34], expressed on a different cell type [32], at a different developmental stage [35] or expressed of a different type of protein than in the case of cancer [32]. Generally, it has been found that the cancer antigens arise due to dysregulation or relocation of the enzymes present in the Golgi apparatus, where both under- and over-expression of different enzymes can be a cause [27, 36] (Figure 4). The most common cancer-associated antigens - and those of interest in this study, are described below.

3.3.1 The Tn- and STn-antigens

Tn- and STn-antigens often appear together on proteins of cancer cells. The Tn-antigen is expressed in over 80 percent of human cancers, and comprises a single α1-linked GalNAc unit on Ser/Thr of proteins [37].

STn is α-2,6-sialyl Tn and is associated with poor prognosis in cancer patients. It

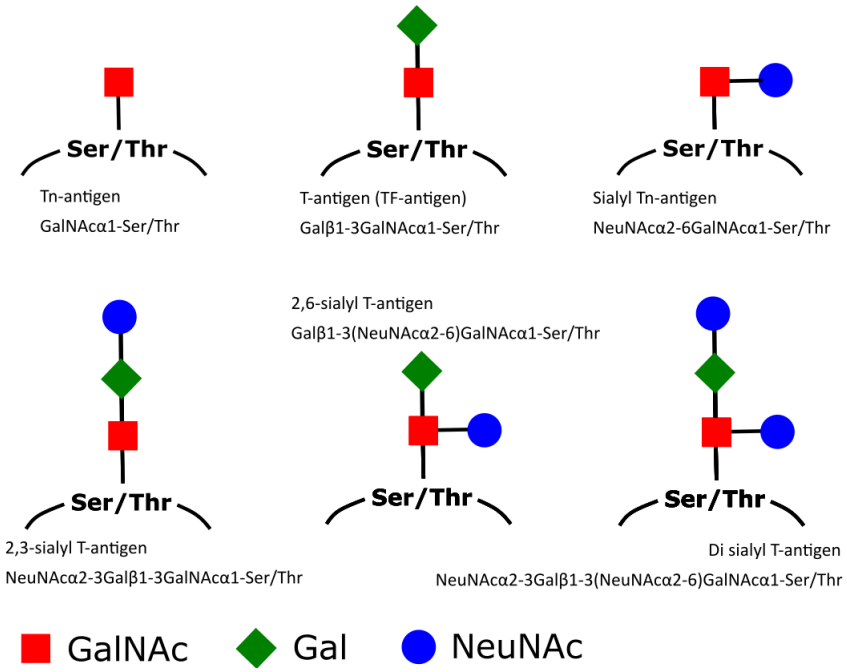

Figure 3: Common tumor-associated carbohydrate antigenson proteins, with their structure described. These are the antigens on MUC1 that have been in focus the most. As shown, there are three possible varieties of the ST-antigen, where more than 80% is of the 2,3-ST.

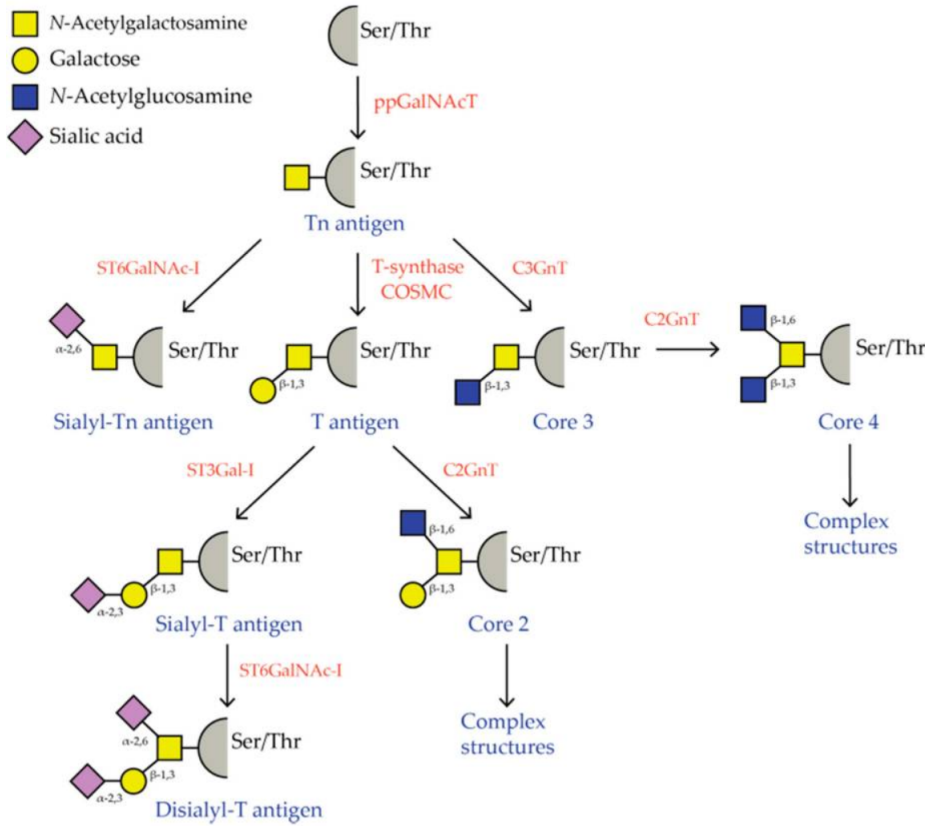

Figure 4: A small overview of how some cancer-associated tumor antigens are generated. All of the orange-coloured enzymes are glycosylases and glycosyltransferases that have abnormal activity when cancer antigens are detected on the cell, except COSMS, which is a chaperone. Reproduced from Cornelissen and Van Vliet, 2016 [33]

is the most tumor-specific antigen, and is expressed by about 30% of breast cancers. Normally, this antigen is only expressed by parts of the gastrointestinal tract. It has been shown that the STn-antigen is often a result of endogenous of exogenous activation of the sialyl-transferase ST6GalNAc1, which overrides the expression of the core 1 and core 2 O-glycans [28].

Recently (2008), one of the mechanisms for expression of two of the most commmon TACAs was found. It was discovered that the Tn and STn antigens, can result from genetic mutation or epigenetic changes in the gene for chaperone COSMC [38]. COSMC is a single-exon gene at locus Xq24 in the human genome. This chaperone is responsible for the correct folding of the T-synthase (β3galactosyltransferase) polypeptide into the functional dimer, before it is sent to Golgi for further processing. Without enough COSMC in the ER, the T-synthase polypeptide creates aggregates [39]. GRP78/BiP is a ER-residing chaperone that plays a mojor role in quility control of proteins [40]. T-synthase is a transmembrane protein; when it creates aggregates it interacts with GRP78, the lumenal part of T-synthase is cleaved off by an unknown protease. The free part is translocated back into the cytosol (HRD1 complex), where it is polyubiquitinated and degraded by proteaosome 26S [40]. The lack of T-synthase in the Golgi leads to expression of Tn. Tn is often accompanied by the expression of STn [41], when there is an abundant amount of enzyme ST6 N-acetylgalactosaminide alpha-2,6-sialyltransferase 1 (ST6GalNAc1) [42, 28], which sialyates Tn.

It has been found that GRP78 is not only involved in quality control, but also involved in survival of cancer cells that involves tumor progression and resistance to drugs. In some cancerous cells, GRP87 is also present of the cell surface, which may give it a possibility to interact with cell-surface receptor of other cells (gain of function). This can be therapeutically relevant [40].

3.3.2 The T-antigen

The T-antigen is also called TF-antigen (Thomsen-Friedenreich), and consists of a galactose bound onto the Tn-antigen (Ser/Thr-bound GalNAc). It has been claimed to have been found in over 90 % of pancreatic, breast and lung cancers in humans [43] [37] and aiding in metastasis of cancer by interacting with galectins [44]. In cancer cell lines from mice, it was shown that metastatic cancers had much higher expression of the T-antigen [26]. T-antigen was also found to increase with the progression of urinary bladder cancer, which could be used in the diagnosis of the disease [45]. The T-antigen has been found on colon cancer cells of moderate and high progression [46].

Aditionally, higher epression of the T-antigen was shown to result in a higher susceptibility to lysis by natural killer (NK) immune celles. Both in the animal model and in tumors from humans, *in vitro* and *in vivo*, which could be potentially interesting for vaccine targeting [47].

3.3.3 The ST-antigen

The ST-antigen is comprised of a galactose and a sialic acid bound to the GalNAc. The ST-antigen is the most common antigen on cancer cells [48]. Sialic acids are common as a terminal resdue on glycoproteins and glycolipids in humans, and results in hydrophilicity and a negative charge on such structures due to the deprotonation of its caboxylic residue at physiological pH [36]. The three sugars that make up the ST-antigen can be bound in three different ways (Figure 3):

1) both the galactose and the sialic acid are bound directly onto the GalNAc, the galactose is not sialyated

2) both the galactose and the sialic acid are bound directly onto the GalNAc, the galactose is syaliated

3) the sialic acid is bound to galactose, which is bound to the GalNAc.

It was found by mass spectrometry, that over 80% of the ST-antigen is bound in the latter described way, and thus should be the main contributor to whatever the effect of ST-antigen is on the interactions.

Sialomucins, which are mucins with abundant sialyation, were first found to be able to suppress the immune system in mice. Cells with abundant sialomucin could be transplanted between different mice without rejection, while cells without this type of mucin were rejected by the immune system [49]. Later it was found that highly sialyated mucins in humans were overexpressed on tumor cells [50] [51], and that sialic acid was found to greatly affect the metastatic potential of cells [52]. Some of the metastatic potential has been thought to possibly be due to sialo-binding lectins, such a galectin-3 (Gal3), which are receptors that might have the potential to capture cells with abundant sialyation during their metastatic migration [53] [54].

Sialic acid is most abundant in the human brain, on glycolipids. The strong negative charges of polysialic acid on neural cell adhesion molecules (NCAMs) prevents the cross-linking of cells in the synapses by these cell adhesion molecules [55]. It is currently unknown whether some of the same anti-adhesive mechanisms might act between other types of cells due to sialic acid. However, experiments have been done where cells from a mammary epithelial cell line have been transfected with a gene for episialin - a mucin-like molecule. This cell line does not normally express this molecule.When micing cells without episialin with cells expressing high mounts of episialin, the episialin-expressing cells did not aggregate with the other cells. When episialin was expressed in amounts comparable to those in cancer cell lines, they did not aggregate efficiently with neither each other nor cells that did not express episialin. The conclusion of the experiments were that episialin might be able to mask other adhesion molecules in its surroundings and strongly affected cell aggregation. This was likely to not be only due to the negtive charges of episialin, as when treated with neuraminidase (sleaves off sialic acid), the aggregation ability was restored only partly [56].

Episialin expressing cells have been successfully made to regain the ability to attach to surfaces by the use of antibodies that aggregate them into pactches, and by capping the sialic acid residues. This causes the adherence and spread of cells,

which showed the ability to migrate [57]. This can be good or bad news. Normally, cells that are meant to be stationary are anchorage-dependent, which means that their survival is dependent on the attachment to a substratum - often this is ECM components. However, when tumor cells lose their anchorage depence, they are able to create metastases [58]. If cells that express high amounts of sialic acid are transformed cells that have lost their anchorage-dependence, anchoring them could be the equivalent of a metastasis.

3.4 MUC1-molecule

Mucin 1 (MUC1) is a member of the mucin family of proteins. Mucins are proteins that form protective mucosal layers on epithelial surfaces. Some mucins are free, but MUC1 is a surface-bound protein that can be found on the apical side of many glandular epithelial cells. The distribution of MUC1 in humans is well characterized and a transgenic mouse model that has a very similar distribution has been established [59]. Examples of tissues where MUC1 can be found are breasts, pancreas, esophagus, lining of the lungs, kidneys and bladder. Some abnormal plasma cells can express MUC1, but it is also normally found on some normal cells, like resting T-lymphocytes and proerythroblasts. Examples of tissues that lack MUC1 in the large intestine, skin epithelium and all mesenchymal tissues [60].

The MUC1-protein became of interest in cancer research in the late 1980's, when it was discovered that it contained a breast cancer-specific epitope. A monoclonal antibody was created to bind to this epitope, which was accessible on breast carcinomas and chemically deglycosylated MUC1, but not on any form of healthy breast tissue and tissue from benign tumors. It was found that the binding of the antibody depended on the glycosylation status of the MUC1 protein, as the antibody bound unglycosylated and partly glycosylated protein, but not when it was fully glycosylated, like in healthy cells [61].

Later, it was discovered that, additionally to the underglycosylation, the expression of MUC1 on breast cancer tissue was 10-100 times larger than on normal breast tissue [34]. MUC1-overexpression was found to be a common theme in many different types of cancer, and often correlated with metastatic potential of the cells. Overexpression of MUC1 was found to correlate with the movement of cancerous cells into the lymphatic system and with further advancement of the cancer stage in gastric carcinoma [62] and in colorectal cancer [63]. Normally, the expression of MUC1 is restricted to the apical side of the epithelium, but in cancer cells, the polarity of expression is often lost, and the protein is expressed accross the entire cell membrane. This seems to decrese the ability interaction between the cancerous cells and cells of the immune system, and to promote invasion and metastasis [64]. In a different study, it was found that the overexpression of MUC1 inhibited the integrin-mediated cell-adhesion to ECM components [57].

The development of drug that promote rejection of tumor tissue has long been a goal in cancer immunology. Further experiments using solid phase enzyme-linked immunosorbent assays showed that different cancer-specific antibodies reacted to a peptide-region of the MUC1-tandem repeat with the sequence PDTR. The threonine

(T) in this sequence is one of the 5 potential glycosylation sites on the tandem repeat. It was thus hypothesized that this threonine might be underglycosylated in breast cancer cells. The sugar moities were believed to either shield the epitope or change its conformation. This began the investigation into other antibodies that preferentially bound cancer-specific mucins, and what sequences these antibodies bound to, as this might offer both a means of diagnosing and possibly also treating cancers that show an obnormal MUC1 phenotype [65].

In humans, the mucin MUC1 molecule is expressed from the MUC1 gene. The MUC1 molecule consists of two subunits: a transmembrane C-terminal subunit (MUC1-C), and an extracellular N-terminal subunit (MUC1-N) that is normally highly glycosylated in healthy cells [66, 67]. The C-terminal subunit is involved in cell signalling, while the N-terminal end participates in cell adhesion [1]. The transmembrane subunit tethers the extracellular subunit to the cell membrane by non-covalent bonds (Figure 5). The extracellular subunit normally consists mainly of tandem repeats of 20 amino acids (PDTRPAPGSTAPPAHGVTSA, Figure 6); the number of repeats reported has been varying, but is in the range from about 20 to 120, with 40-80 being the most common number in Europeans [66] [67]. The tandem repeat structure has been resolved by NMR, [68] and is arranged in a structure that has been called "poly-proline β-turn-helix, and each creates a structure of a knob followed by a spacer, which makes up one repeat).

As the MUC1-protein is normally heavily glycosylated, hydrophobic interactions between parts of the protein are largely sterically prevented by the hydrophilic interactions between the sugar moieties. This makes the normal protein extended but flexible. The average length of one tandem repeat is 5 nm, which results in a protein that extends about 200-500 nm outwards from the cell surface; most other proteins are confined within the first 50 nm of the cell surface [69], which is much further than many receptor-proteins. The stiffness and extension of the protein has been found by using light scattering and NMR, and by AFM-studies. The glycosylated conformation was found to be a random-coil-peptide, which is the case when a peptide does not have any specific strong stabilizing interacting groups, and is not locked into one specific conformation. The glycosylated MUC1 is extended due to interactions between GalNAc residues and adjacent amino acids in the core protein. The sugar moiety linked to the GalNAc can also have an effect, but additional sugar moieties have little-to-no effect. Unglycosylated polypeptide has a different conformation, where it was collapsed into a globular shape. Persistence length can be viewed as the length on a protein at which it would be likely to see a significant change in the curvature of the protein, and is a measure of chain stiffness. The persistence length of glycosylated MUC1 is estimated to be about 145Å, or about 14.5 nm, by using NMR and light scattering. To put this into perspective, a peptide with no glycan substitutes has an average persistence length of about 10Å [70, 71, 72]. Studies done by AFM found a different persistence length, of about 36 nm [73]. In any case, the persistence length compared to the full length of the MUC1-protein means that there is quite a lot of flexibility over the stretch

[1] `https://www.ncbi.nlm.nih.gov/gene/4582`

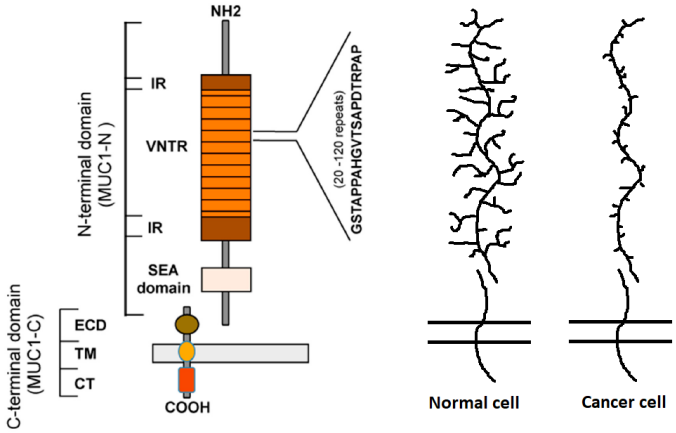

Figure 5: To the left is a schematic overwiew of the MUC1-protein, which consists of two peptides, connected with hydrogen bonds. IR: imperfect repeat of the VNTR-sequence. VNTR: variable number of tandem repeats of 20 amino acids. SEA: sea urchin sperm preotein-enterokinase-agrin domain. ECD: extracellular domain, which has the ability to bind extracellular ligand. TM: transmembrane domain. CT: cytoplasmic tail, which has prolines that can be phosphorylated. On the right, the difference in glycosylation patern of normal vs. cancerous cells is shown, where the side shains represent O-glycans. Reproduced from Cascio and Finn, 2016.

of the whole complex.

There are several MUC1 alleles, and the number of repeats vary among them. Each of the tandem repeats have 5 sites that can be O-glycosylated, but it varies how many of these actually are. Normally, the MUC1 protein is only expressed on the apical side of epithelia. In some transformed cells, MUC1 sometimes does no longer localize exclusively to the apical side of the cell, but also to the basolateral [64]. It has been found that high expression of MUC1, especially in the cytoplasm, is a marker of bad prognosis in several types of carcinomas. In patients with carcinoma, also elevated serum levels of circulating MUC1 can be found, as the N-terminal part of MUC1 is shed from cells [74].

In some cancers, overexpression and abnormal glycosylation of MUC1 is suspected to be an important driver for metastasis and protect the cancer cells from the immune system. There are several ways that over-expression of MUC1 is thought to promote tumorigenicity. Because of over-expression, the mucins are thought to mask other cellular membrane molecules and prevent normal interactions between cells, or cells and the ECM. Some of the mucins self-associate, which might contribute to these effects, but also to hiding tumor-associated motifs from immune cells. The mucin overexpression might prevent small molecules that normally interct with the cells from reaching their receptors. In other cases, the abberantly glycosylated mucins can lead to interactions that are not normally initiated, such

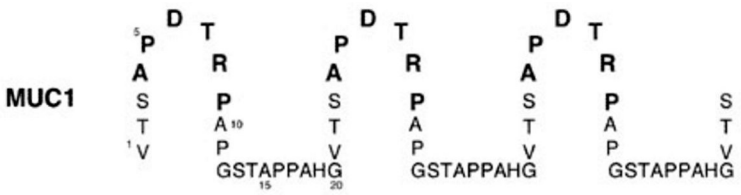

Figure 6: Part of the MUC1 VNTR, showing the 20 amino acid-sequence repeated trice. The VNTR-region has been reported to be repeated 20-120 times in human MUC1. The shape of the peptide sequence does not represent the conformation of the protein, but of the extended tandem repeat, and highlights the PTDR-sequence which often becomes accessible on transformed cells, assessed by antibodies.

as those between cancer-associated mucins and new potential anchoring sites for these cells. An example is between mucins on metastatic cells in the blood stream and the galectin-3 (Gal3) lectin receptor on endothelial cells. Interactions between cancer-associated cell-surface molecules might promote cell adhesion and aggregation, and extravasion . Finally, the aggregation of mucins in the cell membrane might stabilize certain receptor tyrosine kinases (RTKs) in the membrane and by this, cause prolonged abnormal signalling from these signaling proteins [37]

In a studies of esophageal cancer it was found that esophageal cells with overexpression of MUC1 on their surface gained proliferative and invasive properties. Upregulation of MUC1 resulted in bigger tumors following xenografts, and was a marker of tumor progression in this type of cancer. The biological properties of a MUC1-deficient esophagial cancer cell line were investigated. It was shown that the MUC1-deficient cancer cells were less proliferative and less invasive, and had reduced growth after xenografting. [75].

It was found that there is an overexpression of MUC1 on breast cancer cells. Higher levels of expression correlated with a further stage of progression of the cancer, and finally, metastasis [76]. The same was found for epithelial ovarian cancer, where overexpression of MUC1 was associted with cancer, and increased with increasing progression of the disease, in tissue samples [77]. In both cases, over 90% of the cancers of these organs exhibited MUC1 overexpression. In colon cancer, 60-70% of the investigated samples were found to have overexpression of MUC1 [78]. Similar findings are true for other types of cancers, such as that of lung, renal cell carcinoma, epithelial tumors, thyroid and pancreatic cancer, and more [29].

In addition to overexpression of the MUC1, in near all epithelialn pre-cancerous lesions, there is a change in glycosylation of the protein that consists of shortening of the glycan chains. One of the long studied changes of interest has been the expression of truncated O-linked glycans. Normal cells express glycans of quite a different length than certain epithelial cancers or cells from pre-cancerous lesions [79]. The shortened glycans means that the abberantly glycosylated proteins express

a different set of glycan epitopes, that might not normally be exposed. The change in glycosylation has been expected to be important for the cells' interactions with other cells, both through proteins that recognize the new epitopes [67] but also through the interaction between the MUC1 molecules on different cells [79]. There has been interest in investigating whether the aberrant glycolylation pattern could be used as an epitope that the immune system could be directed to.

3.5 Tumor-associated antigens might promote cancer through lectins

Altered glycosylation appears on both proteins and lipids of cancerous cells, and seems to be strongly affected by oncogenesis. Much research exists on the characterization and expression pattern of tumor-associated cancer antigens, but not a lot is yet known about how the altered glycan expression contributes to the progression and behaviour of cancer cells. Among the suspected mechanisms for this are the interactions between the sugar moieties and lectins, which are sugar-binding proteins. These proteins can be expressed in a variety of cells. Some of the cells can be those normally in vicinity of the transformed cell. The altered glycosylation can lead to binding or unbinding from such proteins, which can lead to signalling cascades that alter the behaviour of nearby cells. Another important group of lectins are those present on immune cells, which might lead to recognition of the transformed cell, or to down-regulation of the immune response and thus, masking of the transformed cell [33]. Several studies have found receptors that seem to be important in interactions with cancer-associated glycans, and that might mediate some of the effects of them.

3.5.1 Macrophage galactose-type C-type lectin

Macrophage galactose-type C-type lectin (MGL, lso referred to as CLEC10A or CD301) is a receptor protein that can be found on macrophage and monocyte-derived immature dendritic cells (DCs) (and lacking in mature DCs) of the immune system [80]. It belongs to a class of proteins called lectins, which are carbohydrate-binding proteins that bind sugar moieties on both proteins and lipids. In animals, their main role is to facilitate cell-cell contact. Several types of lectins have multiple binding sites, and can, additionally, oligomerize. Thus, lectins often interact with many carbohydrates on a cell surface, simultaneously. The interactions between carbohydrate and each lectin binding-site are relatively weak, but becomes strong because of their multiplicity. Unlinking is still possible, if needed [81].

Lectins are divided into classes bases on their sequence and properties. C-type lecting is one of the biggest classes, and is classified by its 120 amino acid carbohydrate-binding domain, which requires calcium (*C*-type) to bind carbohydrate. The sarbohydrate interacts with the sugar hydroxyl groups, which leads to their organization and makes the sugar-lectin bond possible. The same lectin can sometimes bind several different sugar moieties, which is due to interactions between different amino acid residues and the calcium [81].

The human MGL-receptor, also called CD301, stems from one single gene in humans, named CLEC10A [2], found at locus 17p13. The mRNA has 9 exons and 8 introns (9 then, I guess) [82]), which can be alternatively spliced, to give rise to several mRNAS, but only a single MGL variant is found in humans [83].

The MGL-receptor is a homotrimeric receptor, with each subunit having one extracellular binding site for N-acetylgalactosamine (GalNAc). The trimers are held together through an α-helical coiled-coil between the extracellular parts of the receptor, extending from the cell membrane, to the globular carbohydrate-recognition domains (CRDs) [84] (Figure 7). MGL is a transmembane receptor, whose intracellular domain has signalling activity

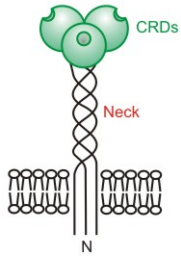

Figure 7: Schematic drawing of the structure of the macrophage galactose-type C-type lectin (MGL) receptor. This lectin is able to dimerize and trimerize, and here, the trimerized receptor is shown. Each MGL unit consists of an extracellular globular carbohydrate-binding domain (CDR, pronounced "card") and neck-region, which is able to induce clustering through coiling. The N-terminal part of MGL is transmembrane, and has signalling activity. Figure reproduced from Kurt Drickamer, 2011.

MGL has been found to bind several TACA, including terminal GalNAc (including Tn antigen), STn and sialyl LewisX (sLeX) and LewisA epitopes [85]. Tn has been described previously, and comprises a single α1-O-linked GalNAc unit on a Ser/Thr on the MUC1-protein. The human MGL (hMGL) has the ability to bind to α- and β-linked GalNAc, and has previously been found to bind to the Tn and the STn (Neu5Ac(α2,6)GalNAc) preferentially, antigens on polypeptides or synthetic backbones. This was studied by NMR spectroscopy, and essential amino acid residues for this binding were identified. The binding happened mainly through the GalNAc moiety, especially the H2-proton, as well as the H3 and H4 protons. The Ca^{2+}-ion was found to make contact with the 3' and 4' hydrohyl groups of the Gal/GalNAc. When the Tn was presented on the MUC1-protein (described below), it was also shown to make contact with some of the protons of the amino acids [86]. MGL has shown to be able to bind to ST-antigen, but not the T-antigen [41]. It has been found to have a marked specificity to the MUC1-protein [80].

[2]http://www.uniprot.org/uniprot/Q8IUN9

The MGL can, because of its ability to bing TACAs make contact with tumor cells. It can also attach to T effector cells through the glycoproteins CD43 and CD15. Downstream, this leads to attenuation of T cell mediated signalling, and thus downregulate the T cell activity and proliferation, and increased their cell death [87]. T effector cells are a part of the adaptive immune responce and regulate immunity and inflammation. The downregulation of their activity against a specific substance means that is is tolarated in the body, which is bad news when it comes to cancer.

However, the MGL-receptor is an endocytotic receptor, which mediated uptake of glycosylated carbohydrates, via clathrin-dependent endocytosis [82] in DCs. It is a type of receptor that is internalized after the binding of substrate. During ins migration through different intracellular compartments, it generally releases its cargo at pH values ¡6.0. Recycling of the receptor has not been demonstrated. After the uptake of polyacrylamide-Tn glycoconjugate, it was shown that the antigen was targeted to the lysosomes and degraded. After incubation of responder T cells with DCs that had internalized the polyacrylamide-Tn conjugate, it was shown that efficient activation of the responder T cells was achieved. This shows that it is possible to initiate an anti-tumor response through the correct activation of DCs through the MGL receptor [88].

As seen from the results of several studies, how the antigens interact with a receptor is of great significance, as the cellular response to similar antigens can be qualitatively different. This suggests that the molecular recognition processes of antigens should be characterized in fine detail to be able to optimize the design of vaccines against TACAs [89, 86].

3.6 Therapeutic molecules that target MUC1-positive cancers

Carbohydrate antigens on many types of cancer cells have been found as some of the most common changes of the cancer cell membrane, and have gained much attention during the past few years. Many of these have been found on the MUC1-molecule, which is upregulated in several types of cancers. Several different strategies have been attempted to target both the N- and C-terminal subunits of the MUC1-molecule for detection by immune cells, as the protein has been found to be overexpressed in many different cancer tissues. The upregulation has found to be possible both due to the upregulation of expression and due to amplification of the gene [90].

It has been shown to be difficult to devolop carbohydrate antigens as vaccines for cancer. Many of the TACAs are recognized by the body as "self" antigens, and the immune response to them is suppressed. It has been attempted to create antigens against the Tn- and STn-antigens, which are present on cancerous cells, but absent from healthy ones, and the presence is often associated with the cancer progression. However, at this point, such antibodies have only been used as tools in diagnosis and prognosis, but not in treatment. These antigens have also been attempted targeted by vaccines, but these have till now not been successful in clinical trials.

As carbohydrate antigens have been found to be some of the most relevant targets in cancer cells, several metohods have been developed to attempt to enhance the immune responce to TACAs.[91].

A DNA aptamer (MA3) that targets MUC1-positive cells preferentially was developed in 2008. Its target is the N-terminal (exstracellular) subunit of the MUC1-protein. It carries the cancer drug Doxorubicin, and was shown to signifficantly improve the delivery of the drug to MUC1-positive lung and breast cancer cells while reducing the intake in MUC1-negative cells. The aptamer targeted the drug to cells where the core peptide sequence APDTRPAPG was exposed, which was chosen as target because of its high immunodominancy. MA3 also recognized the whole VNTR sequence of MUC1. Any drug should exhibit high binding frequency to the target and low to non-target molecules. MA3 showed low affinity for albumin, which is the most abundant protein in serum. The uptake of Doxorubicin bound to the aptamer was same to slightly lower than that of free drug. The aptamer could be potentially useful, but in vivo animal studies must be done to evaluate its effects [92].

Immune cells are often unresponsive to the MUC1-protein as it is expressed on the apical side of some cells. However, patients with breast- and ovarian cancers that have IgM antibodies against MUC1 have been identified, which gives hope of inducing immunicity against the protein in other humans. In vivo studies in mice showed that it was possible to reverse this tolerance of MUC1 in transgenic mice with MUC1-expression similar to that of humans, by immunization the mice with a fusion construct of dendritic cells and the MC-38 MUC1-positive carcinoma cell line. This lead to the expression of CD8+ T-cells that recognized the MUC1 tandem repeat and had antitumor activity, but did not appear to be reactive to normal tissue [93].

It has previously been studied whether poly(acrylic acid) polymers functionalized with carbohydrate antigens would be able to be taken up by the immune cells . PAA is an example of a type of polymers called synthetic polyelectrolytes. Polyelectrolytes are able to stimulate the membrane receptors of immune cells to change the flux of ions through the membrane, which contributes to the uptake of the polymer and enhance the immune responce to the antigen bound to the polymer [94]. Studied showed that when PAA of low molecular weight was used *in vivo*, it showed no effect, but the effects becomes prominent with increasing molecular weight of the PAA, and it was in this way found to be an efficient adjuvant [95] [96]. Polyacrylic acid has previously not been found to induce cytotoxicity in murine macrophage cells [97], and thus, it has been of interest to study whether this polymer could be used to activate human macrophages through uptake of a PAA-conjugate. PAA is also a carrier that can potentially be used for treatment of cancers in the gastrointestinal tract; it can pass through the stomach and gastrointestinal tract without being digested, but is broken down by the microflora in the colon [98].

Other adjuvants that have been tested out as enhancers of the immune responce against TACAs have also been under investigation. Novel carrier systems of carbohydrate antigens have been under investigation, and have shown promising results. A group at the Michigan State University has been developing several

different new carrier systems for TACA antigen presentation. One of the studed systems is lipopeptide-coated iron oxide nanoparticles with carbohydrate antigens. The nanoparticles were coated with phspholipid-functionalized Tn-antigen-bearing glycopeptides. These delivery systems showed to be highly efficient in activating B-cells of the immune system, and leading to high expression of antigens against TACAs in mice. These antigens were able to recognize both mice- and human cancer cell death, and lead to destruction of tumors through complement-mediated cytotoxicity [99].

Another carrier system that has been tested by the above-mentioned group is the presentation of Tn-antigen on viral capsids. The group found that it is possible to induce a much stronger cancer immune responce against carbohydrate antigens by presenting them in a highly organized form. For this, the bacteriophage Qbeta was modified to carry the Tn-antigen. This conctryct was injected into mice with the highly aggressive TA3Ha-tumors. The construct was highly efficient at inducing immunity against the cancer cells, and resulted in signifficant improvement in survival of the mice: 0% vs 50%, in 6 mice [100]. It has been shown that both geometry and linker-design of the conjugate can play an important role in the anticancer response [101].

Also the T-antigen has been attemptes as a target of cancer vaccines, however, this has been studied much less than vaccine targeted against the Tn an STn antigens. The T-antigen is a Gal bound to a GalNac. Previous studies showed that the the glycosidic bond makes this structure flexible, which might be contributing to its low immunodominancy. It was suggested that glycan-engeneering might be used as an approach to make the the structure of the glycan more rigid, which might enhance the antigenic effect [102]. A more rigid structure of this antigen did indeed show to create an immune response in mice [103, 104], but there is yet a limited amount of research vaccines against the T-antigen.

3.7 Fumonicin and yeast

Within the investigation of interactions of carbohydrates, it was also possible to look at some of the interactions between carbohydrates present in the yeast cell wall and a mycotoxin called fumonisin B1. As the carbohydrates of the yeast cell wall are different from those present on human cells, it was believed that this investigation could result in a broader knowledge of interactions of carbohydrates.

Different species of *Fusarium* produce different fumonisins, and in this study, the focus is fumonisin B1 (right frame in Figure 8), produced by *Fusarium moniliforme* (left frame in Figure 8). *Fusarium* is a genus of fungi that are often found in soil or associated with plants, and fumonisin is a mycotoin produced by this microorganism. Fusarium is a filamentous fungi and characterized as a mold. It produces three classes of mycotoxins that have been proven to cause disease in animals: trichotecenes, fumonisins and zearalenones. Fumonisins are structurally similar to sphinganine, which is a sphingosine-backbone precursor, and can inhibit sphingolipid metabolism [105, 106].

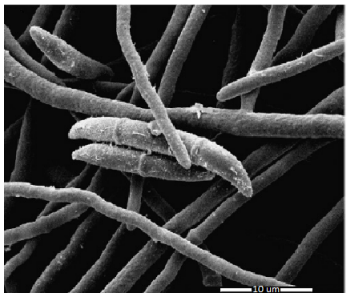

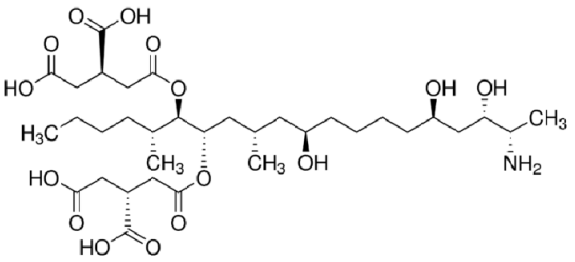

Figure 8: The left frame shows an electron microscopethe fungus *Fusarium moniliforme*. The white bar at the bottom right corner is 10 μm long. Adapted from Plodpai et al., 2012 [107]. In the right frame, the structure of fumonisin B1 is shown, which is one of the mycotoxins that the *Fusarium* is able to produce.

Fumonisin B1 has been found in corn [108], oats and wheat [7], and can sometimes be observed as a grey or white, fuzzy layer. Fumonisin has been shown to cause cancer in humans [11, 12], cancer [8] and edema in farm animals like pigs and horses [9, 10]. Wheras the toxin has been found to get into food produced for humans less often, it is a much bigger problem in feed produced for consumption by farm animals. The toxin can severely affect the productivity and welfare of farm animals [109]. It is therefore of interest to see if a cheap and effective system for the extraction of this mycotoxin can be established.

The removal of toxins from food can sometimes be challenging without affecting other characteristic of the product, like taste and the availablity of vitamins and minerals. When producing animal feed, the price is very important, a cheap way of removing unwanted chemicals is highly desirable. Using microorganism for the

removal of toxins is an example of such a method [13], and yeast species has been a popular choice. Usually, the cells are treated in a way to remove the cell-portion, and only the cell wall is used in the detoxification process. This method has been used for detoxification of animal feed for almost two decades, however: it was used for the removal of zearalenone, another toxin produced by *Fusarium moniliforme*, and not fumonisin [14, 15].

The dry yeast cell wall components are mixed into the animal food, and are left there. When animals eat the feed, contaminated by mycotoxin, the cell wall components bind strongly to the mycotoxin, and are indigestible. In this way, although the animal does consume the toxin, it is prevented from entering its blood [14]. The yeast cell wall and mycotoxin passes through the digestive tract of the animal. Recent studies have attempted to find out which components of the yeast cell wall bind the toxin. With this information it could, potentially, be possible to optimize the process of trapping of toxins by yeast cell walls.

3.7.1 The composition of the *Saccharomyces cereviciae* cell wall

Yeast are eukaryotic cells that are protected by a thick cell wall (Figure 9). It is composed of 85-90% carbohydrates, while the rest is protein [110]. The cell wall of the yeast *Saccharomyces cereviciae* is composed of β-glucan, chitin, proteins and mannan. The mannoprotein-layer is the outermost layer, and consists of mannosylated proteins. Mannan is a polymer made of mannose sugar units. The type of mannan that is found in the cell wall of *S. cereviciae* is a linear α-1,6-linked backbone with α-1,2- and α-1,3-linked branches [111] (Figure 10). Mannan makes up 30-40% of the dry weight of the cell wall of this yeast [110].

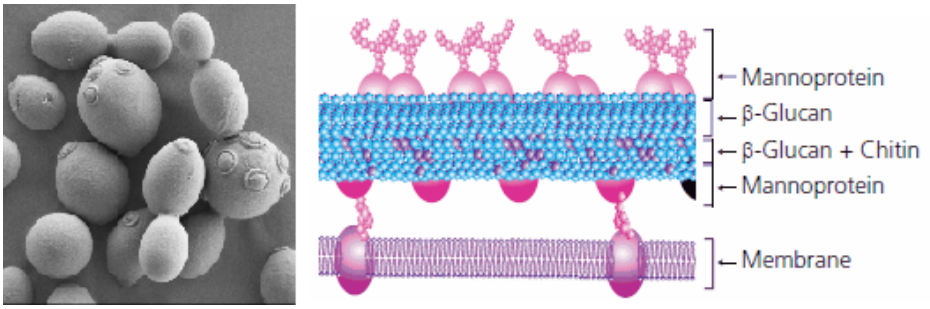

Figure 9: Left: SEM picture of the yeast *Saccharomyces cereviciae*. The craters are bud scars. Adapted from Kiseleva et al., 2007 [112]. Right: he yeast cell wall: a schematic drawing of the placement of components. Mannoproteins are drawn in pink, β glucan in light blue and chitin in purple. reproduced from SigmaAldrich.

The middle layer of the cell wall is made up of β glucan, which is a glucose polymer composed of β-1,3-linked backbones with β 1,6-linked side chains and interlinks between the backbone (Figure 11). The β glucan makes up about 30-50%

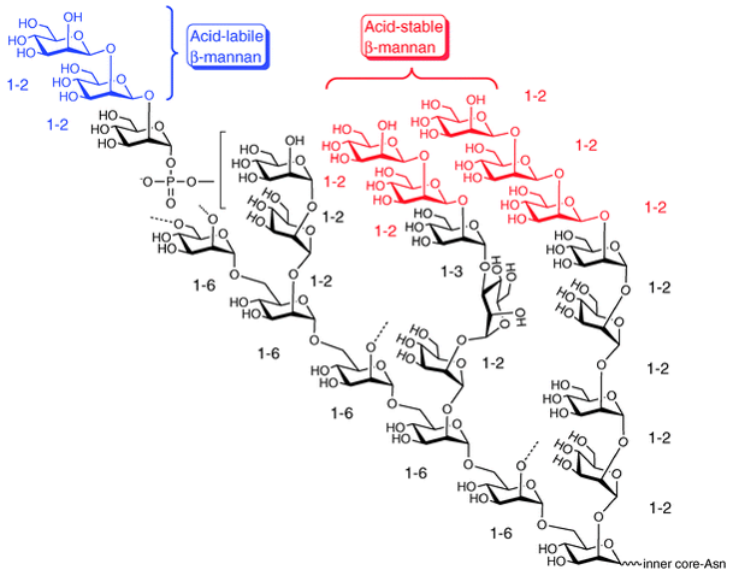

Figure 10: *Saccharomyces cereviciae* mannans [113], which, together with proteins, makes up the outermost layer of the yeast cell wall.

of the cell wall. It is important for the structure and rigidity, as it has numerous times before been shown that it links together all of the other components of the cell wall [114].

The innermost layer of the *S. cereviciae* is composed of chitin (Figure 12), but it is also found to be exposed on the cell surface, in a ring around the bud scar (exclusively) of the yeast cells. The bud scar is a crater-shaped structure left on the mother cell after budding (division in yeast) [115]. The structure of chitin was found in 1929, by Albert Hofmann. It is a long polymer of repeating β-1,4-linked N-acetylglucosamine (N-acetyl-D-glucosamine) units [116]. Chitin is very similar to cellulose, but with an acetylamine group instead of a hydroxyl group [117]. This allows chitin to bond to adjacent chitin units, mostly due to hydrogen bonds [118, 119]. The chitin content of *S. cereviciae* cells does not make up more than 1% of the dry weight of the cell wall [110]. Chitin is highly insoluble in most solvents [120].

It has long been known that glucan and proteins, chitin and proteins, glucan and chitin, and glucans and glucans in the cell wall interact. The mannan was found to react neither with other polysaccharides nor with proteins, making the outer side of the cell wall highly inert to certain substances. The mannans seemed to be attached to glucan through a proteins, which are N- or O-mannosylated [121].

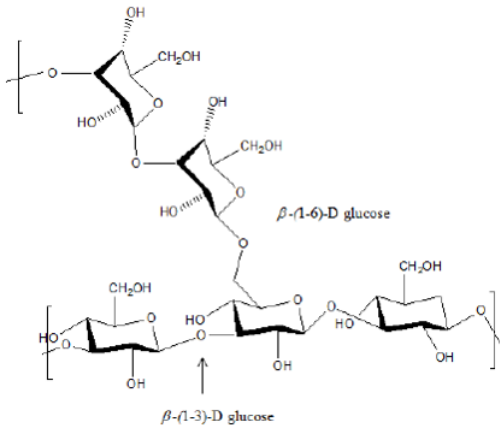

Figure 11: The structure of β-glucan, which makes up the middle layer of the *Saccharomyces cereviciae* cell wall, and binds together the other components of he cell wall: mannoproteins (outer layer) and chitin (inner layer). It is this component of the cell wall that contributes the most to its structure and rigidity.

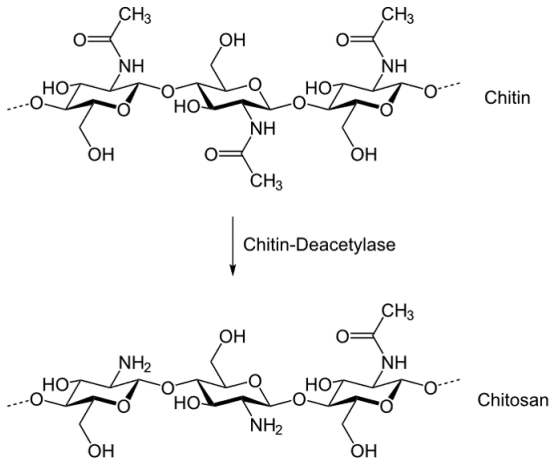

Figure 12: The structure of chitosan, which makes up the inner layer of the *Saccharomyces cereviciae* cell wall. It is the least abundant component of the yeast cell wall.

3.8 Dynamic force spectroscopy

Dynamic force spectroscopy (DFS) is the study of forces that are required to manipulate molecules, such as unbinding, unwinding, stretching, unfolding or twisting. DFS techniques can be used to measure different properties of molecules: bond strength, elasticity, protein movement along a polymer, conformation changes and more. When performing such measurements, rupture strength of the bonds will not be constant, but will result in a distribution of forces, because the strength of a bond, among other things, depends on the loading rate of the bond [122]. This distribution of forces is sometimes refered to as a dynamic power spectrum, and displays force as a function of the logaritm of the loading rate.

How molecules interact can be influenced by temperature [123], pH and ionic strength [124], cation valence [125], the hydrophilicity of the medium they are studied in [126], and more. Neither the bond strength or how molecules interact is affected by their concentration. The above-mentioned factors can be interesting and important to study, but will not be explained in further detail, as it is outside the scope of this project.

In this study, intermolecular bonds will be investigated, and an attempt will be made to measure and compare some of these interactions. DFS can be useful in such studies as they are able to detect whether molecules bind, and if so the strength of the bonds. Furthermore, some of the calculated parameters can be used to find other properties of the interactions, such as the energy landscape of the intermolecular bonds, the lifetime of the complex, and the amount of energy needed to break the bond. The ability of molecules to interact and the stability of the complexes have long been known to be important in cell biology. Information like that about the lifetime of complexes has been found to be of great importance in pharmacodynamics of medicines [6], as it determines much of the pharmacological activity of a drug. Binding affinity and lifetime can also be important in various industrial applications.

Several techniques are available today for the measurement of intermolecular interactions of single molecules; this is called single-molecule force spectroscopy. Different techniques can be used, depending on the desired sensitivity, and also on properties that are examined (stretching, twisting, bond strength, etc). Some of the existing techniques for measuring forces between molecules is atomic force microscopy (AFM), optical tweezers (OT), magnetic tweezers (MT) [1], acoustic force spectroscopy (AFS) [127]. As seen below (Table 1), OT is a sensitive method, which made it possible to measure the strength of weak interactions.

Table 1: The order of magnitude available with different force spectroscopy techniques.

Method	Force range (pN)	Working Principle
AFM	10 - 1000	Force probe
OT	0.1 – 100	Laser light
MT	0.0001– 100	Magnetic field

3.8.1 Unbinding of single molecule pairs

In this thesis the forces between polymers that bind and unbind are measured using optical tweezers by bringing two molecules together, let them interact and then pull them apart while recording the loading rate and magnitude of the interaction. The forces are measured along a dissociation pathway, limited by the movement of the beads the molecules are immobilized to. In addition to the forces that will be applied to the polymers by the optical tweezers, molecules in solution experience the Brownian motions of particles around them, which adds thermal energy. Different bound molecules can be held together by different forces, the bonds have different lifetimes and, and different binding geometries lead to different energy landscapes of the interaction. Because of the multiple factors that can affect binding, the shape of the energy landscape of a complex can be illustrated as a 3D field, where many factors can affect whether the molecules are in a bound or free state (Figure 13).

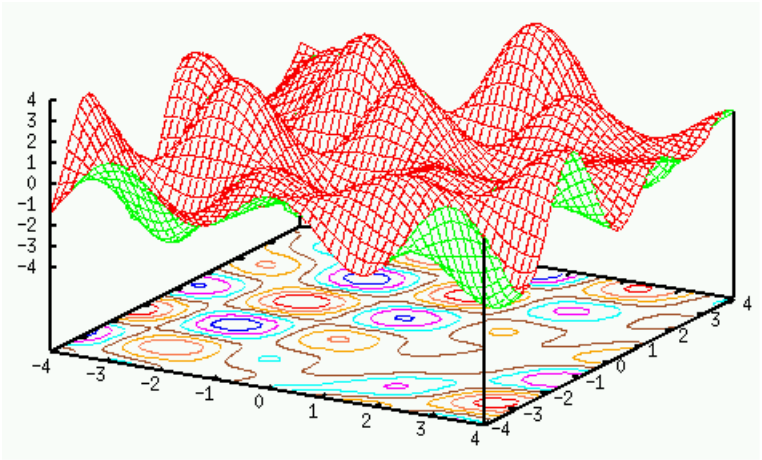

Figure 13: An example of the shape an energy landscape of a complex of two bound molecules could have. Where in the landscape the complex is depends on its internal energy. Reproduced from Ruye Wang, 2016.

However, because of the almost endless possible states of a complex, it is common to project the energy landscape along a reaction coordinate X (Figure 14), although this is a big simplification, it is still useful. The energy barrier is represented by an X,Y-coordinate system, where the x-axis represent different states of the complex, while the Y-axis represents its energy. It is preferentially to occupy the minima in the energy landscape because it is the energetically favourable state.

When the energy landscape represents the bound and unbound state of the molecule, it can be illustrated as in Figure 14. The first (leftmost) well in the curve (Figure 14) represents the most stable state - for example the bound state. The following peak is the transition state of the molecule, and has the highest

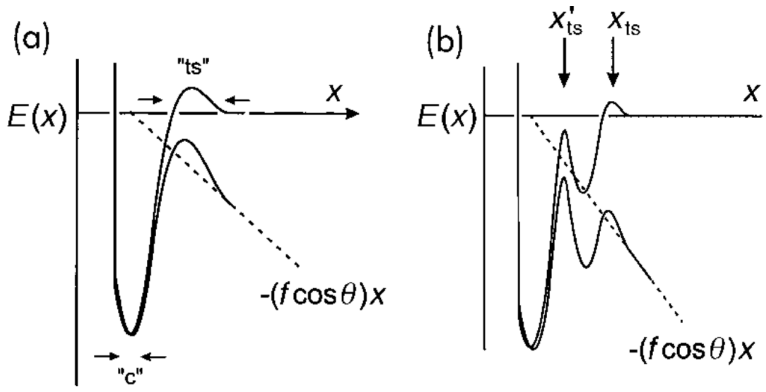

Figure 14: Here, the X-coordinate can represent the stretching of the complex, while the Y-coordinate represents the energy. "c": the stable complex, "ts": a short-lived transition state that the complex has to overcome to break apart. (a) Example of an energy landscape of a complex with a single activtion barrier. (b) Sometimes a complex muct go through several transition states before the molecules are free. The tilted stippled lines highlight the tilting of the energy landscape when external force is applied. When several barriers are present, tilting can change their relative importance. Reproduced from Evan Evans, 2001 [128].

potential energy and a brief lifetime before it proceeds to the next step. The energy difference between the complex and the transition state is called the activation energy (or "activation barrier"), which is the energy required to go from bound to free molecules. The transition state has higher energy than the bound and free states. Sometimes, the unbinding of molecules requires that they overcome several activation barriers before they are free - this might mean that some new bonds are formed and broken during the process of complete release.

3.8.2 The Worm-Like Chain model

The worm-Like Chain (WLC) model is one of the models that predict how a polymer can behave when it is being stretched. It describes the relationship between pulling length of a polymer and the force it experiences. This model deals with polymers that are continuously flexible (not only at certain segments), rod-like - particularly stiffer polymers, that have a smooth, curve-like conformation. This model is well suited for biological polymers like DNA, and proteins, that roughly follow the behaviour described by the model [128, 129]. The force experienced by such a polymer is described by Equation 1:

$$F(x) = \frac{k_B T}{L_p} \left(\frac{1}{4\left(1 - \frac{x}{Lc}\right)^2} - \frac{1}{4} + \frac{x}{L_c} \right) \tag{1}$$

F is the external force, and x is the pulling distance (or extension). The L_p is persistence length. Persistence length describes the stiffness of a polymer where it deviates significantly from a straight line, defined as half of the Kuhn length. L_c is contour length, which is is a molecular phycics term that refers to the maximum length a polymer can be extended. k_B is the Boltzmann constant and T is the absolute temperature in Kelvin [128, 129].

The WLC model is often applied to the force-extension curves on proteins up to several hundred pN, and often guides the analysis where single-polymers are being stretched, in terms of what the shape of a stretched polymer should look like. However, it is applicable also when two interacting polymer are stretched. The increase in force of the polymers should roughly follow the shape the model predicts (Figure 15) [128].

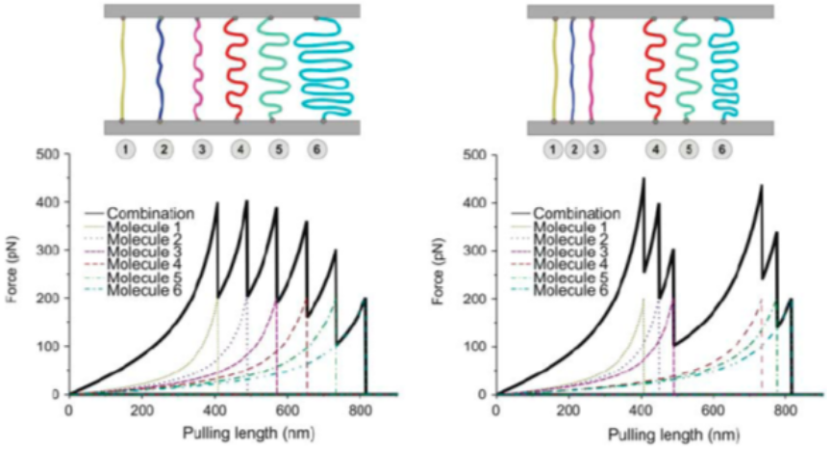

Figure 15: The left side shows the extension curves of molecules of different contour lengths before they are released or bonds break, as described by the Worm-Like Chain (WLC) model. The right side shows how the combined pulling of molecules. Reproduced from a PowerPoint presentation by Wuy Siev Tan, 2008.

However, when multiple bonds are present (right side Figure 15), the situation is not actually that simple, as they affect the shape of the other curves and, consequently, affect the parameters that are fitted to the stretching curves. In general, it is easier to avoid multiplicity of bonds to get good estimations of parameters of the bond [130, 131].

3.8.3 Probing the energy landscape of binding molecules

Some of the characteristics of the energy landscape can be found by studying an ensemble of molecular unbinding events in the presence of applied external force. While the height of the energy barriers is affected by external force, the positions of the transition states are not. Because the rupture events are stochastic processes, the quantification of the bond strength requires many measurements of individual bond rupture events. The interactions strength (f) is plotted against the logaritm bond loading rate (r_f); this should result in a linear relationship between the two. This distribution of points is then divided into k number of subdistributions, where k depends on the size of the dataset. Each subdistribution has a mean loading rate, $\langle r_f \rangle$. A histogram is fitted to each of the subdistributions (Figure 16) - this is called the Bell-Evans histogram plot, and a most probable force ($f*$) is found for each $\langle r_f \rangle$. To achieve a good estimate of the force-loading rate relationship, a big amount of data is needed. The $f*$ and r_f are related throught (Equation 2):

$$f^* = \frac{k_B T}{x_\beta} \ln\left(\frac{r_f x_\beta}{k_{off} k_B T}\right) \tag{2}$$

Where x_{beta} is the thermally averages distance from the complex-state to the transition state. k_B is the Boltzmann constant and T is the absolute temperature in Kelvin. r_f is the actual loading rate and k_{off} is the rate of dissociation.

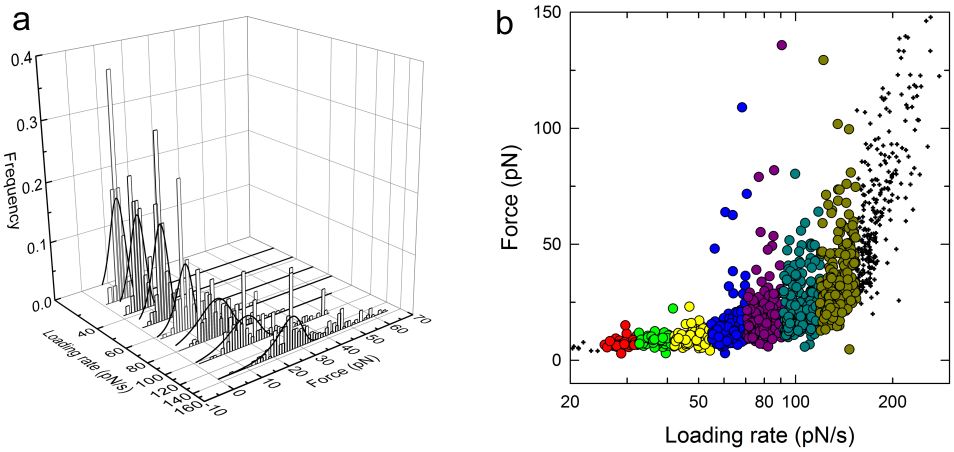

Figure 16: Example of histograms that have been fitted to subdistributions of loading rates. Reproduced from Hadjialirezaei et al, 2017 [132].

The resulting mean loading rate of subdistributions and most probable force can then be plotted against each other, and should result in a plot similar to that shown in Figure 17. This plot is called a dynamic strength spectrum. The left

side of Figure 17 corresponds to the energy landscape on the left in figure 14, and the right side should correspond to the right side of that figure. Thus, when a bond between a pair of molecules has several energy barriers, it will, according to the theory, yield a dynamic strength spectrum with multiple energy barriers, represented by discontinuous linear parts. Two transition steps means that there are two possible intermediates between bound and unbound state, and that two steps need to be overcome. The inner barrier is called the configurational state, while the second barrier is called the orbital or centrifugal state. Without any force applied, the outer barrier is the rate-determining barrier, but when force is applied, the outer barrier is driven below the inner by k_BT.

An important parameter here is x_β, which is the thermally averages distance from the complex-state to the transition state, or in other words: the characteristic bond length. It can be represented in Figure 14 as the distnce from the "c" well to the "ts" hill. The bond length is a parameter that tells something about the properties of the bond. Generally, a shorter length of the bond means than more electrons are involved in the binding, and that the strength of the bond is higher and requires more energy to break.

The x_β can be found through Equation 3:

$$f_\beta = \frac{k_BT}{x_\beta} \tag{3}$$

Where x_β, which is the thermally averages distance from the complex-state to the transition state. f_β is the force governed by the distance x_β. k_B is the Boltzmann constant and T is the absolute temperature in Kelvin.

Another Important parameter is k_{off}. Under a constant loading force (f), k_{off} - the rate of dissociation increases exponentially with the force (Equation 4):

$$k_{off}\left(f\right) = k_{off}\left(0\right) exp\left(\frac{x_\beta f}{k_BT}\right) \tag{4}$$

The $k_{off}\left(0\right)$ is the dissociation rate extrapolated to zero loading force. The rest of the parameters are described above. k_{off} again be used to find the lifetime of the bond, called $\mathcal{T}$ (Equation 5):

$$\mathcal{T} = \frac{1}{k_{off}} \tag{5}$$

Thus, by carefully mapping the dynamic power spectrum it is possible to map the energy landscape of a pair of interacting molecules, and even identify multiple interaction barriers, if such exist. It is also possible to find the thermal energy needed to break the bonds using additional equations, and equations for the probability of bonding forces exist, but this is not relevant to this work.

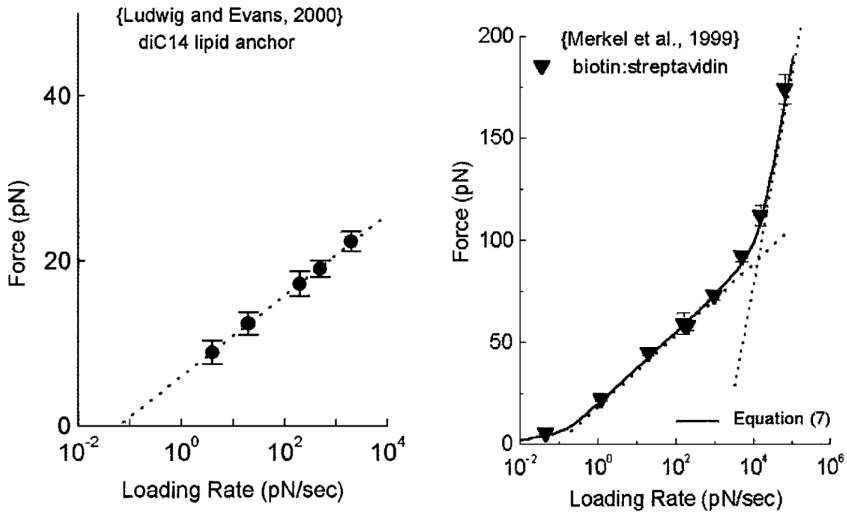

Figure 17: Dynamic strength spectra of two different molecules, one with a single activation energy barrier (left frame) and one with two barriers (right). The multiple energy barriers are represented by the discontinuous lines if the spectrum. Reproduced from Evans, 2001 [128].

3.9 Optical tweezers

The method of optical trapping was discovered by Arthur Ashkin in 1970. He found that micron-sized beads in a solution were propelled in the proparation direction of a high-powered laser with high speed. He noticed that beads were pulled into the path of the beam and accelerated forward. From this, he got the idea of trapping objects using light. In the first optical traps, objects were immobilized by using two opposing laser beams [133]. Later, it was discovered that it is possible to use a single laser beam for trapping, which is the method that is normally used today [134].

Objects that are small, mostly transparent, dielectric particles, can be held in place while forces and displacements of the objects are measured with high accuracy and sensitivity. [135]. When the object is small enough (<100 μm), the radiation pressure from a tightly focused laser beam can be used to trap the objects in three dimensions. This is achieven by using an objective with high numerical aperture, which focuses the light down to a small spot, or laser waist (Figure 18). The lasers are monochromatic, which means that they have a narrow range of wavelengths, linearly polarized and continuous. [136]. Optical tweezers have been used in various applications, like measuring the forces exerted by molecular motors [137], the elasticity of cellular membranes [138], forces required to unzip DNA [139], trapping and moving living bacteria and viruses with no apparent damage [140], and unfolding of proteins [141].

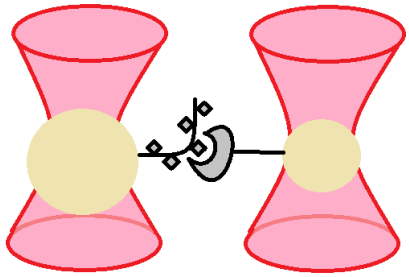

Figure 18: A schematic drawing of optical traps, which are created by tightly focusing a laser beam. Mostly transparent, dielectric object of size less than ca 100 um, with refractive index higher than that of the medium can then be held in place by the forces acting upon them by the laser. Here, two interacting molecules are stretched out between two trapped beads.

Most cells are possible to trap with a laser, given that they are not too small. When studying biological molecules, such as polymers, proteins, or even structures like viruses, these are all too small to be trapped by a laser directly. Instead, they are immobilized onto micro-spheres, which are of sufficient size. The microbead size used in optical tweezer experiments typically range between 10 nm and 4 μm (JPK technical note), and are often made of polystyrene [136].

In order to use a laser to manipulate objects, the objects must fulfil certain requirements. The refractive index (n) of the particle plays an important role, and an index of 1.2-1.3 is optimal, which is what polystyrene beads have in water (1.2). The object must have higher refractive index than the surrounding medium: objects with higher refractive indices, it will be trapped, while objects with lower refractive indices will be propelled forward, in the direction of the propagation of laser light [136].

Light is an electromagnetic wave. When light exerts force on matter, it is due to an electric field that exerts force on charges, and a magnetic field that exerts force on currents. For the particle to be trapped, it must be dielectric: made of a material that can be polarized in an electrical field, but has low conductivity. The laser beam used in optical tweezers has a Gaussian intensity profile, which means it is most intense at the center, with decreasing intensity the further out. When the particle is polarized and moves toward a highly focused laser beam, it will experience a gradient in the electric field. This causes it to be drawn to the region of greatest light intensity (in case of higher refractivity than the medium) laterally (in the X,Y-direction). It also experiences a scattering force, which pushes the particle in the direction of the propagation of the light (in the Z-direction) (Figure 19). The photons from the laser also exert a radiation pressure, which pushes the particle in the direction of light propagation. For the particle to be trapped, the gradient force must be greater than the scattering force and the radiation pressure from the

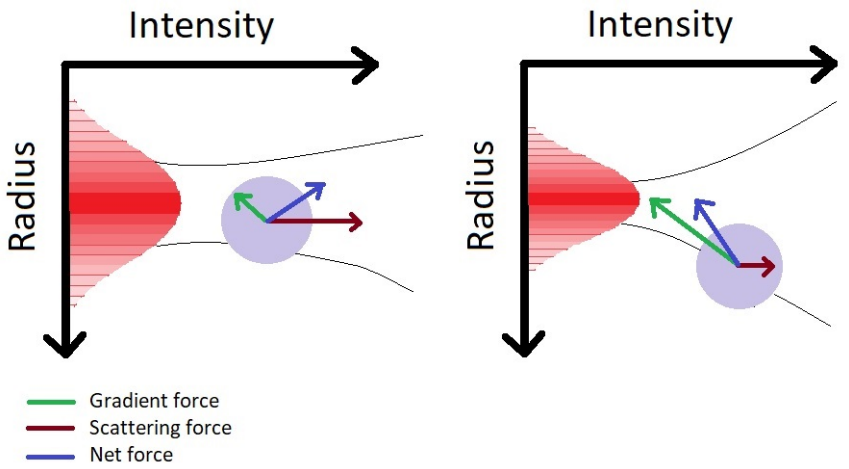

Figure 19: The forces acting on a bead in an optical trap; the radition pressure form the photons is not shown, but it acts in the drection of the propagtion of the laser (left to right). The Gaussian intensity profile of the trapping laser is illustrated in red. The curvature of the laser beam is marked in black, and shows that the beam on the right is more focused than the beam of the left. As is shown by the vectors, in the left case, the less focused laser will not be able to hold the beam, as the scattering force is greater than the gradient force. In the case on the right, the laser is more tightly focused, and the predominant gradient force restores the position of the bead towards the center of the optical trap.

protons [136].

Scattering force can often be excluded, as the laser is highly focused. The two remaining force components: the gradient force and the force of the radiation pressure create an equilibrium position for the bead trapped by the laser beam. This is in the center of the beam, slightly (100-500 nm, normally about 150 nm) behind the beam waist because of the radiation pressure. In a focused laser, the trapping volume has an eliptical shape. This is because there is better control of the laser focus in the lateral directions than in the axial, because of the diffraction limit of light, and according to Abbe's expression of axial and lateral resolution in optical microscopy [3] [136].

Lastly, for a laser to be able to trap an object, it must be sufficiently powerful to overcome other types of forces acting on the object, such as gravity, movement of surrounding liquid and other types of pushes-and-pulls the object might experience. If all of the other properties of an object are kept constant, and fulfils the requirements above, the greater the size of the particle, the more loosely it is held in the optical trap [136].

[3] http://zeiss-campus.magnet.fsu.edu/articles/superresolution/introduction.html

3.9.1 Principles behind force measurements

While it is impossible to measure the forces exerted by the laser directly, it is possible to use the light scattered by the trapped object to accurately measure external forces - other forces (than the trapping force) acting on the object. These forces pull or push the trapped object out of the center of the trapping beam, and can be for example the Brownian motions of the liquid around, collisions with other objects in the solution, or pulling forces generated by molecules connecting the surface of the trapped object to something else. The forces acting on the beads are calculated from the trap stiffness and the displacement of an object out of the trap center [1].

The trapping force of an optical trap with a Gaussian beam profile will behave similar to a spring, in that it will be linearly proportional to the displacement of the particle out of the beam center, up to a certain point (outside of the linear response area of the quadrant protodiodes). This follow Hook's law, that states that the force a spring will experience is linearly proportional to the distance it is stretched (or compressed) (Equation 6) [1]:

$$F = -kx \tag{6}$$

Where F is the force - in this case: the force a bead pulled out of the trap experiences. k is the spring constant of the trap, also called the trap stiffness - how strongly the optic trap is holding an object. k is the displacement distance of the bead out of the trap center. In the case of stretching a polymer, the force will not be negative, but an absolute value of the expression.

To find forces experienced by a trapped object, the spring constant k must be known. This is achieved by calibration of the optical traps. Calibration can be achieved in multiple ways, all of which are about finding the forces experienced by a particle when certain forces exerted on it are known [1]. One of the ways to calibrate the optical trap is to measure the Brownian motion of the trapped particle. Brownian motion that occur due to the diffusive movement of the fluid molecules in the sample, which act on the particle to a considerable extent because the relatively weak forces of an optical trap. The particle does not stand completely still in the trap, but can move around in the focal volume of the trap. Brownian motions can be determined, in one dimension at a time through equations 5 and 6 :

$$\langle x^2 \rangle = 2Dt \tag{7}$$

$$D = \frac{k_B T}{3\pi\eta d} \tag{8}$$

$\langle x^2 \rangle$ is the mean square displacement (distance) of the particle due to Brownian motion, D is the diffusion constant of the trapped particle, and t is the time. In the

equation for the diffusion constant, k_B is the Boltzmann constant - a fixed number. T is the absolute temperature (in Kelvin), which should be known by measuring the room temperature where the experiments are conducted, and adding a few degrees due to heating of the sample by the laser. η is the viscosity of the surrounding fluid medium, which can be retrieved from registers for viscosities of different fluids. d is the diameter of the trapped particle, which should be known to the researcher. From these parameters, it is possible to calculate the movement of the particle in all three directions. The positions of the particle are tracked by a quadrant protodiode (QPD), which is a detector that converts light lignals it receives (affected by the position of the particle in the trap) to a voltage [142, 143].

The thermal motion of beads in fluid is believed to follow a distribution that can be fitted the Lorenzian equation (Equation 9). The power-spectrum of the Brownian motions of the particle, held by an optical trap with stiffness κ are thus fit to this equation [143]:

$$S\left(f\right) = \frac{k_B T}{\gamma \pi^2 \left(f_c^2 + f^2\right)} \tag{9}$$

$S(f)$ i the function for the Lorenzian power spectrum (Figure 20), γ is the viscous drag coefficient, which can be found through rearrangement of equation 10 [143]:

$$F = 3\pi\eta dv = \gamma v \tag{10}$$

As a result, it is possible to find the characteristic roll-off frequency of the power spectrum, f_c (Equation 11) [143]:

$$f_c = \frac{\kappa}{2\pi\gamma} \tag{11}$$

f_c is used to find the stiffness of the optical trap, κ. The stiffness of the trap gives the conversion factor from displacement to force, as shown in equation. To get the measurement of forces, the signa from the QPD, is multiplied with the sensitivity (β) constant of the trap, which yealds a change in position of the bead. This is again multiplied wth the stiffness of the trap to get the force measurement.

Often, it is possible to change the stiffness of the traps by varying the laser power of the trap. There is a trade-off between increasing stiffness and sensitivity of the optical traps, as one decreases as the other increases. By having a stiffer trap, the sensitivity decreases - the trap will no longer be as sensitive for small changes in the position of the particle. Thus, a weaker trap is better at measuring small forces because the bead will be affected by them (pulled out of the trap center) easier. The minimum force that can be measured is then dependent on the trap stiffness. At a given radius of the beam waist, the trap stiffness is highest for particles with the same radius. When the radius of the particle is smaller, the restoring force will have a rapid decrease, but a particle that is bigger in radius will have a much lower decrease in restoring force [1].

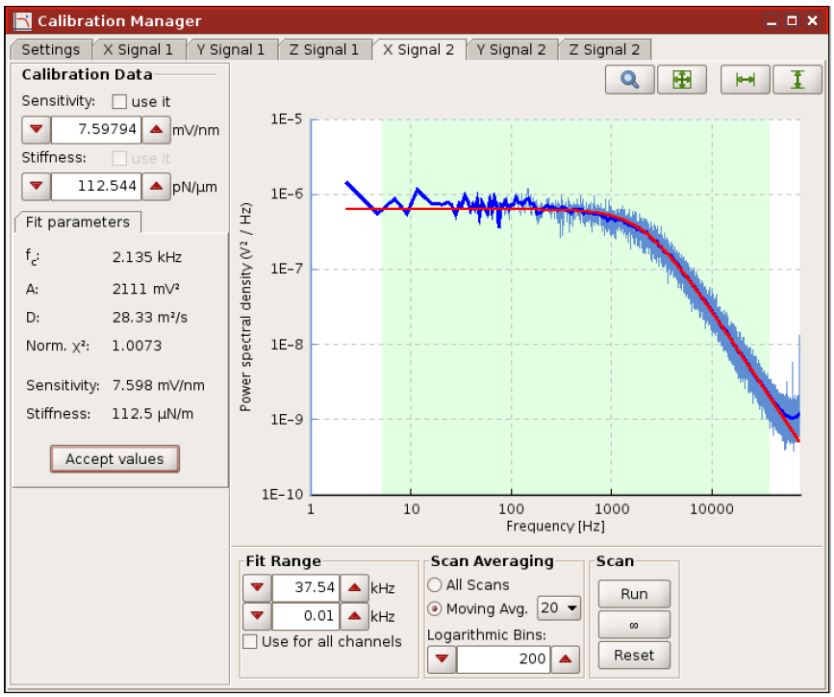

Figure 20: A screen print of the calibration procedure in the program NanoTracker 2, which is used to control the optical tweezers from JPK. The blue curve are the sampled frequencies of the Brownian motions of a trapped particle. The red curve is the Lorenzian power spectrum function, fit to the sampled data. As seen from the tabs, this is the calibration of movements of the particle in trap 2, in X-direction. The frequency at which the curve bends downwards is called the corner frequency, and is used to find the stiffness of the optical trap (N/m)). This fit of the Lorenzian power spectrum is also used to find the sensitivity (m/V) of the measurements. Both of these measuremens can be seen at the left-side panel of the window, together with information about how good the fit is. The figure is reproduced from JPK Technical Note for Optical Tweezers, "Characterizing quantitative measurements of force and displacement with Optical Tweezers on the NanoTracker".

4 Materials and methods

4.1 The set-up of the JPK optical twezers

The optical tweezers used in these experiments are NanoTracker from JPK (Figure 21), integrated with a Zeiss Axio Observer Inverted optical microscope. The instrument is kept in a temperated room with a constant temperature of 23 deg C. To dampen vibrations, the instrument is placed on a vibration isolation table. The schematics of the set-up is shown in the figure below. The TEM_{00} trapping laser has a power of 3W, with the option of tuning, a wavelength of 1064 nm, with a Gaussian beam profile. The laser beam is controlled by galvanic mirrors in the X and Y directions. To get the two traps used in the experiments, a polarized beam splitter with a tunable split-ratio is used. The two traps can be controlled independently.

The sample chamber (described later in the methods) is mounted onto a sample holder, which is placed inside the instrument. The sample holder can be moved in the lateral directions by a motorized sample position system. The trapping and detection objectives are both water-immersion objectives with 63x magnification and 1.20 numerical aperture. A LED light source illuminated the sample, and the sample was imaged with a CCD camera, with a 1064 nm laser reject filter.

The position of beads in the traps is detected by back focal plane (BFP) interometry, by quadrant photodiods. The movement of each of the two beads is detected in the X,Y-direction, and another photodiod is also used to detect the position in the Z-direction, to increase the Z-sentsitivity.

To reduce the vibrations due to movement in the building, the optical tweezers were stationed atop of an air vibration isolation table.

NanoTracker 2.0 software was used to record the results, which could later be revisited in the Analyzer software, which visualized the force-curves obtained for both beads in three directions separately. The software is available for computers with the Linux operative system.

4.2 Preparation of the liquid cell

A liquid cell is a closed chamber that was used to study polymer-covered polystyrene beads in solution. Circular coverslips (30 mm diameter, thickness number 1) were overlaid with a solution of BSA (1 mg/mL in MilliQ water, filtered using 0,2 μm Acrodisc Syringe Filter from Pall Corporation) for about 15 minutes, washed lightly with MQ-water and dried with N_2 gass. This method was found to be an effective way of preventing polystyrene beads from sticking to the surface of the glass by Kristin Elisabeth Haugstad, during her work on her Master thesis at the Department of Physics at NTNU. To prevent excess of BSA from dissolving in the solution that was to be applied to these glasses later, it was decided to wash the glasses lightly with destilled water before drying them. The glasses were stored BSA-side up, without stacking them to avoid affecting the BSA-layer. Glasses could be stored in room temperature for several weeks, in closed petridishes, but were washed before

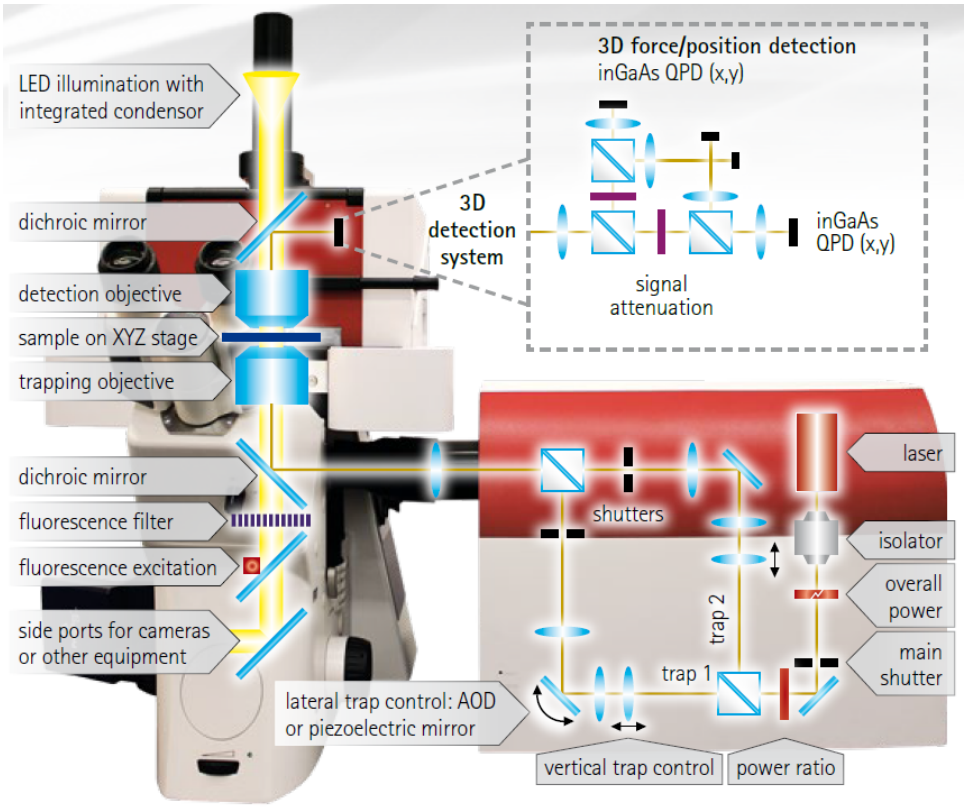

Figure 21: A schematic diagram of the JPK NanoTracker Optical Tweezers [144].

use. Some molecules still bound strongly and rapidly to the BSA-layer and made taking measurements difficult. A different way to solve the problem is to attach molecules onto smaller beads instead.

The liquid chamber (Figure 22) for the sample was prepared right before a sample was ready to be studied. Small pieces of double-sided tape were used to create a narrow passage (about 4 mm wide), at the center of the glass. A 20 x 50 mm coverslip (thickness number 1) was placed on top, to create the channel of the liquid cell. Such a coverslip was found to be a good choice to stabilize the liquid chamber inside the sample holder. About 6-8 uL of sample was sufficient to fill the channel. A drop of sample was placed at one end of the channel and dragged into the liquid cell by capillary forces. The volume of the liquid chamber was 5-8 uL. The chamber was sealed using nail polish to prevent the sample from drying out during measurements.

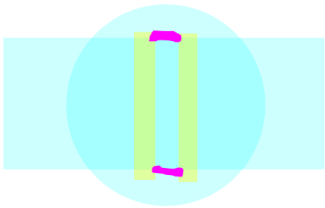

Figure 22: A liquid cell, composed of a circular cover glass and a rectangular cover glass, held together by two strips of sticky tape (yellow). The sample is applied in the passage made between the double-sided tape and dragged into the chamber by capillary forces. Nail polish (pink) is used to seal the cell on both sides, after the loading of sample.

4.3 Calibration, measurements and analysis of the results

4.3.1 NanoTracker Control Software

NanoTracker is the software used to record unbinding forces. This software calibrates the parameters needed for finding the force of the interactions (see section 3.9.1). The calibration is done by the NanoTracker software that is a part of the JPK NanoTracker optical tweezers platform. The user needs to know how to operate the software, and be able to evaluate whether the fitted calibration curve for the power-spectrum is sufficiently good. If the sampled frequency data (Figure 20) has big deviations from the calibration curve, the causes might be that the trapped particle is not perfectly spherical or might be stuck to something hindering its motion. A new particle should then be chosen.

First the instrument is turned on, followed by the software (see Guide Manual). Due to the time it takes (1 - 2 hours) for the laser power to stabilize, the instrument was left running for this time, and measurements did not begin prior to the stabilization of the laser.

The sample was prepared, loaded into the liquid chamber (Figure 22), and added immersion oil from Zeiss with refractive index 1.67, provided by a JPK representative, to be used with this specific optical tweezer setup. When a sample was loaded into the optical tweezers, the first step is to adjust the trapping and detection objectives to get the sample in focus. Then the microscope was adjusted to Köhler illumination, which is when both the sample and the blender are in focus. After this, two beads were trapped using the lasers.

The power of the laser was set to maximal force (3W), with the power equally distributed between the two traps, even though this meant that two beads of unequal size would be trapped with different force. All of the measurements were done at room temperature, which should be 21° C. As the laser will always heat the liquid chamber slightly, the temperature for calibration of the trap stiffness was set to 25° C. Viscosity was set to 0,890 mPas. The fit range was 30.00 -0.01 mPas, and the exclusion range was 20.00 kHz - 0,20 kHz.

Beads that were picked had to have a completely spherical shape and the correct size, determined visually, based on what looked like the most common size (Figure 28) . If the size of a bead stood out from what appeared to be normal, a different bead was trapped. No visible particles or filaments should be seen stuck to the bead. The beads that were trapped with the laser were lifted about 2-4 μm above the bottom of the sample chamber in order to prevent them from being affected by the BSA-layer on the glass, and to make sure that molecules on the bead were not and could not be attach to the glass surface.

The height of the beads was adjusted in the Z-direction so that they were in the same plane. This was done by monitoring the change in their contrast as they were moved up and down in the z-direction. When beads are in the same plane, they have equal contrast. After this, the beads were placed on a line in the x-plane, which would be the direction of the the approach-retract movement. It was chosen to always have the smallest bead (when two different sizes were used) in trap 1, which would be the trap that would be moved back-and-forth during measurements. The optimal inter-bead distance will vary depending on how far polymers are able to extend from the surface of the bead, and how strong the measured forces can be. Generally, beads were kept 1-2 μm apart during these experiments. It is advisable to not have an unreasonably large inter-bead distance, as larger distances will generate bigger files that take longer to process later on.

Next, the detector response was set to image the bead in the center of the QPD, which is achieved using the NanoTracker 2.0 software (Control $\rightarrow$ Offset correction $\rightarrow$ mark both traps and press the "Trap 1" and "Trap 2" buttons). To ensure good results, it is necessary to calibrate the stiffness and sensitivity of the optical traps every time new beads are caught. The stiffness and sensitivity of the traps were calculated by fitting the Lorenzian function to the measured power spectrum of Brownian motions of the particles. The motions of the particles is measured and calibrated one particle at the time, in X, Y and Z directions separately. The Brownian motions were recorded for 9 seconds, as this results in less noise than recordings for 5 seconds, which is the default for this instrument. The recorded spectrum did not seem to improve beyond that. The calibration of stiffness and sensitivity is found by the software, by calculating the corner frequency, or roll-off frequency, of the fitted Lorenzian power spectrum. The fit suggested by NanoTracker's online calibration manager was most often used as it was sufficiently good.

Among the parameters that are possible to vary is the speed of approach and the hold-time (dwell time). In almost all of these experiments, a speed of 1 μm/sec was used, with a dwell-time of 1 sec. The dwell-time was added to increase the interaction frequency. The force beads are pressed together is also an important variable. In these experiments, a pressing power of what could be estimated to 4-10 pN was used for most of the experiments. The beads had to be in contact, but not be pressed so hard together that it lead to an easily observable displacement from the trap center. After this, the measurements began.

The force curves were recorded using the JPK NanoTracker software. The resulting files were in the format "force-save-YYYY.MM.DD-hh.mm.ss.jpk-nt-force".

4.3.2 Analyzer visualization software

The files can be viewed in the Analyzer-program from JPK. This software visualizes force curves for each of the beads in all three directions, separately. Using this program, files were manually sorted into two categories: curves with or without force jumps. Files were sorted into folders according to the system studied (i.e: MUC1-Tn - self), the date the measurements were done, the number of the bead pair that was studied. The size of the beads, speed and dwell time was noted. The desired number of retract-approach-curves was recorded for many types of different bead pairs.

4.3.3 Conversion of .jpk-nt-force force files to .txt files

Curves of interest - mainly curves with force jumps, were converted using software from JPK, available for Linux. This generated ".txt"-files, with information about the values of parameters for both beads, as well as their stepwise position in X, Y and Z-directions.

4.3.4 iNanoTrackerOT3DPreProcess2.pro

In this study, the software of choice was IDL Data Visualization Software, with programs written by Bjørn Torger Stokke, Professor at the Department of Physics at NTNU. The first program, iNanoTrackerOT3DPreProcess2.pro, integrated the information about the forces in the X, Y and Z positiond for both of the two beads, and generated a single position-coordinate. As there is displacement of both of the beads when they interact, this change was combined into a single force-value using the Equations 12 and 13:

$$\Delta F = F(retract) - F(approach) \tag{12}$$

$$\sum F = \Delta Fx + \Delta Fy + \Delta Fz \tag{13}$$

Finding $\sum F = \Delta$ for both beads and adding them generated a combined curve of the forces. This also evened out the baseline of the approach-retract-curves and gave a horizontal baseline. This generated a new ".txt" file, which was further processed with iNanoTrackerOT3DPostProcess2.pro.

Recently, JPK made a change in their NanoTracker software, which is not compatible with iNanoTrackerOT3DPreProcess2.pro, so iNanoTrackerOT3DPreProcess3.pro must be used for conversion of some of the files, recorded in May 2017.

4.3.5 iNanoTrackerOT3DPostProcess2.pro

iNanoTrackerOT3DPostProcess2.pro was written by Bjørn Torger Stokke. This program plotted the generated force curve, and let the user manually fit the slope of the loading rate (r_f) to the curve, according to Equation 14:

$$r_f = \frac{\Delta y}{\Delta x} = \frac{\Delta f}{\Delta d} \tag{14}$$

The estimation of the unbinding force was done by the program by fitting a vertical line from the baseline to the force jump. The vertical line would only be fitted well to a coherent vertical line. An example of these estimations can be observed in multiple figures in the result section. The force and loading rate estimations were written to a "out.txt" file.

4.3.6 iNanoTrackerGallery.pro

This software was used to generate galleries of interactions. It imports a selected number of "out.txt" files and lets the user vary the degree of smoothing, distance between force jumps and length of the baseline. It generates a ".txt" file with parameters of datapoints of force vs. distance for the force jumps.

4.3.7 SigmaPlot

All figures depicting DPS, histograms and galleries of force-jumps were generated using SigmaPlot mathematical and statistical software.

4.3.8 Energy landscape parameters - unconstrained and constrained fit

This analysis was conducted by Marit Sletmoen, by employing ForceLifetimeFit.pro software developed by Bjørn Torger Stokke. The software calculated the most probable unbinding force and mean loading rates for the loading rate intervals, according to the theory in Section 3.8.3. This is called the unconstrained fit. It is possible to estimate a better fit for the data, according to the predicted probability function (Haugstad et al., 2015[145], and supplementary material). If the Bell-Evans relation for the data is good, the values of these parameters should be close to the values of the parameters for the constrained fit.

4.4 Chemicals used in the experiments

Chemicals purchased from Sigma Aldrich:

HEPES (4-(2-Hydroxyethyl)piperazine-1-ethanesulfonic acid)), >99.5% (titration-grade). Molecular Weight 238.30 g/mol. Useful pH range: 6.8 - 8.2. CAS Number 7365-45-9.
Boric acid (H3BO3). BioReagent, for molecular biology, suitable for cell culture, suitable for plant cell culture, >99.5%. Molecular Weight: 61.83 g/mol. CAS Number 10043-35-3.
Calcium chloride ($CaCl_2$ 2H2O) dihydrate, for molecular biology, >99%. Molecular Weight: 147.01. CAS Number: 10035-04-8
Manganese(II) chloride tetrahydrat (MnCl2 4H2O). Molecular Weight 197.91. CAS Number: 13446-34-9
Bovine Serum Albumin (BSA), lyophilized powder, BioReagent, suitable for cell culture, >96% (agarose gel electrophoresis). CAS number: 9048-46-8.
Phosphate-buffered saline tablets. One tablet in 200 mL water resulted in a 137 mM NaCl, 2.7 mM KCl and 10 mM phosphate buffer solution (pH 7.4 at 25 ° C). MDL number: MFCD00131855.
EDC (1-ethyl-3-(3-dimethylaminopropyl)carbodiimide hydrochloride) (abbreviated as EDC). Chrystalline. CAS Number: 25952-53-8.

4.5 Samples

4.5.1 Mucin experiments

The samples of naked MUC1, MUC1-ST, MUC1-T, MUC1-Tn and MUC1-STn were kindly provided by Gianofranco Picco, rasearcher of glyco-oncology at King's College in London.
Unglycosylated MUC1-was expressed in CHO-K1 (Chinese-hamster ovary K1) cells. This mucin was created by fusing murine IgG2a Fc domain and an enterokinase clevage site to the MUC1 using PCR and amplifying the sequence in *Escherichia coli* XL10 Gold using as plasmid. CHO-K1 cells were transfected with the plasmid and selected based on the highest expression of the MUC1-IgG protein into the culture medium. SDS-PAGE followed by western blotting with 3 antibodies that can detect MUC1 tandem repeat. The binding of the antibodies is affected by glycosylation, and thus, the affinity of the antibodies indicate the glycosylation status of the protein [146].
MUC1-ST was expressed from CHO-K1 cells were the expression system for these mucin. The protein contains the who ECD of MUC1, including 16 MUC1 tandem repeats, with murine IgG Fc and an intervening enterokinase cleavage site for the removal of the Fc tail. The CHO-K1-cells shed the protein into the cell culture medium. The protein was purified using a two-step procedure: clevage at the enterokinase cleavage site and purification using ion exchange chromatography. Liquid capillary chromatography followed by MS analysis revealed that the main O-glycans on this MUC1 were T-antigen (Galβ1-3GalNAc, core 1) and mono- and

disyaliated T-antigen. On average, 4.3 of the 5 available glycosylation sites on each MUC1 tandem repeat were occupied, determined by nano liquid chromatography - MS. The procedure for production and purification is described in Beckstrom et al., 2003 [147].
MUC1-T was prepared from the MUC1-ST (decribed above) by treatment with neuraminidase. Another sample of the same mucin was made, where the IgG-domain was cleaved off [147].
MUC1-Tn and MUC1-STn was prepared as described in Beatson et al., 2015 [41]. The two mucins were produced in wild-type CHO cells that were were previously transfected with human MUC1 with IgG2a Fc fusion construct [147] (16 VNTR tandem repeats), were transfected with the gene for ST6GalNAc-I. Clones that expressed MUC1 were cultured in serum-free medium in biorectors [146]. The MUC1-protein was filtered and concentrated from the serum, and the Fc-region was cleaved off using enterokinase enzyme. MUC1-Tn and MUC1-STn was purified using affinity chromatography. Concentration and purity was determined by amino acid analysis.
Several different mucin samples were provided by Thoman Gerken at Case Western Reserve University. Unfortunatly, there was only time to work with TR-PSM H8-I in these experiments. TR-PSM H8-I is a porcine submaxillary mucin (PSM), that has been reduced and trypsinated. The high MW fractions (peak 1) were collected after gel filtration on Superdex 200. The composition of the glycosyltion pattern is 31, 17, 12, 40, 41 : mono, di, tri, tetra, NeuNGl. This is a natively fully glycosylated mucin, with a complex glycosylation pattern. This sample is similar to Fd-PSM, used by Kristin Haugstad earlier [145], and prepared like described in Tom Gerken's article about determination of the O-glycosylation pattern, from 1997 [148].
Human recombinant MGL/CLEC10A was ordered from R&D Systems (Cat. number 4888-CL-050). Expressed from a mouse myeloma cell line, NS0-derived Gln61-His316, with an N-terminal 6-His-tag, which was used for affinity purification. Predicted Molecular Mass: 29.6 kDa. SDS-PAGE: 40-43 kDa, in reducing conditions.

4.5.2 PAA-experiments

To attempt to study how the density of Tn-antigen affects the intraction forces and frequency, a polyacrylic acid (PAA) polymer with two different densities of Tn were used: PAA-450K-10 and -40. 450K refers to the molecular weight of the polymer in Daltons, and the last number represents the percentage of Tn-substituted carboxyl groups. The samples were kindly provided by Xuefei Huang, Professor in Chemistry at Michigan State University, USA.

To study the role of the C4 OH-group and the C2 N-acetyl group of the Tn-antigen, PAA, which is here poly[N-(hydrohyethyl)acrylamide, with different sugar moieties were ordered from Lectinity. The PAA chains had a molecular mass of about 30 kDa, according to gel filtration, where protein was used as a marker for the molecular mass. The carbohydrate content was 20% mol. The PAA had 5% mol biotin label for easy immobilization only streptavidin-coated polystyrene beads. The product arrived as dehydrated polymer. To assess the functionality of

the C4 OH-group, PAA-GalNAc (GalNAcb-sp3, Cat number 0031-BP and PAA-GlcNAc (GlcNAcb-sp3, Cat number 0029-BP) , which are epimers, were ordered. To assess the importance of the N-acetyl group, PAA-Gal (Galb-sp3, Cat number 0024-BP) and PAA-Glc (Glcb-sp3, Cat number 0022-BP) were ordered, which have an N-acetyl group instead of an OH-group. For the control experiments, PAA-$HOCH2(HOCH)4CH2NH_2$ (Cat number 0000-BP) was used.

4.5.3 Fumonisin-experiments

Fumonisin B1 from *Fusarium moniliforme* was ordered from Sigma Aldrich, in powder form, and dissolved in acetonitrile, for storage in freezer (see Product Information Sheet from SigmaAldrich). CAS number: 116355-83-0.

Laminarin and mannan was purchased and modified to have amino groups, by Marit Sletmoen, professor at the Norwegian Institute of Science and Technology (Norges Teknisk-Naturvitenskapelige Universitet, NTNU), so it could be bound to surfaces with carboxyl groups. Laminarin is an algeal β glucan.

Chitosan and mannan was prepared by Marianne Dahlsbråten, at NTNU. The chitosan had an FA=0.69 and (n)=771 ml/g.

Two types of yeast cells were used in this work. Wild type yeast wild strain BY4741a, and an mnn9-mutant, with a mutation in a gene encoding a protein for mannan synthesis in the cell wall. Both of the strains were supplied by Marion Schiavone, PhD at INSA, Tolouse. The yeast were grown by Åshild Samseth, as described in her Master's Thesis (samseth2016immobilisering). One yeast colony was incubated in 25 mL of yeast peptone dextrose (YPD) at 30 ° C in an incubator, at 250 rpm. The YPD medium consisted of 10 g/L yeast extract, 20 g/ bacterial peptone and and 20 mg/L glucose, in destilled water. The medium was autoclaved for 20 minutes, at 120 ° C.

Limited information is available on the preparation of some of the biopolymers above. These substances were provided by Marit Sletmoen at NTNU. For additional information contact her directly.

4.6 Protocol for preparation of the samples

Optical tweezers were used to measure the binding forced between sets of two different molecules, immobilized on polystyrene beads (SPHERO Tm Carboxyl/Amino Polystyrene Particles, 5 % w/v), functionalized with either carboxyl or amino groups, respectively. The functional groups are located on the surface with alkyl linker arms. The content of functional groups is different for the two types of beads, with amino-functionalized beads having about 1/3 as many as the carboxyl-functionalized. The refractive index of the beads is 1.59. when experiments where the interactions between two different polymers were probed, different sizes of beads were used to recognize beads with different molecules.

Prior to using the beads, they were washed with 200 uL MilliQ water, centrifuged at 6000 rpm for 1 min, and the water was removed. This was done to remove the storage-buffer the beads are kept in, which contains PBS, sodium azide and BSA

[4]. Because the reaction with EDC is executed in unbuffered boric acid, even small amounts of PBS buffer can alter the pH.

The immobilized molecules were covalently attached to the beads in a chemical reaction using (1-ethyl-3-(3-dimethylaminopropyl)carbodiimide hydrochloride), also called EDC or EDAC. EDC activates the conjugation of carboxyl groups to primary amino goups, and is called a "zero-length carboxyl-to-amine cross-linker" because no part of it is incorporated into the cross-bond between the reacting groups. The reaction product of EDC is isourea (Figure 23) [149]. The reaction was conducted in a solution of boric acid (50 mM, pH 5.8, prepared by Gjertrud Maurstad), filtered using Sterile Acrodisc 0.2 μm Supor Membrane 32 mm syringe filters, from Pall Corporation, REF: 4652. The boric acid provided the correct pH for the reaction to take place. The concentration of molecules was varied in different experiments according to the goal of the measurements and the types of molecules used. The samples were incubated for 40 minutes.

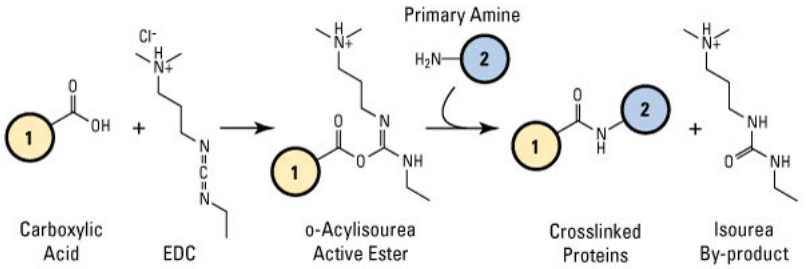

Figure 23: The crosslinking reaction with EDC, which has the ability to create covalent bonds between amino- and carboxyl groups. EDC is a zero-length crosslinker, which mens it does not incorporate itself into the product. The reaction product is isourea.

After the incubation, the samples were centrifuged for 1 minute at 6000 rpm. The speed and time was chosen because 1 minute is the shortest centrifugation cycle, and 6000 rmp was the smallest speed needed to sediment the beads. Such a low speed and short time was chosen to avoid pressing the beads together for too long, in case this might somehow affect the proteins immobilized on them. As much of the supernatant as possible was removed to get rid of the unreacted EDC, isourea, free mucin and boric acid.

The sample was then washed with HEPES (described below) to ensure that as much of the above-mentioned chemical were removed. 200 uL was the chosen volume used because it was close to the maximal volume that could be used - at higher volumes it was very difficult to concentrate the beads by the chosen centrifugation speed and longevity. The washing was repeated twice, and consisted of re-suspending the beads in HEPES, centrifuge the sample at 6000 rpm for 1

[4]http://www.spherotech.com/technical%20notes/comptrol%20STN-18.pdf

minute, remove the supernatant, and repeat the whole process. Finally, the sample was diluted in an appropriate amount of HEPES, which is usually 300-500 uL, when the samples are made as described below.

It is highly recommended to filter the boric acid and HEPES about every week or two. As time goes by, the solutions were found to accumulate contamination that may interfere with the measurements and constitute a source of error. Some of the contaminants were visuble under the microscope, but some might be impossible to see, but might sometimes be pulled into the optical traps or stick to the beads.

4.6.1 Preparation of HEPES-buffer

HEPES (4-(2-hydroxyethyl)-1-piperazineethanesulfonic acid) is a buffering agent commonly used in cell-culture studies because of its good buffering capacity with changing CO_2-concentrations, compared to bicarbonate buffers.

Two different buffers were used under the experiments. Far most of the samples were studied in buffer number 1:
1) 100 mM HEPES with $MnCl_2$ (1 mM) and $CaCl_2$ (1 mM), pH 7.2
2) 10 mM HEPES, pH 6.9

The HEPES-buffer was made with MilliQ water. The starting pH of MilliQ water is about 5.5, which is normal, and varies depending on how much CO_2 is dissolved in the water. When preparing HEPES it is important to first dissolve the HEPES in the water and then adjust the pH. 10 mM NaOH was used for pH adjustment because of the strong buffering capacity of HEPES. The salts should be added as the last step. If the salts are added before the pH is adjusted, high local pH results in the precipitation of $Mn(OH)_2$ salt (brown colour), which has low solubility at the pH and temperature of the working conditions. If the salt is added before the pH is adjusted, it will be filtered out in the nest step; the buffer was filtered using Sterile Acrodisc 0.2 μm Supor Membrane 32 mm syringe filters, from Pall Corporation, REF: 4652.

HEPES has earlier been found to react with organic compounds when exposed to light, which lead to the production of hydrogen peroxide (HOOH) [150, 151, 152], and the buffer was thus exposed to light the least possible amount by wrapping the container in aluminum foil and keeping it in a refrigerator. This also means that after samples are prepared they might accumulate hydrogen peroxide over time, which might limit the time they should be used. Thus, samples were kept in dark conditions as much as possible. This might be of much higher importance when working with cells, but as the chemistry of the buffer was not inverstigated further, caution was exhibited just in case.

4.6.2 Ingredients for MUC1- and PAA-450K-coated beads

This is the protocol used for making samples for experiments with MUC1, MUC1-T, MUC1-Tn, MUC1-ST, MUC1-STn, TR-PSM-H8. For almost all of the experiments, protocol 2 (below) was used.

Two different protocols were used during the experiments: one with higher concentration of all of the reactants, and one with lower. The latter was an attempt to conjugate the molecules to the beads at fewer points, in order to try to achieve interactions a greater distance away from the bead surface. As this did not seem to work, it is suggested that protocol 1 be used if it is desirable to repeat these experiments. For one reaction mixture, either 1 uL of polystyrene beads with diameter of 2.01 μm was used, or 2 uL of beads diameter of 3.36 μm. Both sizes of beads were used for all of the mucins, but 2um size beads are recommended whenever possible, especially for polymers that sticks strongly to the surface of the liquid chamber.

Protocol 1	**Protocol 2**
50 uL boric acid (50 mM, pH 5.8)	200 uL boric acid (50 mM, pH 5.8)
Polystyrene particles of desired size	Polystyrene particles of desired size
0.2 mg/mL mucin	0.05 mg/mL mucin
2-3 mg/mL EDC	2-3 mg/mL EDC

Normally, 2 mg/mL EDC was used, but when it was expected that the EDC was losing its effect, more was used. The washed beads were mixed with the mucin. The EDC and boric acid was mixed to the desired concentration immediately before it was to be added.

4.6.3 Ingredients for MGL-coated beads

50 ug MGL was reconstituted in 250 uL sterile PBS, to a concentration of 0,2 mg/mL. PBS was purchased from SigmaAldrich. One tablet dissolved in 200 mL of deionized water yields 10 mM phosphate buffer, 2.7 mM KCl and 137 mM NaCl, pH 7.4. The solution was immediately divided into batches enough for on sample preparation and stored in the freezer at -20° C. MGL solution can be stored in the freezer for up to 3 months after reconstitution. All of the experiments using MGL were executed in 10 mM HEPES-buffer without $MnCl_2$ (1 mM) and $CaCl_2$.

MGL-coated beads
50 uL boric acid (50 mM, pH 5.8)
3 uL carboxyl-functionalized polystyrene beads, 2.10 μm
3 uL 0.2 mg/mL MGL in PBS
0.2 mg EDC (4 mg/mL)

4.6.4 Ingredients for PAA-450K-coated beads

Two different PAA-polymers were used in these experiments: PAA-450K-10 and PAA-450K-40. PAA-450K is a polyacrylic acid polymer with molecular mass 450 kDa, with 40% of its carboxylic acid groups substituted with GalNAc. The polymer will be immobilized to amino-functionalized beads by the carbocyl groups, available along the whole polymer. The samples were provided in dehydrated form, and

dissolved in PBS, to a concentration of 2 mg/mL. The PBS used was purchased from SigmaAldrich. One tablet dissolved in 200 mL of deionized water yields 10 mM phosphate buffer, 2.7 mM KCl and 137 mM NaCl, pH 7.4. The solution was stored in a refrigerator at 4° C.

PAA-450K-coated beads
50 uL boric acid (50 mM, pH 5.8)
3 uL amino-functionalized beads, 3.36 μm
7.5 uL 2 mg/mL PAA-450K-x (x = percentage of Tn-substitution) in PBS
0.2 mg EDC (4 mg/mL)

For further studies, it would be advisable that these polymers would be dissolved in boric acid, in order to avoid changing the pH of the boric acid during immobilization.

4.6.5 Ingredients for PAA-GalNAc/-Gal/-GlcNAc/-Glc-coated beads

PAA-GalNAc/-Gal/-GlcNAc/-Glc/without carbohydrate was purchased from Lectinity, and was dissolved in HEPES (100 mM in MilliQ water, with $MnCl_2$ (1 mM) and $CaCl_2$ (1 mM), pH 7.2), to a concentration of 2 mg/mL. PAA is poly[N-(2-hydroxyethyl)acrylamide], and has about 20% mol carbohydrate content, and about 5% biotin-label. These polymers were immobilized onto streptavidin-functionalized beads, using the following procedure:

PAA-coated beads
5 uL PAA-x, 2 mg/mL in HEPES (x = percentage subsitution with Tn)
2 uL streptavidin-functionalized beads, 3.05 μm
195 uL HEPES (100 mM in MilliQ water, with $MnCl_2$ (1 mM) and $CaCl_2$)

In these experiments, the beads were much more heavily coated with polymer as the concentration of beads-to-polymer was about 10 times higher, as the bead dilution was 10 times higher than in all other experiments. This made it impossible to wash the beads after the immobilization of polymer.

4.6.6 Ingredients for samples for fumonisin-experiments

Before immobilizing the polymers onto beads in these experiments, the beads were dissolved in 200 uL MilliQ water, centrifuged at 6000 rpm for 1 minute, and the supernatant was removed before the polymer was added. The incubation was done with sonification to distribute the molecules more evenly in the solution. Otherwise, the molecules tended to aggregate in solution, and the beads tended to clump together.

Mannan-functionalized beads
7.5 uL mannan (7 mg/mL) in acetic acid (1 M)
2 uL carboxyl-functionalized beads, 3.07 μm
0.6 mg EDC
200 uL boric acid (50 mM, pH 5.8)

Laminarin-functionalized beads
10 uL laminarin (1 mg/mL) in acetic acid (1 M)
2 uL carboxyl-functionalized beads, 3.07 μm
0.6 mg EDC
200 uL boric acid (50 mM, pH 5.8)

Kitosan-functionalized beads
10 uL kitosan (5 mg/mL) in acetic acid (1 M)
2 uL carboxyl-functionalized beads, 3.07 μm
0.6 mg EDC
200 uL boric acid (50 mM, pH 5.8)

Fumonisin-functionalized beads
10 uL fumonisin (5 mg/mL) in acetic acid (1 M)
1 uL amino-functionalized beads, 2.01 μm
0.6 mg EDC
200 uL boric acid (50 mM, pH 5.8)

4.7 Control experiments

To exclude the possibility of interactions between the beads themselves, amino-functionalized and carboxyl-functionalized beads were tested for interactions. This was performed in water, and also after treatment with the same chemicals that beads with immobilized molecules go through. The process involved incubating the beads with boric acid and EDC for 40 minutes, centrifuging the beads at 6000 rpm and removing the supernatant. The beads were then washed twice with HEPES-buffer, with centrifugation and removal of supernatant as previously, and finally, resuspension in an appropriate amount of HEPES. Sch beads will from now be referred to as "non-coated beads".

To ensure that the breaking bonds that were to be observed were due to binding between polymers of interest, control experiments were conducted. Beads that had been treated with everything except the polymer of interest were probed with. Both amino- and carboxyl-functionalized beads were tested against themselves and each other in water, boric acid and EDC, HEPES, and treated as beads are when molecules are to be immobilized on them (non-coated beads).

Amino-functionalized beads were chosen for the MUC1-experiments, and non-coated amino beads were tested against beads coated with the different MUC1-polymers (MUC1-T/-Tn/-ST/-STn/-naked).

No control experiments were done for the PAA-450K-polymers. Naked PAA-

polymer was not available to test whether GalNAc had any interactions to this backbone. Previously done experiments had shown no interactions between the PAA-polymer and beads.

Control experiments for the fumonisin-study were done, where both carboxyl- and amino-functionalized non-coated beads were tested against beads with all polymers and fumosin. These control experiments might not have been necessary, as the beads for these experiments were coated with a large amount of polymers, so that the surface of the beads would be unlikely to be available.

For the PAA-GalNAc/-Gal/-GlcNAc/-Glc samples, PAA-functionalized beads without glycosylation were tested against each other. No experiments were done to test whether sreptavidin-functionalized beads (without any immobilized polymer) would bind to beads with PAA-polymer, due to the unavailability of beads of two different sizes, suitble for these experiments.

5 Results and analysis

After obtaining force-distance curves, the loading rate for each force jump is fitted manually. This requires some experience of how force-jumps should look. A lot of the obtained data could not be fitted with loading rate slopes because of multiple bonds breaking too close apart. Multiplicity affects the shape of the force-jump curve in a way that makes it impossible to determine the correct loading rate for a single bond rupture event. When multiple bonds break at the same time, the curves will be more flat, and the loading late will be lower than for single bonds. From the obtained data it was clear that force-distance curves could have a variety of different shapes - this is examplified in section 7.3.

The noise in the system used was about +/-1 pN, which made forces below 4 pN hard to characterize as an unbinding force rather than an unspecific interaction or accumulation of noise. Forces up to about 320 pN have been measured in these experiments; however, a much narrower range of forces is actually useful, as will be shown later in the results.

5.1 Control experiments for the mucin studies

In all of the experiments, performed as part of he current Master Thesis studied biopolymers are immobilized onto polstyrene beads that are brought together and apart in order to assess whether the polymers interact. When performins such experiments, interactions between te biopolymer and the bead surfacewould, if they exist, complicate the interpretation of the results. If the polymer binds to the surface of the bead, it is important that the bead is either fully coated with polymer, so that unspecific interactions rarely happen, or that the unspecific interactions differ in some way from specific ones. In the latter case, the unspecific interactions can be filtered out as part of the data analysis. It is thus essential to know whether the molecules in study interact with the bead surface; otherwise the interactions obtained can not with certainty be attributed to originate from the binding of target molecules.

Neither amino-functionalized nor carboxyl-functionalized beads showed any self-interactions in MilliQ water (pH 5.5). When the beads were dissolved in boric acid (50 mm, pH 5.8), a few interactions could be observed with some pairs of beads. For these interactions to happen, the beads had to be pressed together strongly. Both the amino-functionalized beads and carboxyl-functionalized beads exhibited the same behaviour in MilliQ water and boric acid. When these beads were placed in HEPES-buffer (100 mM, pH 7.2, with or without 1 mM $CaCl_2$ and 1 mM $MnCl_2$, the result was the same as for the boric acid: a few, nonspecific interactions, or interactions with abnormal force-curves. Carboxyl-functionalized beads were early on found to have frequent interactions with beads coated with MUC1-STn (almost in 50% of the curves). Amino-functionalized beads were initially found to rarely have interactions against beads with immobilized mucin, and they were thus chosen to be used in the mucin-experiments. When amino-functionalized beads were treated the same way the beads are when biopolymers are to be immobilized on them

(incubated in a solution of boric acid and EDC, and later washed with HEPES-buffer), the frequency of interactions increased dramatically. The first time this control experiment was done, 409 out of 840 force curves (49%) were found to have interactions, with some even being multiple.

Small contaminants in the sample sometimes had a refractive index that allowed them to be pulled towards and into the traps, which might affect measurements. Sometimes it has also been observed that small impurities were stuck to the bead surface; it is not known how this might affect interactions. Many steps were taken in order to attempt to reduce the unspecific interactions to zero by practising good hygiene during these experiments; pipette tips and cover glasses used for the experiments were exposed to the air in the lab for a minimal amount of time and all solutions used were filtered at least once a week (0,2 μm syringe filter). This reduced the amount of interactions to 150 out of 795 curves (19%).Glasses used for the bottom of the liquid chamber were washed immediately before use, Eppendorf tube racks were washed frequently to avoid accumulating dust on the outside of the Eppendorf tubes, glasses that the buffers would be made in were rinsed with MilliQ water before use. When tested after implementing all of this, the interaction frequency was 50 out of 861 curves (6%). It was hypothesized that the EDC might be the direct cause for these interactions. In order to test this hypothesis a signifficant amount of EDC was added to the same sample, which resulted in 23 out of 467 curves (5%). The conclusion was that the EDC did not participate directly in the interactions, but might have immobilized something onto the surface of the beads. Thus, 5-6% of interactions was the lowest frequency of interactions achieved. This extra steps taken improved the sample quality and lowered the amount of unspecific interactions, but did not bring the frequency to an absolute zero. Eppendorf tubes were later examined thoroughly for contamination, and blown clean by using nitrogen gas before use. It is unknown whether this gave any further reduction in unspecific interactions.

Amino-functionalized beads were initially found to rarely have interactions against beads with immobilized mucin, and they were thus chosen to be used in the mucin-experiments. The control experiments were repeated at a much later point, and a different result was found. This time it was found that MUC1-Tn (16%), MUC1-STn (close to zero) and MUC1-ST (17%, vs 37% when MUC1-ST - self) were all able to bind to the surface of uncoated beads, but not MUC1-T (0%, . MUC1-Tn and -STn did not have frequent interactions with the bead surface, but were not possible to distinguish easily from MUC1-Tn and -STn-self interactions. MUC1-ST had frequent and strong interactions with the amino-functionalized beads, but the force curves differed from those obtained for MUC1-ST self-interactions in both strength and shape (MUC1-ST - self interactions were weak and had flat curves). It was found that the MUC1-protein is highly inert and did not exhibit self interactions, and was equally unreactive to any of the glycosylated mucins, except MUC1-STn, which it seemed to react to.

At this point, there is no way of identifying the point of rupture of an interaction due to how the program for the analysis works. This was suggested early on during this work and was implemented for the AFM-platform, but was more challenging

to do for the optical tweezers. The program for the optical tweezers estimates the force of the rupture by subtracting the approach-curve from the retract-curve. The result is a curve when only the events present in just one of the curves, as for example the force jumps, remain. When beads are pressed together hard enough to displace them, the distance of displacement will be added as extra distance before the interaction-curve. Thus, all of the examples of curves given in this work can be expected to show bond ruptures that actually happen at a lesser distance from the bead surface than is depicted.

5.2 Factors that can affect the frequency of interactions

Frequency on interactions was found to be a poor method for quantification of the adhesiveness of two polymers. Although it would be very convenient to be able to estimate the frequency of interactions, this is not an easy task due to several reasons. It is important to have control of both how long and hard beads are pressed together, as both of this factors will affect the frequency of interactions. As not all of the beads are equally and evenly coated, it is important to have measurements from many pairs of beads, from many different time points to even out the differences. Because the efficiency of EDC decreases quite rapidly, the frequency of interactions measured weeks or months apart has been shown to vary in frequency. It is also not always easy to filter out the nonspecific intractions. All of these moments are explained and exemplified further below.

5.2.1 The reactivity of the EDC

It was noticed early on that EDC seemed to lose its reactivity quite rapidly. The first findings of this was while studying MUC1-Tn molecules, which are known to have frequent interactions. After working with these before versuS after the two months of summer vacation, there was a sudden strong decrease in the frequency of interactions. As these molecules are themseles stabile when stored at -28 ° Celcius in the freezer, this was attributed to a possible decrease in the reactivity of EDC. The effectivity of EDC has an important role in determining the amount of molecules that will be attached to the surface of the microbeads, which affects the multiplicity of interactions.

It has been observed that the reactivity of the EDC seems to decrease over time from; this is supported by Figure 24. At the same time, experiments involving the same EDC were conducted on a different pair of interacting molecules. The AFM curves showed that force curves had high multiplicity of interactions in september, and many more single bond ruptures only a couple of months later.

It would thus be advisable to find a way to test this. During this study, it has not been possible to test the reactivity of the EDC in any direct way. As the point of many of the experiments that were carried out was to confirm or disprove interactions between biopolymers, it is extremely important to be able to control the density of the polymer. The way the immobilization procedure was assessed during these experiments was to make both positive and negative control

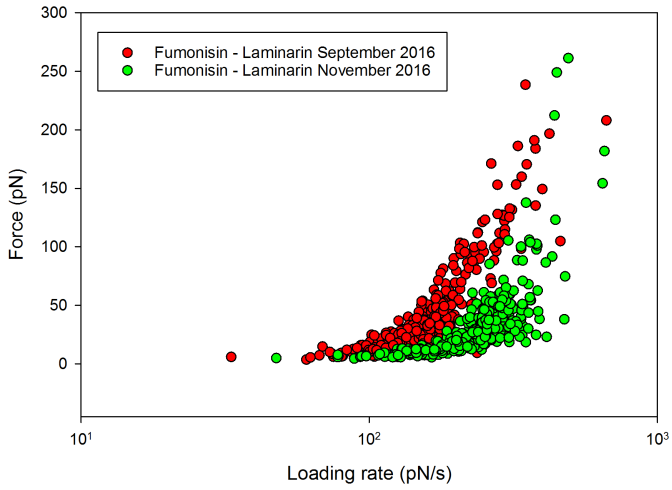

Figure 24: The dynamic power spectrum for fumonosin - laminarin interactions, recorded about three months apart. The difference in the gathered data is believed to be due to the reactivity of the EDC, which had just been purchased before the first measurements, in September.

samples in addition to the sample that was to be studied. The mix of EDC and boric acid for the immobilization was made as one batch, and then distributed to all of the samples. The negative sample was amino-functionalized beads that underwent the same preparation procedure as the beads that were to be decorated with molecules. If a lot of unspecific interactions were found in this sample, all other samples prepared would not be used, and solutions were used to prepare the samples were made anew or filtered. The positive control sample was a mucin, MUC1-STn, that had been found to have frequent and strong self-interactions. If no interactions were obtained for the positive control, it was assumed that the immobilization procedure did not work in the other samples either.

5.2.2 The alignment of the optical traps

An issue that was noticed during this work is the importance of aligning the optical traps every time before experiments are carried out. Slight misalignment of the optical traps in the Z-plane was not thought to be an issue, but it was later found to be of major importance. An experiment was carried out where 702 approach-retract-curves from 9 different pairs of beads with immobilized MUC1-STn resulted in 14 interactions. When it was suspected that the alignment was the problem and the traps were re-aligned, the same sample was used to test the hypothesis. 321 interactions were found among 626 attempts, from 8 pairs of beads that all exhibited interactions. The misalignment of traps can thus alone result in the

wrong conclusion being drawn from an experiment where the main interest is the presence or absence of interactions.

The optical traps were monitored the next few days, and it was found that they had to be re-adjusted every time the liquid chamber was changed, and sometimes several times during an experiment. The misalignment of traps is easily visible at a specific distance from the camera, and is recognizable by different contrast in the colour of the beads; unfortunately, no screen shots of these was taken. The variation in the contrast is not linear at distances further away from the camera, and thus, small differences in the Z-position of the beads might not be noticed. Being aware of this is even more important when experiments with beads of different sizes are carried out, as it is more difficult to see when beads of different sizes are misaligned; same size beads should be used to align the traps.

During the experiments it was noticed that it took around 2 hours for the lasers in the optical tweezers to stabilize. This stabilization could be observed by the reduction of noise in the force-curves, and less movement of the beads in the XY-plane while a series of measurements was carried out. It was noticed that, if the lasers had not stabilized yet, a change of the position of the beads could be observed over time, until the trapping power had stabilized. Beginning the measurements before the stabilization of the lasers was avoided.

5.2.3 The distribution of polymer on the surface

The distribution of polymer on the beads is a factor that strongly affected the frequency of the interactions. The best case would be that polymers immobilized on beads were distributed evenly on the surface of the bead, and that different beads had an approximately equal amount of polymer. Unfortunately, this is not so. Early on during the experiments it was hypothesized that polymers are not equally distributed on the beads, as some of the beads had many interactions while others had few. In any case, it was decided to always record interactions from many different pairs of beads. When data was sorted in this way, it was immediately obvious that the distribution of interactions could vary greatly between different pairs of beads in the same sample.

While some beads could show no interactions, even when approached from different sides, other beads could have up to about 65% interactions. This is exemplified by some statistics employed on data from MUC1-STn self-interactions and TR-PSM-H8 self-interactions. 15 pairs of beads with TR-PSM-H8 were studied. The percentage of interactions for every bead was found, and the average and standard deviation was calculated. This resulted in an estimat of interaction frequency of 8.5% +/- 8.5%. The same was done for 43 different pairs of beads with MUC1-STn, which resulted in 19% +/- 14.5%. This can mean that the frequency of interactions are not normally distributed around the average - some beads experience interactions frequently, while many, not at all.

Table 2: The force beads are pressed together with affects the number of interaction. The table shows one of the quantified examples of this that was observed by the number of increasing interactions. At distance 0.00, the beads were barely touching.

Added distance (μm)	**Number of interactions**
0.00	0/30
0.01	5/30
0.02	8/30
0.03	13/30
0.04	20/30
0.05	20/30
0.06	35/50

5.2.4 How hard beads are pressed together and the hold time

A few tests were done early on to see how the force (Table 2) beads are pressed together with and the time beads are kept together (hold time) can affect the results. It was found that the frequency of interactions could be increased in both ways. However, when beads were pressed together strongly, there was an increase in unspecific interactions. Some of these look like the entanglement of molecules, but others might have a more normal stretching curve examples of such curves are presented in Section 5.3. When pressed together strongly enough, any type of coating on the beads could result in interactions, some of which might be between a polymer and the surface of a bead. It was determined that pressing beads together should be avoided to attempt to decrease the amount of unspecific interactions. Some of the data are shown in the table below (Table 2).

5.2.5 Not all interactions can be analyzed

A fraction of the force jumps can not be analyzed due to that the loading rate cannot be determined accurately (Figur 26). This challenge is more pronounced for systems that have many strong interactions. As these interactions can not be analysed, they will also not be represented in the subsequent histograms.

5.3 Criteria for identifying specific interactions

As there are many possibilities for interactions between molecules, and there is no way to directly observe what kind of molecules are binding, it is important to define some criteria for how useful interactions are distinguished from those that should be excluded. It has been chosen that specific interactions are those between target molecules, while all other interactions are referred to as non-specific. Examples of unspecific adhesion is peeling of a molecule from a surface and entanglement of molecules that causes pulling. Interactions that originate due to contact between target molecule and bead surface are defined as non-specific, even though they might originate from some kind of specific intermolecular binding events.

All of the molecules that have been studied are relatively rigid and will not be unfolded during the stretching by optical tweezers, due to the limited forces optical tweezers are able to exert. This results in interaction curves with a distinct polynomial shape before the bond rupture, illustrated in Figure 25. The goal of the experiments was to measure mostly single-bond rupture events. The main criterion for identifying such events was the shape of the force curve immediately before a bond-rupture. According to the worm-like chain model for polymers, used to describe stiffer polymers, the more the polymer will be stretched the less flexibility it will have. This will result in a behaviour where the force exerted on the polymer will grow more rapidly the more the polymer is stretched, and will give a force curve with an increasingly steeper slope before the bond ruptures. The MUC1-protein has a certain elasticity, and thus, when it is stretched, the force that is exerted on the molecule will not be linear, but increase the more the molecule is stretched. This will result in curves that have polynomial growth. Figure 25 shows a force-distance curve of an interaction originating from binding between MUC1-Tn - self, with a correct shape according to what should be observed when two relatively rigid MUC1-molecules are being pulled apart during an interaction.

Some examples of specific interactions are shown below (Figure 25). These interactions are defined by a slightly increasing slope (right to left), which should correspond to the stretching of an elastic molecule, according to the worm-like chain model. To be able to estimate the loading rate of the interactions correctly, the shape of the curve immediately before the bond breakage should have fairly low noise, and there should not be large differences in the slope of the fitted loading rate when the area that is fitted to is increased or decreased slightly. The stretch of the force curve that the loading rate is fitted to is marked by a red tilted line in the figure (Figure 25). As there will always be some variation in how much thermal energy a bond experiences additionally to the pulling force exerted on it, the loading rate will have some variation for the same strength of forces. As long as the shape of the stretching-curves looked normal, this variation in loading rate was accepted and thus included in the data for the different systems investigated in this study.

In many cases, it was not possible to determine the loading rate for an interactions accurately, and there can be several reasons for this. The measurements can often be affected by random noise. If the noise appears right before a bond breaks, which is the area of the force curveused for loading rate determintion, the loading rate determined can vary strongly depending on how large a stretch of the curve is used for the fitting (Figure 26, upper left). Such force curves are excluded from the analysis. The reliability of the determination of the loading rate is also significantly reduced if two bonds rupture simultaneously or nearly simultaneously. In this case, the rupture curve will look slightly different: it can either be jagged (Figure 26, upper right) or flattened (Figure 26, lower right). In any case, the loading rate is likely to be significantly underestimated.

When two bonds rupture within a short time frame, it is sometimes possible to correctly estimate the loading rate and strength of the first rupture, but not the second (Figure 26, bottom left). When it was not possible to see most of the curvature in such cases, the second rupture was excluded from the analysis.

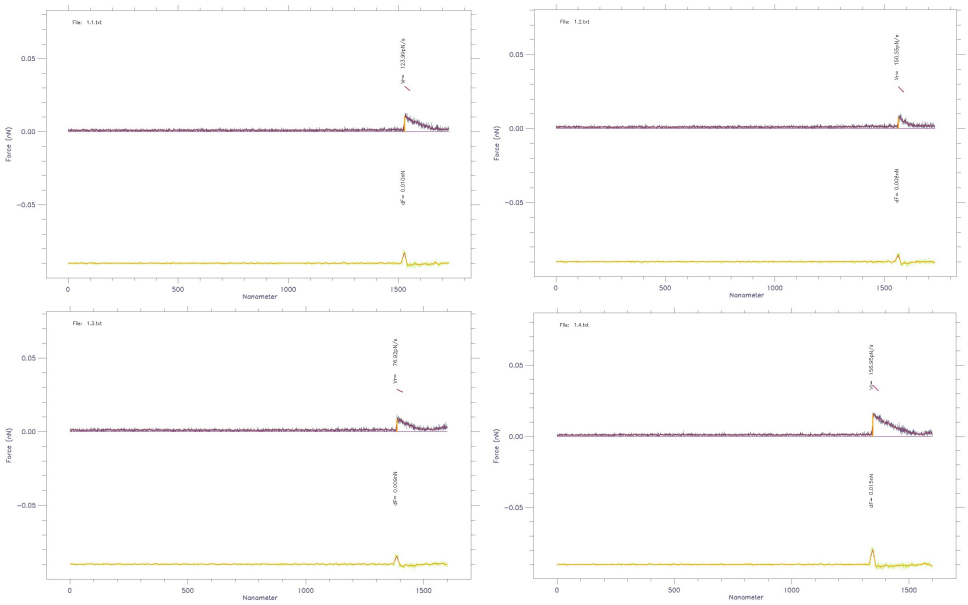

Figure 25: Examples of interactions that can be fitted a loading rate with high accuracy. The frames show how the interactions look in the IDL PostProcessing software, where loading rate is fitted to the curves manually, and is represented by the short red line above the force jump. The X-axis shows a distance in nm, while the Y-axis shows force in pN; the resolution of the figure is poor due to the limited export options of the software.

Both the tilt of the curve and the height of the vertical line (estimated force) is important parameters to notice when estimating the loading rate. Sometimes, the PostProcessing software did not estimate the strength of the interactions correctly, which could be observes in that he yellow vertical line did not reach to the top of the rupture curve (Figure 26, bottom figure). This will affect the tilt of the loading-rate line, as these two lines together are supposed to come to a corner that cups the bond rupture at the side and the tilt. The error in estimation of the force can be due to a bond of lower strength breaking right before the main bond-rupture event.

Beside the interactions that were not used for the analysis due to uncertainty in the loading rate, other interactions that are not included in the analysis are interactions that have a shape that indicated that they are unspecific (Figure 27). There are several types of unspecific interactions. Some are easily distinguishable and can easily be avoided in the dataset, while others are more complex.

One of the unspecific interactions that can often be easily recognized is peeling (Figure 27, upper left and right). Peeling happens when a polymer exhibits interactions against the surface on a bead and sticks along the surface. This results in a gradual peeling when the polymer is being pulled at, which results in a near

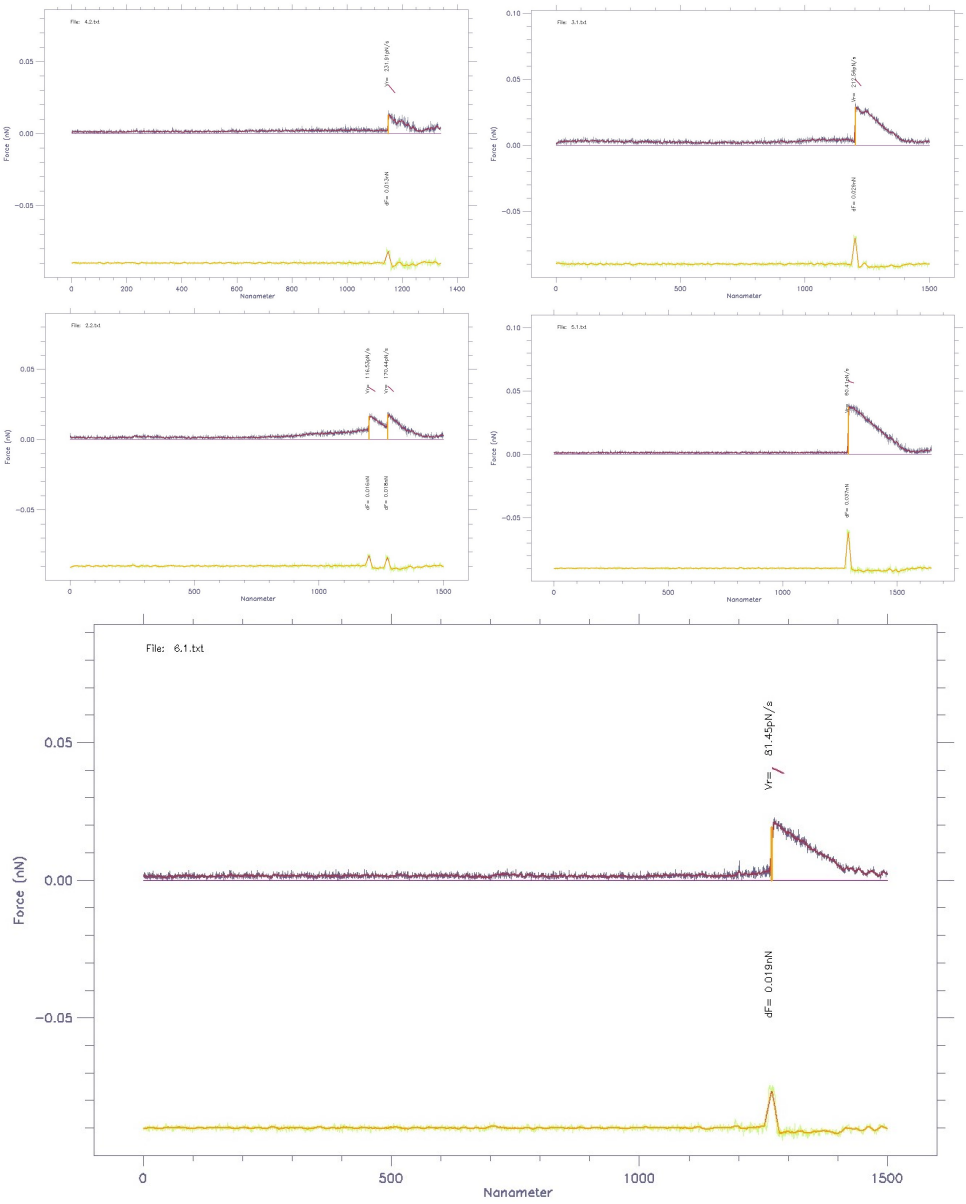

Figure 26: Examples of interactions that should be excluded from the analysis due to difficulty in estimating the loading rate. Upper left: curve characterized by a high noise level. Upper right: two bonds breaking with short distance in-between. Lower left: two subsequent rupture events, where only the loading rate of the first can be estimated correctly. Lower right: curve with linearly increasing force prior to the bond rupture. This indicates stretching of multiple polymers. Bottom right: incorrect estimation of bond strength.

constant force, which is represented by a near horizontal curve. This curve can have different shapes, depending on how many points on the polymer are attached to the surface. The more attachment sites, the smoother the curve is. These interactions were seen between an amino-functionalized bead and MUC1-ST .

Some unspecific interactions can happen between the non-coated surfaces of the polystyrene beads. This is a type of interactions that was not seen very often during these experiments, but is more common when two beads are pressed together strongly, with a some time (dwell time upon contact). These interactions are expected to be due to entanglement of molecules, and/or peeling-effects (Figure 27, lower left).

The last type of curved that were excluded were those where suspected to be due to simultaneous rupture of multiple bonds. In some systems: MUC1-ST - self and MUC1-T - self, such interactions could make up most of the data set. The curves of these interactions have a linear increase in force from the baseline to the bond rupture (Figure 27, lower right). This indicates that there might have been something less elastic that was being pulled at than is expected from the MUC1 protein. At first there was doubt that this was, in fact, interactions between the MUC1 proteins. However, after a long evaluation, these interactions might be due to a high density of mucin at the interacting surfaces. The forces ranged from 5-50 pN.

5.4 Difference in the bead size affects the spread of the data

During this work it was noticed that there is a variation in the size of the beads the molecules are immobilized on. Early on in the process of performing the force measurement experiments, it was decided to save the data gathered for every different pair of beads separately. This was done to later be able to exclude pairs of beads where the force had been calibrated incorrectly due to a difference between the size of the bead provided to the software vs. the actual bead size. It was often possible to see that the resulting calculated forces showed a slight variation in the distribution of data gathered using different pairs of beads. (Figure 28).

The polystyrene beads that were used for these experiments had a finite diameter declared on the box. However, information provided on the webpages of the company providing the beads (Spherotec), indicated a deviation of +/- 0.2 μm. Based on a visual evaluation, the variation seemed to be larger than expected (Figure 29), bases on the information provided by Spherotech. When beads were being chosen for the measurements, the only guide for what the correct size might be was to choose the most typical size of beads. During this work, JPK Systems have modified the software to include a measuring tool. Because of the relatively low resolution of the microscope integrated with the optical tweezers, the estimation of size still has a quite high uncertainty.

The differences between calibration for the same pair of beads was assessed by Marit Sletmoen by doing 30 calibrations for the same bead pair. After statistical analysis of the trap stiffness it was found that there was a deviation of about 5.8 % between calibrations for the same pair of beads. This has relatively little

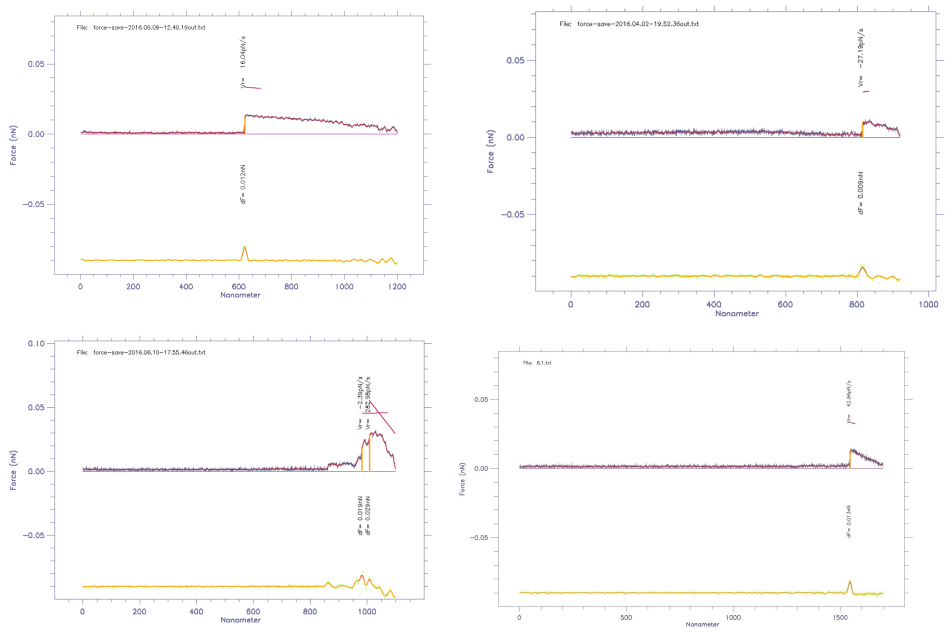

Figure 27: Examples of interactions that should be excluded from the analysis due to unspecificity. Upper left: curve with a large amount of noise. Upper right: two bonds breaking with short distance in-between. Lower left: two bonds, where ontly the loading rate of the first can be estimated correctly. Lower right: flat curve immediately before the rupture that indicates stretching of multiple polymers. Bottom: strength estimated incorrectly.

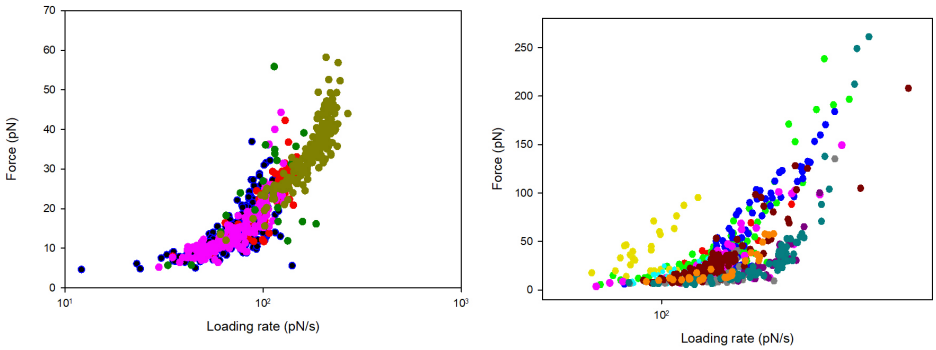

Figure 28: Data from different beads plotted separately. In the left frame, the beige dataset is gathered using smaller beads (2.01 μm), while the rest are gathered using larger beads (3.36 μm). These are TR-PSM H8 self-interactions. In the right frame, the yellow dataset was excluded due to an abnormal location in the dynamic force spectrum. The placement indicates high multiplicity of interactions. These interactions were recorded between fumonisin and laminarin.

significance. However, when the calibration for trap stiffness was compared between different beads that were supposed to be of the same size, there was a much bigger deviation: around 40 %.

During calibration of the trap stiffness, the calibration curve fitted to the Lorenzian power spectrum seemed better for smaller beads (2.10 μm) than for bigger beads (ca 3.36 μm). Small beads were thus preferred in experiments where self-association of molecules was studied. The effect of this seems to be that when bigger beads are employed, it is easier to probe forces at lower loading rates, which are almost inaccessible with smaller beads (Figure 28, right frame). The smaller beads seem to be held more strongly in the traps, and result in a narrower distribution of forces.

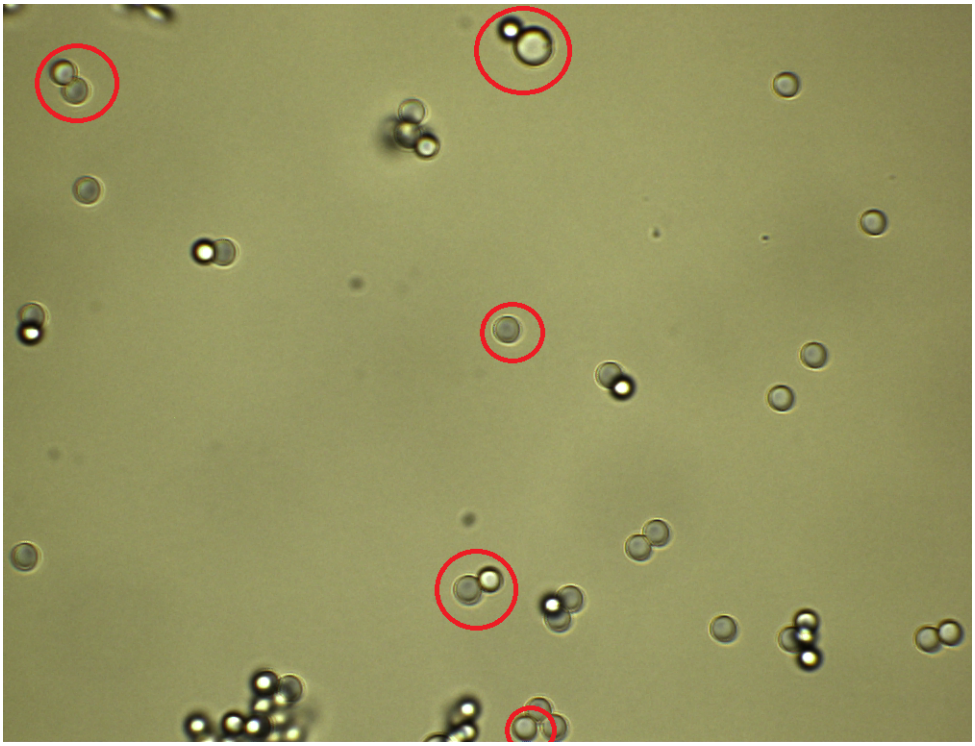

Figure 29: A screenshot from NanoTracker Software from JPK, during measurements. Although beads should be the the same size 3.36 μm +/- 0.2 μm, it is possible to observe a size difference in some of the beads (circled in red), which indicated that their deviation is more than it should be.

5.5 Importance of mucin glycosylation for self-interaction ability

5.5.1 MUC1-Tn - self interactions

The Tn-antigen comprises a single α1-linked GalNAc unit on a Ser/Thr of a protein. MUC1-Tn was found to self-interact. Interactions were observed in two different HEPES-buffers: 10 mM HEPES, pH 6.8, no ions added and in 100 mM HEPES, pH 7.2, added 1 mM $CaCl_2$ and 1 mM $MnCl_2$. No measurable difference was observed in the interaction ability of this mucin in the presence or absence of calcium ions. The dynamic force spectrum (Figure 30) was made based on 531 datapoints. The distribution of forces can be observed as a histogram (Figure 31). The data from the dynamic force spectrum was divided into seven sub-distributions (Figure 32). f^* values were obtained for six of the sub-distributions, together with parameters for x_β and k_0 (Table 3).

Many very strong interactions were observed for this system, but they are not represented in the analysis due to the inability to estimate the loading rate accurately at the point of unbinding. This also means that the histogram below also does not show the true extent of the interactions that it was possible to measure. The spread of the data is greater than for some of the systems analyzed later. This might be due to both less experience with the instrument and the analysis at the time when the data was obtained.

Table 3: The calculated parameters for the sub-distributions of the dynamic force spectrum for interactions between MUC1-Tn - self. The bottom row shows the averaged values for the innermost barrier.

	Bell-Evans analysis				**Constrained fit**	
N	$<r_f>$ **(pN/s)**	f^* **(pN)**	x_β **(nm)**	k_0 (s^{-1})	x_β **(nm)**	k_0 (s^{-1})
20	78.3	6.4	3.74	0.19	0.39	10.05
28	95.7	8.4	1.55	1.44	0.39	6.39
44	112.7	8.7	2.21	0.54	0.39	6.16
70	132.5	10.1	2.14	0.34	0.39	6.05
108	161.4	14.7	0.79	1.77	0.37	4.20
103	190.3	16.5	0.50	3.04	0.37	3.86
-	**-**	**-**	**2.41**	**2.12**	**0.38**	**6.39**

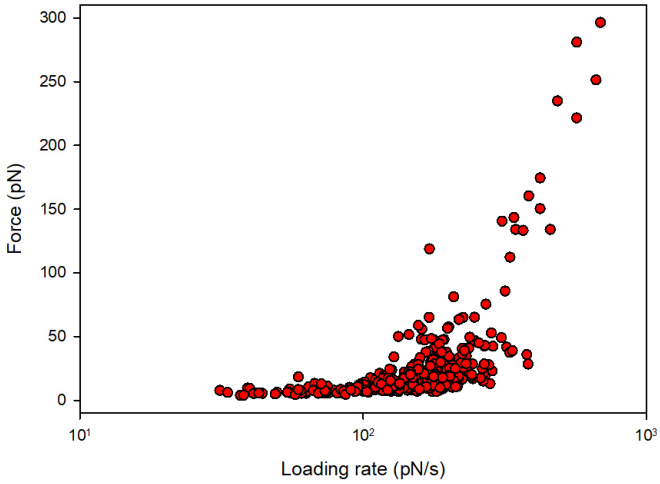

Figure 30: The dynamic power spectrum for MUC1-Tn - self interactions. This distribution is based on 531 observed force jumps. Interactions with strengths above 50 pN were not uncommon, but for these force jumps accurate estimation of the loading rate was often impossible.

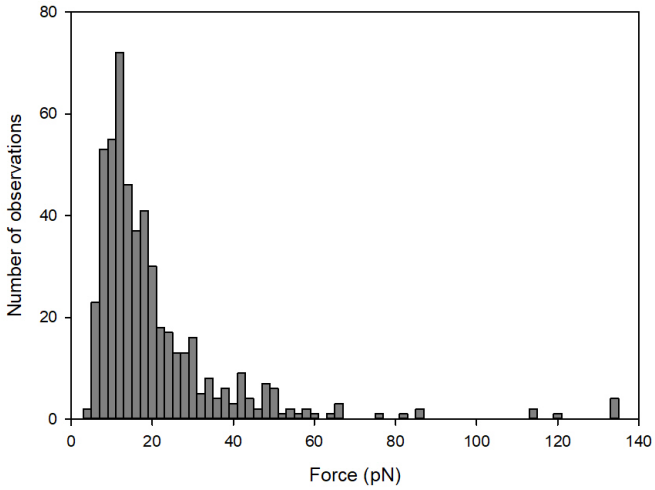

Figure 31: The histogram shows the distribution of unbinding forces between MUC1-Tn - self, and is based on 531 datapoints. Although many interactions with strength above 80 pN were obtained, they are not represented in the histogram due to inability of correctly estimating the loading rate for these interactions.

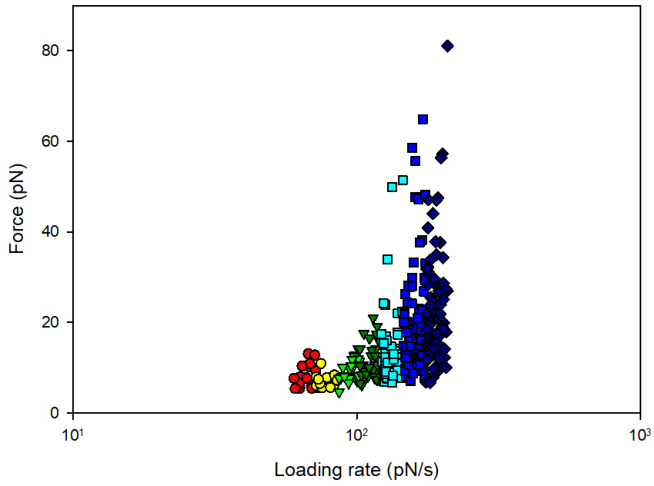

Figure 32: The dynamic force spectrum shows the sub-distributions of unbinding forces between MUC1-Tn - self. Due to an insufficient amount of datapoints in the lower part of the loading rate spectrum, this part of the spectrum was not included in the analysis.

5.5.2 MUC1-STn - self interactions

The STn antigen is comprised of the Tn-antigen with an α-2,6-linked sialic acid. It was of interest to study whether the presence of sialic acid was destructive for the interactions between Tn-antigens. The dynamic force spectrum (Figure 34) is based on 376 data points. The distribution of forces has been visualized by a histogram (Figure 35) . STn exhibited self-interactions more frequently than MUC1-Tn. Thus it was found that sialic acid does not prevent interactions between Gal-NAc groups on MUC1, but seems to promote them instead.

The dynamic force spectrum was divided into eight sub-distributions (Figure 36). f^* values were obtained for seven of the sub-distributions, which were fit histograms (Figure 37). Parameters for x_β and k_0 (Table 4) were found based on the fits of values for $f*$ and mean r_f.

Table 4: The calculated parameters for the sub-distributions of the dynamic force spectrum for interactions between MUC1-STn - self. The bottom row shows the averaged values for the parameters.

	Bell-Evans analysis				**Constrained fit**	
N	$<\mathbf{r}_f>$ **(pN/s)**	$\boldsymbol{f^*}$ **(pN)**	$\mathbf{x}_\beta$ **(nm)**	$\mathbf{k}_0$ (s^{-1})	$\mathbf{x}_\beta$ **(nm)**	$\mathbf{k}_0$ (s^{-1}))
11	107.3	9.2	1.89	0.68	0.33	8.88
20	123.2	8.7	1.85	1.06	0.33	9.99
28	144.1	11.0	1.42	1.04	0.33	8.22
45	163.1	12.7	1.26	0.98	0.33	6.48
58	188.0	13.3	1.64	0.34	0.33	5.63
58	216.1	18.2	1.01	0.57	0.33	4.69
57	247.3	27.7	0.42	1.43	0.09	4.20
42	282.4	33.7	0.59	0.30	0.09	3.58
-	**-**	**-**	**1.26**	**0.68**	**0.27**	**6.46**

From these findings it seems that the α-2,6-bound sialic acid of the STn-antigen does not inhibit the interactions between the Tn-antigens. It is, however, difficult to say whether the α-2,6-linked sialic acid does or does not change the characteristics of the interactions. It may seem like the most probable interaction strength is slightly higher for MUC1-STn than for MUC1-Tn, according to the histograms for forces obtained (Figure 31 and 35), but there is some uncertainty in this data due to less experience with how to use the optical tweezers during the data collection for MUC1-Tn - self interactions.

5.5.3 Comparison of MUC1-Tn - self and MUC1-STn - self

A comparison between the dynamic force spectrum of MUC1-Tn - self and MUC1-STn - self (Figure 38 and 39) shows that there is a significant overlap between the dynamic force spectra of self-association between the two mucins. The historgam fits for the data show that the force distributios (Figure 40 and 41) The difference

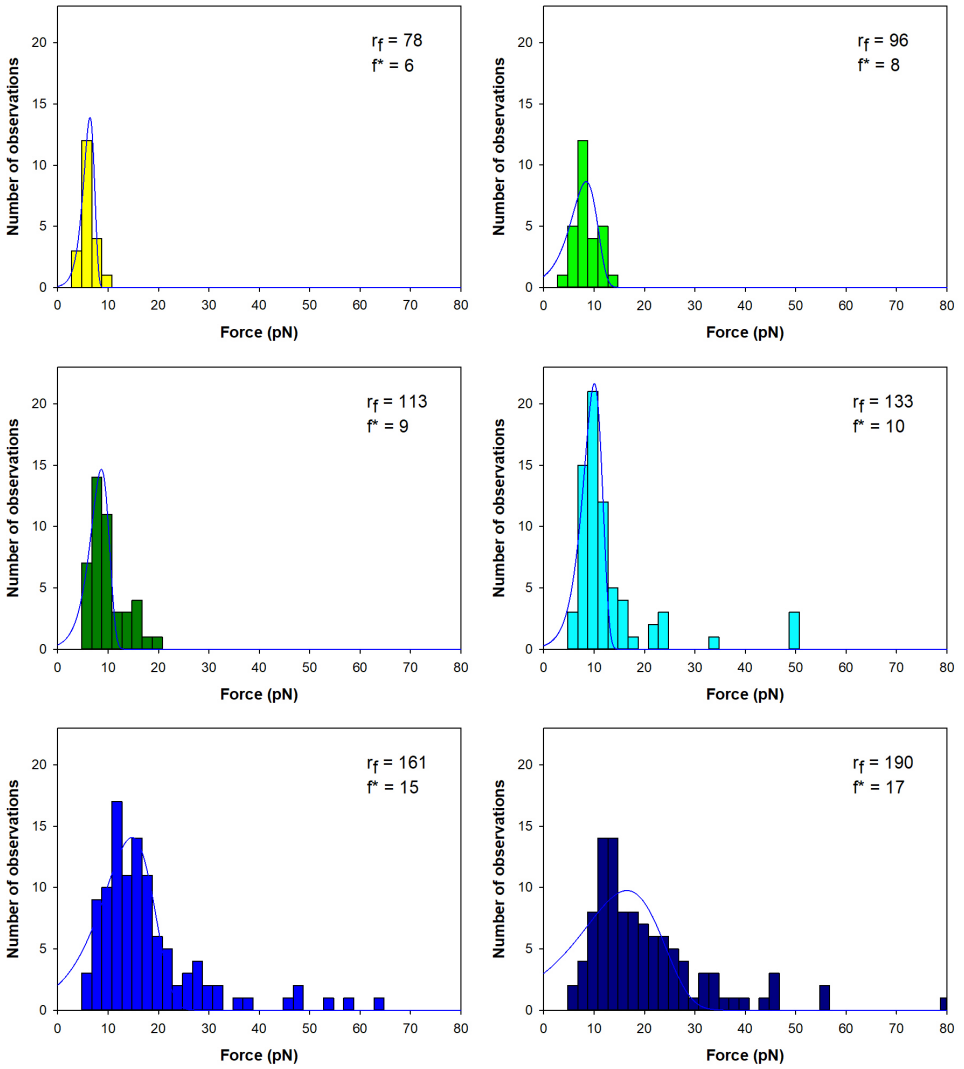

Figure 33: Histograms for most probable unbinding force (f^*) obtained for forces in sub-distributions of loading rate, for interactions between MUC1-Tn with itself.

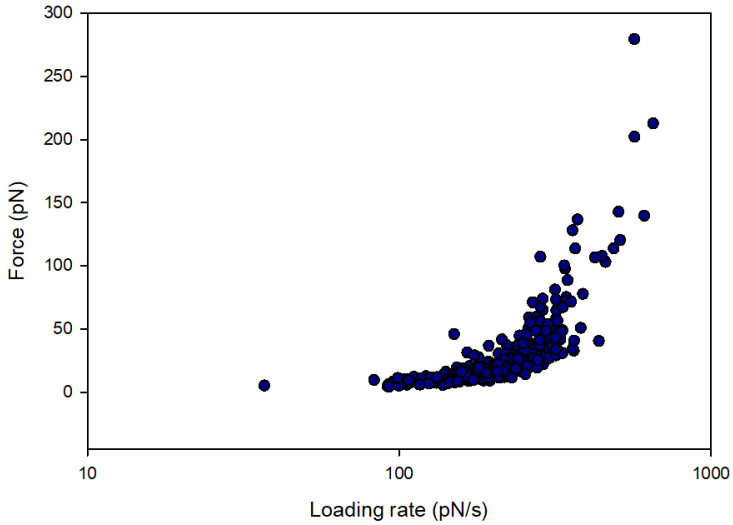

Figure 34: The dynamic power spectrum for MUC1-STn - self. This distribution is based on 376 observed force jumps.

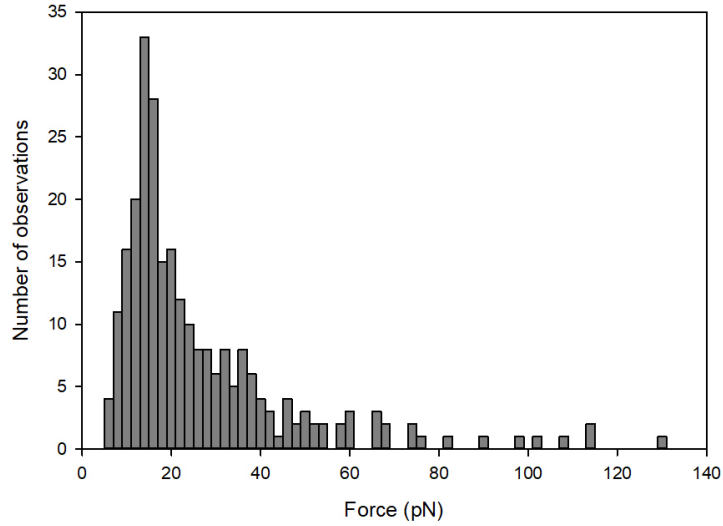

Figure 35: The histogram shows the distribution of unbinding forces between MUC1-STn - self, and is based on 376 datapoints. Although many interactions with strength over 60 pN were obtained, they are not represented in the histogram due to inability of estimating the loading rate for these interactions correctly.

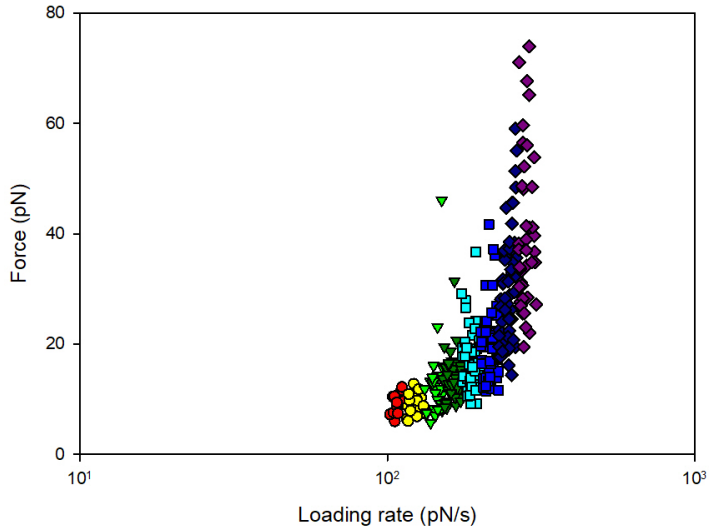

Figure 36: The dynamic force spectrum shows the sub-distributions of unbinding forces between MUC1-STn - self. Due to an insufficient amount of datapoints in the lower part of the loading rate spectrum, this part of the spectrum was not included in the analysis.

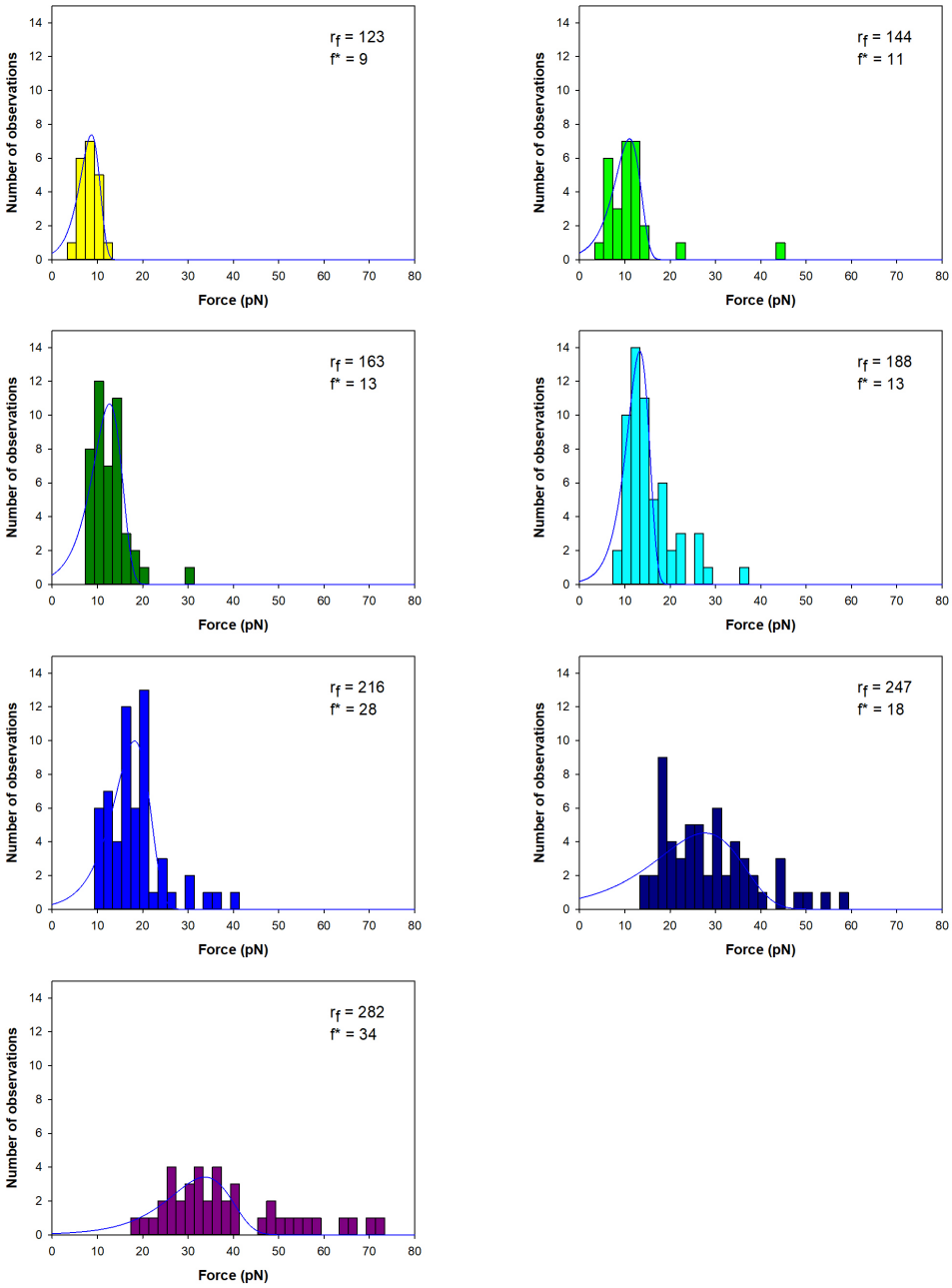

Figure 37: Histograms for most probable unbinding force (f^*) obtained for forces in sub-distributions of loading rate, for interactions between MUC1-STn with itself.

in the spread of the MUC1-Tn - self data might be due to the experience with the analysis of data gained during this work, since some of it was analyzed early on in this work, and some of it much later. Thus, some of the difference observed in the dynamic force spectra might not be due to an actual difference.

For MUC-Tn - self, fewer interactions have been obtained at the lowest loading rates compared to what is observed for MUC1-STn - self. All interactions for MUC1-STn - self have been measured with bead displacement-speed of 1 μm/s and 1 s dwell-time (time beads are kept in contact), with the mucins attached to beads 2.01 μm in size. Some of the interactions between MUC1-Tn - self have been measured with no dwell-time, and on beads 3.36 μm in size. The difference in dwell time and bead size might be the cause of the absense of interactions for low loading rates for MUC1-STn self.

From the histograms, it seems that the average strength for the interactions between STn-groups might be slightly higher than that for Tn-groups, and this is the case with both bead sizes and both 1 s and no dwell time. As mentioned before, there also seemed to be a higher interaction frequency between MUC1-STn - self than MUC1-Tn - self.

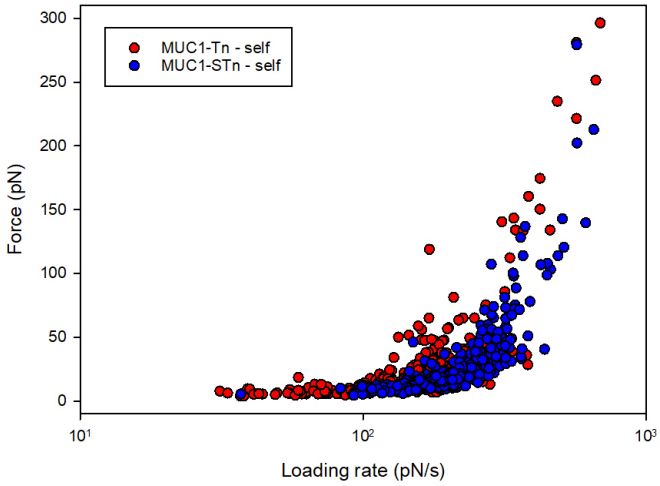

Figure 38: A dynamic force spectrum showing all unbinding forces between MUC1-STn - self compared to MUC1-Tn - self. Interactions between MUC1-STn - self have been obtained by using beads of 2.01 μm and 1 s dwell-time, while those for MUC1-Tn - self have been obtained between beads 2.01 μm and 1 s dwell time, and 3.36 μm beads and 0 s dwell-time. The bigger bead size and dwell-time are thought to be the reason for more interactions at lower loading rates for MUC1-Tn - self.

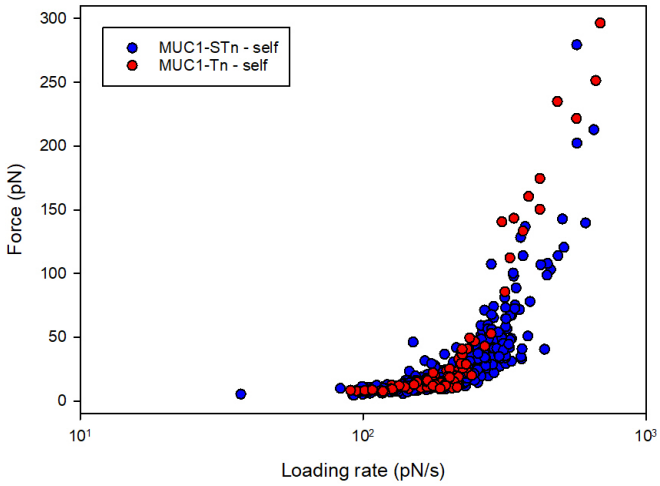

Figure 39: A dynamic force spectrum showing the distribution of unbinding forces between MUC1-STn - self compared to MUC1-Tn - self. Both sets were obtained using 2.01 μm beads and 1 s dwell-time.

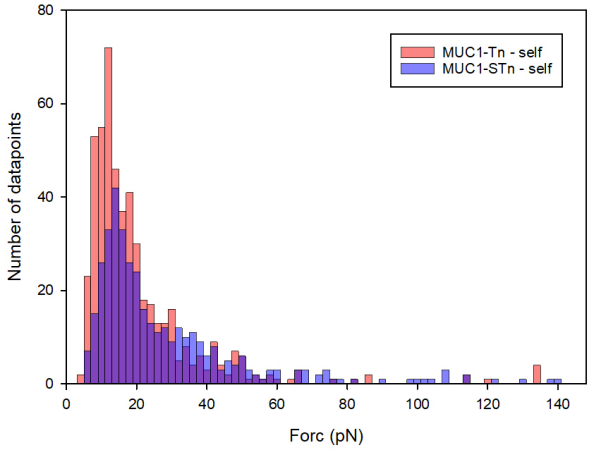

Figure 40: All unbinding forces between MUC1-STn - self compared to MUC1-Tn - self. Interactions between MUC1-STn - self have been obtained by using beads of 2.01 μm and 1 s dwell-time, while those for MUC1-Tn - self have been obtained between beads 2.01 μm and 1 s dwell time, and 3.36 μm beads and 0 s dwell-time.

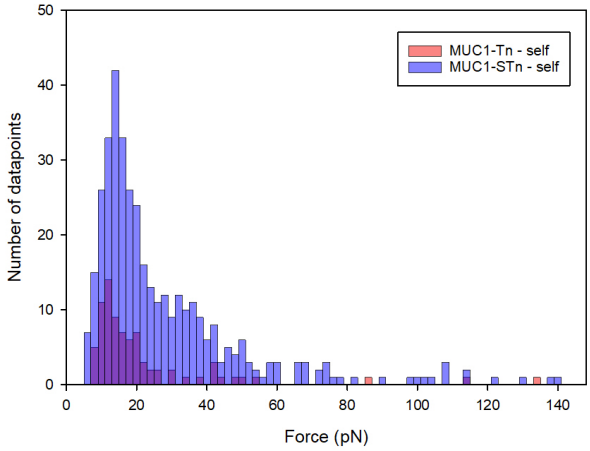

Figure 41: All unbinding forces between MUC1-STn - self compared to MUC1-Tn - self. Both sets were obtained using 2.01 μm beads and 1 s dwell-time.

5.5.4 MUC1-ST - self interactions

MUC1-ST has a galactose and a sialic acid bound to the GalNAc. These sugars can be bound in three different ways (NeuNAcα2-3Galβ1-3GalNAcα1-Ser/Thr, NeuNAcα2-3Galβ1-3(NeuNAcα2-6)GalNAcα1-Ser/Thr, Galβ1-3 (NeuNAcα2-6)GalNAcα1-Ser/Thr), also shown in the background (Figure 3).

When MUC1-ST-coated beads were allowed to interact with each other, quite a few interactions were found, which was surprising, as earlier studies had found that MUC1-ST does not interact [153]. When the interactions were analyzed, it was found that the shape of the force curves differed from those for interactions between MUC1-Tn/-Tn, MUC1-STn/-STn and MUC1-Tn/STn. The interaction-curves either had a linear rise in force all the way, up until the rupture event, or were recognized as peeling (Figure 27). Examples of these interactions are shown below (Figure 42). Many of the recorded interactions were found to be peeling of molecule from the bead surface, and other non-specific interactions.

Some of the interactions were analyzed (Figure 43, 44) to investigate whether the dynamic power spectrum would differ from that of mucins that were know to exhibit interactions in previously conducted experiments. The dynamic power spectrum showed that the interactions were generally of lower strength than between the mucins mentioned above, and that the interactions could only be probed at lower loading rates. The dynamic power spectrum for the interactions looked quite different from the ones for MUC1-Tn - self and MUC1-STn - self.

According to the histogram showing the most probable forces it is possible to see that the interactions forces actually appear to have a normal distribution, but it is centeres at a lower average force, around 9 pN. When first conducting the control

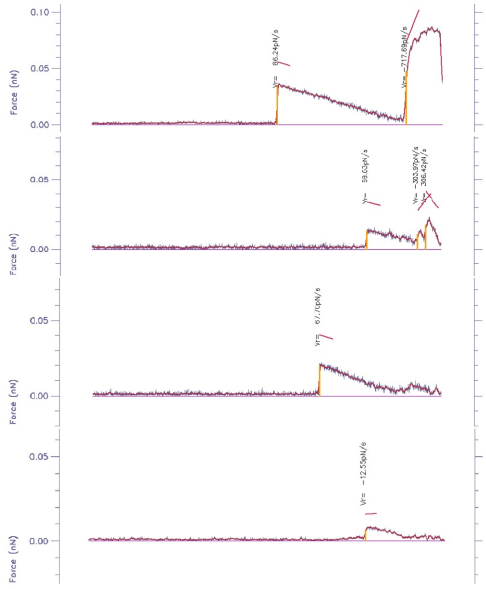

Figure 42: Examples of typical interaction-curves observed for MUC1-ST - self. The poor resolution of the Y-axis (force measured in pN) is due to the limited picture export options of the analytic software.

experiments for interactions between amino-functionalized beads and MUC1-ST, no interactions were found. It was thus surprising that MUC1-ST seemed to exhibit interactions. However, when the control experiments were conducted at a much later point, the control experiment showed that interactions between bead and MUC1-ST were found in 17% of the approach-retract curves. It is thus possible that the interactions are between the MUC1-ST-mucin and the bead.

5.5.5 Intreactions betwen MUC1-ST and MUC1-Tn/STn

MUC1-ST did not seem to interact with neither MUC1-Tn nor MUC1-STn in some of the early experiments. Later, it was found that MUC1-ST interacted with MUC1-STn and MUC1-Tn. The force curves looked normal, like those seen for MUC1-Tn and MUC1-STn self-interactions. The dynamic force spectra for the interactions resembled those found for MUC1-Tn - self and MUC1-STn - self (Figure 45). At a much later point, it was attempted to measure interactions between MUC1-ST and MUC1-Tn/STn again, and they were found to not interact. For MUC1-ST vs MUC1-Tn, 2/351 interactions were found. For MUC1-ST vs MUC1-STn, 0/311 interactions were found.

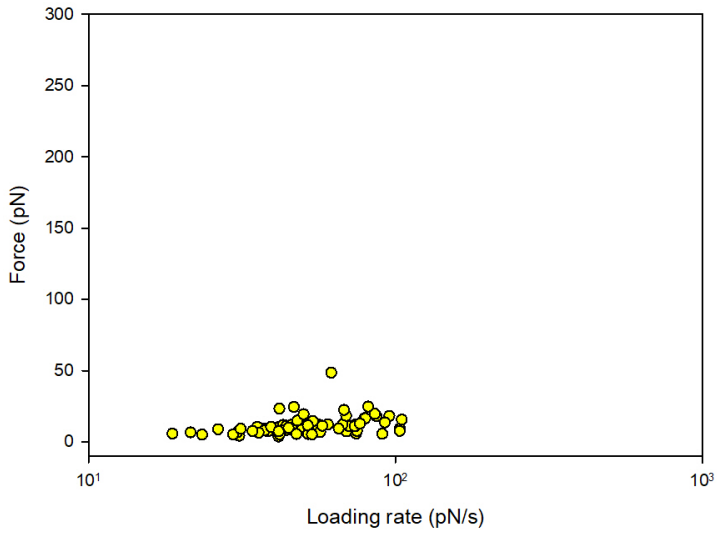

Figure 43: The dynamic force spectrum for MUC1-ST - self interactions. These interactions were obtained by using beads of size 3.36 μm. The limited amount of analyzed data is due to the belief that these interactions were unspecific. This is no longer believed to be the case. Much more data is available for these interactions.

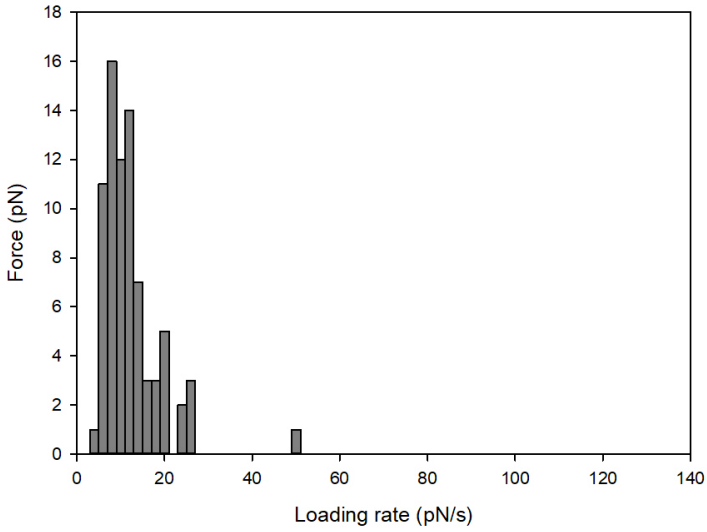

Figure 44: The distribution og forces measured for MUC1-ST - self interactions. The interactions curves for this system had an abnormal shape, and these interactions are thus classified as unspecific.

5.5.6 MUC1-T - self interactions

MUC1-T was in an earlier study found to not interact [153]. It was thus strange to discover that MUC1-T seemed to exhibit plenty of interactions:1750 out of 8127 attempts, where a small amount are expected to possibly be unspecific. Three different samples of MUC1-T were used in these experiments, and all off them had some degree of interaction. One of the samples was obtained by neuraminidase treatment of MUC1-ST, which cleaves off the sialic acid; this sample also had an IgG-domain. The other who samples Did not have an IgG-domain.

The interactions had, as with MUC1-ST, abnormal force curves, where the force increased linearly from the baseline and all the way until the bond rupture. These abnormal force curves resulted in an abnormal dynamic force spectrum (Figure 46), and the interactions were initially dismissed as they were believed to be unspecific. A histogram of the distribution of the forces has been made (Figure 47) Some of the reason for this was that the beads had been pressed together strongly (20 pN and above vs. 2-10 pN for other systems), which can, potentially, cause unspecific binding.

Later, when interactions were obtained during subsequent measurements, it became less clear what caused the abnormal shape of curves. A bigger subset of all of the curves was analyzed. The dynamic force spectrum (Figure 46) seems to indicate a high amount of multiplicity.

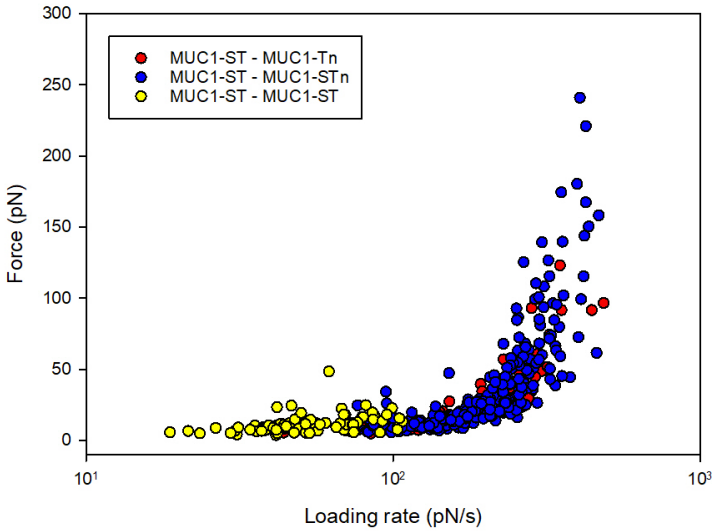

Figure 45: The distribution of forces measured for MUC1-ST and MUC1-Tn/STn. The data for MUC1-ST self-interactions were gathered using beads of size 3.36 μm, while the MUC1-ST - STn and MUC1-ST-Tn data was gathered using one bead of 2.01 μm and one of 3.36 μm. At this point, there is uncertainty around whether MUC1-ST actually interacts with the other two mucins.

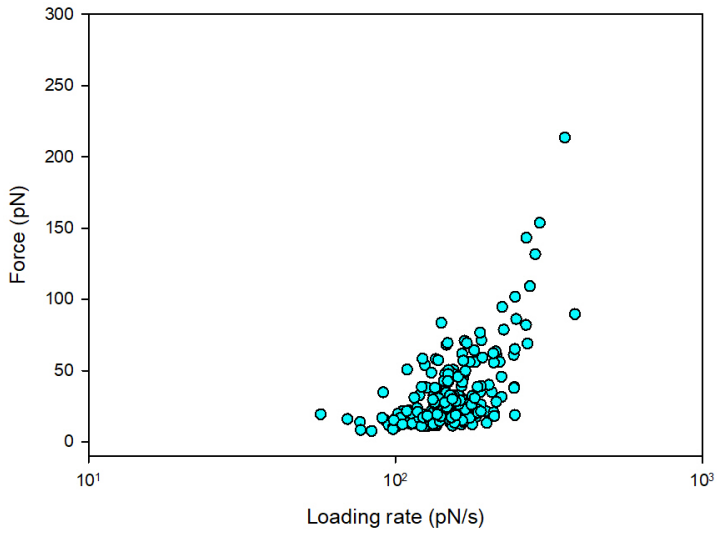

Figure 46: The dynamic force spectrum of unbinding forces for MUC1-T-self. This data was analysed in spite of strange-looking force-curves. The mucin was immobilized onto beads of size 2.01 μm.

5.5.7 Interactions between a more highly glycosylated mucin with itself

The fully glycosylated mucin TR-PSM-H8 (porcine submxillary mucin, MUC1, with 31, 17, 12, 40 : -mono, -di, -tri, -tetra, NeuNGl - N-glycolylneuraminic acid) was studied, as an example of a fully glycosylated MUC1. It was found that this mucin was easy to work with as the strength of the interactions obtained was relatively low, compared to interaction that were often observes between MUC1-Tn and -STn.

The dynamic force spectrum for this mucin is shown (Figure 48), together with a histogram that shows the distribution of forces obtained for this system (Figure 49). The DFS of TR-PSM-H8 and is also compared with the dynamic force spectrum for the less glycosylated, cancer-associated MUC1-Tn ans -STn (Figure 50). It shows a difference in the strength of interations of this mucin at a given loading rate, compared to the self-interactions between the less glycosylated mucins MUC1-Tn and MUC1-STn.

Enough data was gathered for this system to perform a Bell-Evans lifetime analysis. The data was divided into ten subdistributions (Figure 51) that resulted in histograms with a good normal distribution (Figure 52) and 53), nine of which could be used for a Bell-Evans lifetime analysis (Table 5).

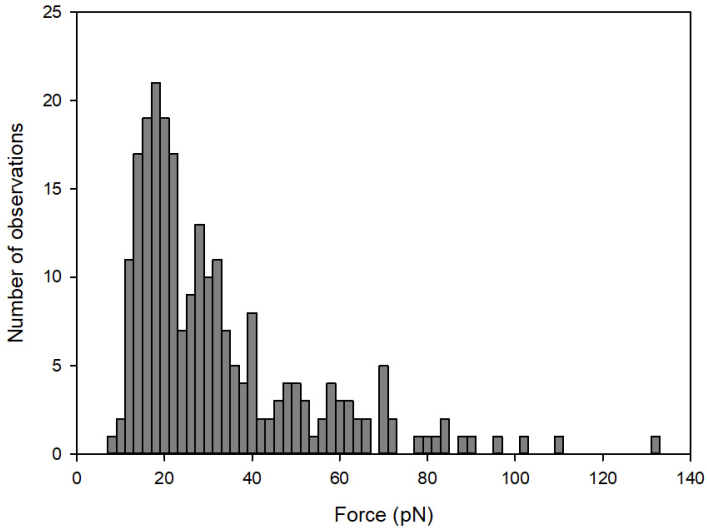

Figure 47: The distribution of unbinding forces for MUC1-T-self. This data was analysed in spite of strange-looking force-curves.

Table 5: The calculated parameters for the sub-distributions of the dynamic force spectrum for interactions between MUC1-protein TR-PSM-H8 - self. The bottom row shows the averaged values for the parameters. 10 sub-distributions were made, but only the first six characterized the first barrier of the self-interactions of this mucin. Parameters could not be calculated for the second barrier.

	Bell-Evans analysis				**Constrained fit**	
N	$<\mathbf{r}_f>$ **(pN/s)**	$\boldsymbol{f}$*** (pN)**	$\mathbf{x}_\beta$ **(nm)**	$\mathbf{k}_0$ (s^{-1})	$\mathbf{x}_\beta$ **(nm)**	$\mathbf{k}_0$ (s^{-1})
25	43.9	8.0	2.44	0.21	0.22	5.42
32	51.4	9.0	1.82	0.40	0.22	4.51
43	59.3	10.6	2.20	0.10	0.22	3.89
60	70.2	13.4	1.39	0.24	0.22	3.04
96	82.0	15.1	1.09	0.38	0.22	2.92
105	96.5	19.3	1.00	0.20	0.22	2.42
-	**-**	**-**	**1.66**	**0.26**	**0.22**	**3.72**

5.5.8 Summary of interactions between mucins

Interactions between all of the available mucins: MUC1-Tn/STn/T/ST and also unglycosylated MUC1 have been studied. Conflicting results have been obtained for some of the systems. MUC1-ST have shown to interast with MUC1-Tn and

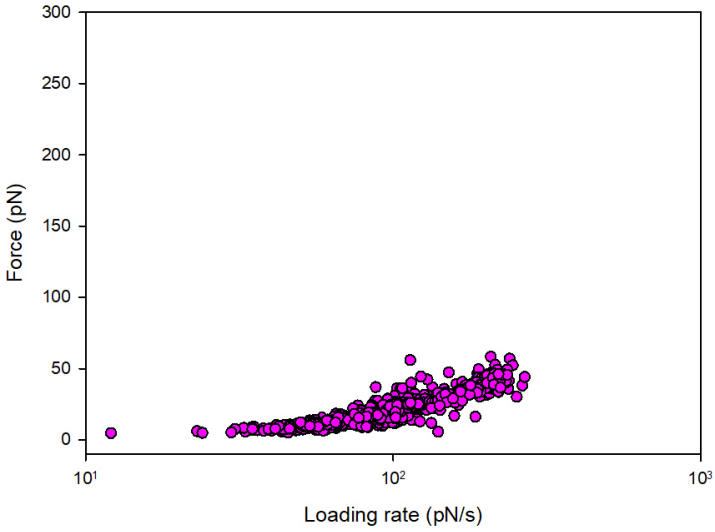

Figure 48: A dynamic force spectrum showing the distribution of unbinding forces between TR-PSM-H8 - self.

MUC1-STn in some cases, but not others. Some of the mucin interactions have not been studied extensively, or specifically: only one or two samples have been studied. Conflicting results have been found for relatively well-studied systems, where 6-12 samples were studied and several thousand interactions were observed. Based on this, when only a few samples were studied, it was decided that not enough data was available to draw conclusions yet.

The dynamic power spectra of self-interactions between all of the studied mucins have been compared (Figure 54). MUC1-Tn self-interacts, but it is difficult to say anything about their frequency at this point. It was believed that MUC1-Tn had self-interactions quite frequently, but MUC1-Tn was the first molecule studied during this work, before the realization that the force beads are pushed together with was an important factor. The MUC1-Tn and MUC1-STn were among the best investigated samples in this study. Although the frequencies of interactions are difficult to estimate with certainty, it was noticed during these experiments that MUC1-STn seemed to be more reactive than MUC1-Tn. From the dynamic power spectrum it is otherwise possible to see that the overlap between the MUC1-Tn and STn data is almost 100

It was found that MUC1-Tn and -STn had interactions with themselves and each other. MUC1-Tn and STn were not found to interact with MUC1-T. It was found that MUC1-T - self and MUC1-ST - had abnormal force curves. These were first believed to be unspecific interactions, but are now thought to have been caused

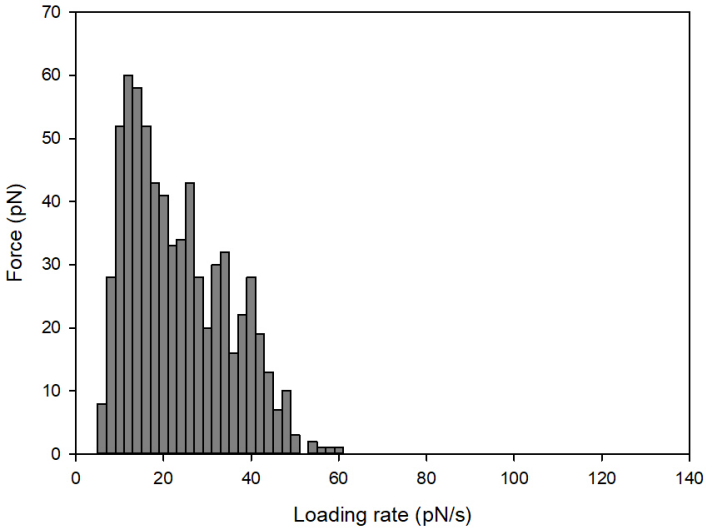

Figure 49: The distribution of unbinding forces between TR-PSM-H8 - self.

by high degree of multiplicity. The curves for these interactions did not have the stretching profile that was expected to be seen when an elastic polymer like MUC1.

MUC1-T was found to interact with itself, but was not found to interact with any of the other mucins. MUC1 showed interactions in very rare cases, or not at all, and there is high certainty that the unglycosylated MUC1 does not easily interact with any of the other mucins.

Conclusions can be drawn for the interactability of some of the systems that have been studied during this work. However, due to contradicting data for some of the mucins, it has been chosen to avoid drawing conclusions for these, as they might create confusion about the certainty of the data. Although all of the mucins have been tested for self-interactions and interactions with each other, unfortunately, some of the results are far from clear (Table 6). More information about the reasons for the choices made can be obtained from the discussion section.

5.6 Interactions between MGL and polymers with GalNAc

5.6.1 MGL vs MUC1-Tn

Experiments showed that MGL and MUC1-Tn did have interactions in 10 mM HEPES, pH 6.8, without $CaCl_2$ and $MnCl_2$ in the solution. It was thus found that the protein seemed to bind MUC1-Tn in a calcium-independent manner. A limited amount of data was obtained for this system due to issues with EDC (the crosslinking agent) and the optical tweezers. As the MGL-protein has a shelf-life

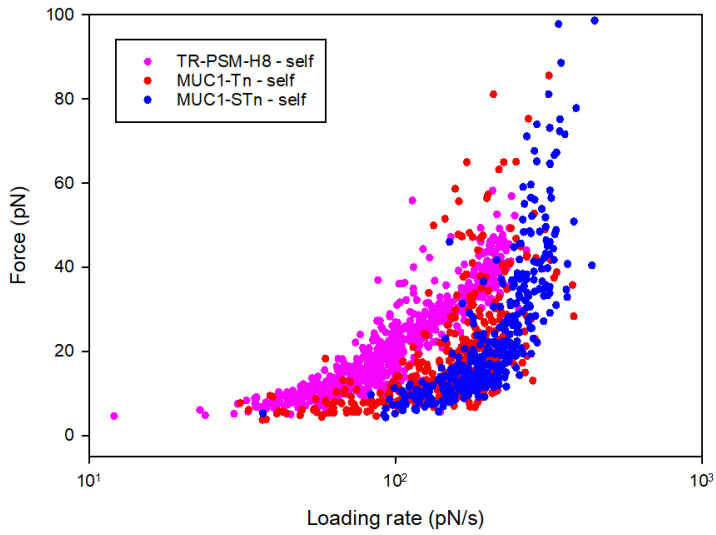

Figure 50: A comparison of the dynamic force spectra of fully glycosylated MUC1-mucin TR-PRM-H8 - self, and the cancer associated mucins MUC1-TN - self and MUC1-STn - self.

Table 6: The result of crossing MUC1-mucins with different glycosylations. A (+) indicates interaction while a (-) means that the mucins hardly ever were found to interact. All of the interactions have been studied, however, conclusions for some of the mucins could not be drawn (?) due to conflicting results or the desire for more data due to experimental difficulties.

Mucin	**MUC1**	**MUC1-Tn**	**MUC1-STn**	**MUC1-T**	**MUC1-ST**
MUC1	-	-	-	-	-
MUC1-Tn	-	+	+	?	+
MUC1-STn	+	+	+	?	+
MUC1-T	-	?	?	+	?
MUC1-ST	-	?	?	?	+

of only 3 months in solution, it was chosen to not continue to use the protein any further to avoid introducing errors due to degradation of MGL.

The interactions of MGL and MUC1-Tn differed from intractions observed for many other systems in that double and tripple bond ruptures could be observed signifficantly more often (Figure 55).

No control experiments where performed for this combinationm, but it is unlikely that the MGL-protein can have interactions with NH_2-functionalized beads, as MGL binds sugar moieties. Earlier control experiments have shown that no interactions

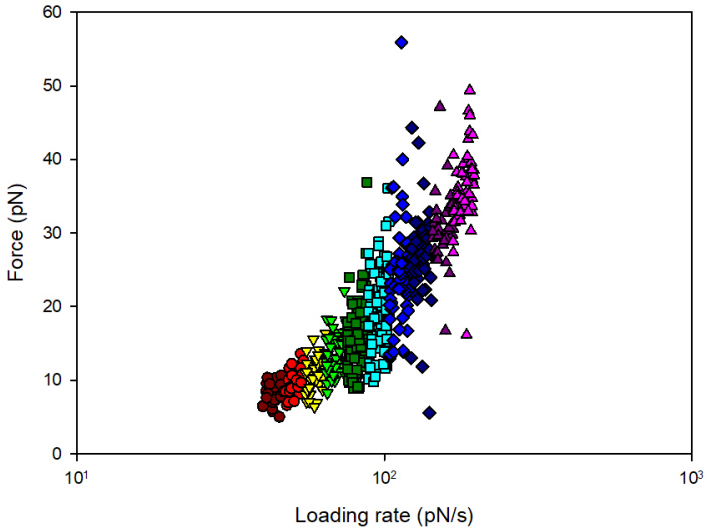

Figure 51: The dynamic force spectrum shows the sub-distributions of unbinding forces between TR-PSM-H8 - self.

were found between the bead surface and MGL. MGL was also not tested for binding to unglycosylated mucin due to no availability of a sample of such mucin at the time of this work.

The dynamic power spectrum of interactions between MUC1-Tn and MGL (Figure 56) is based on 230 interactions. The shape of the distribution can imply that many of the interactions analyzed are multiple.

5.6.2 MGL vs PAA-450K-40

PAA-450K-40 is a polyacrylamide (PAA) polymer of 450 kDa, with 40% GalNAc. This polymer was tested for interactions with MGL, to make sure the MGL actually interacted with the GalNAc group independently of the backbone it was attached to. MGL was not found to interact with PAA-450K-40. However, the amount of data for this system is limited (243 attempts).

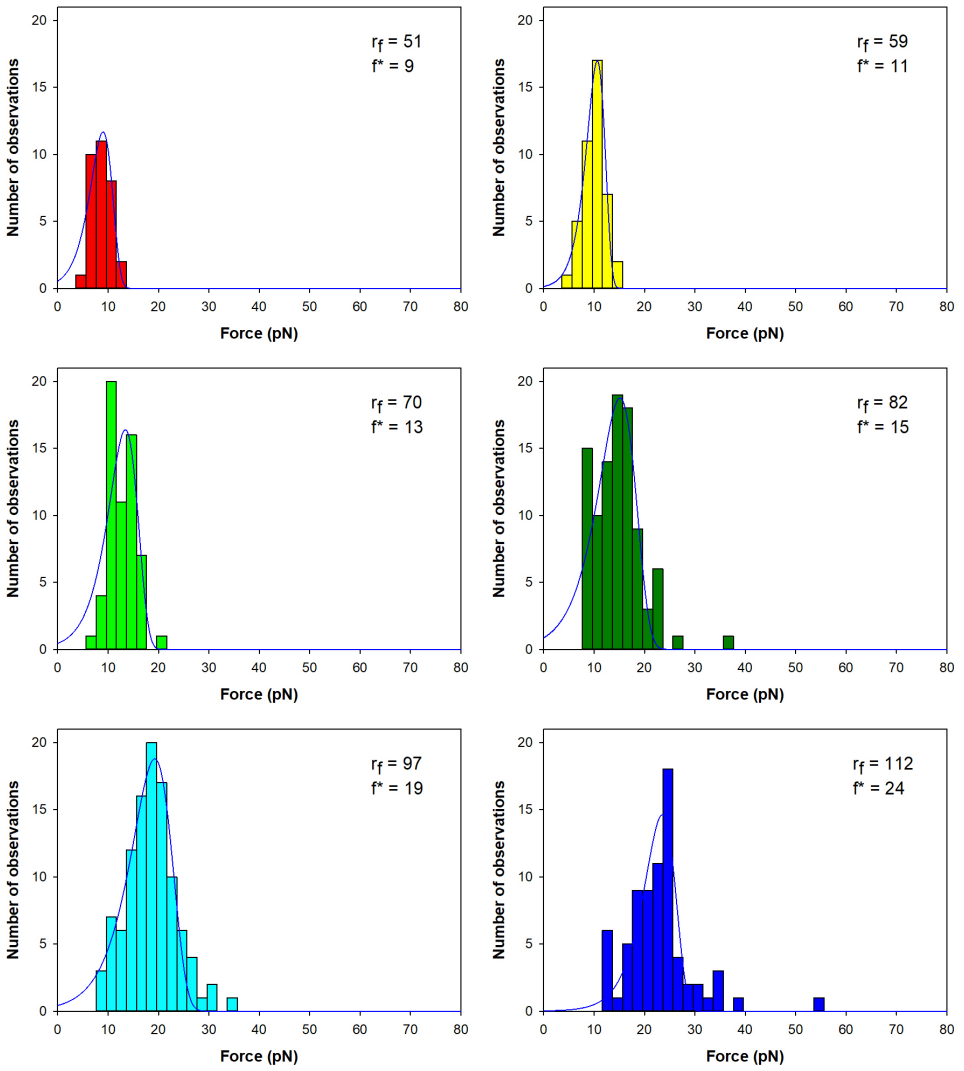

Figure 52: Histograms obtained for forces in sub-distributions of loading rate, for interactions between TR-PSM-H8 with itself

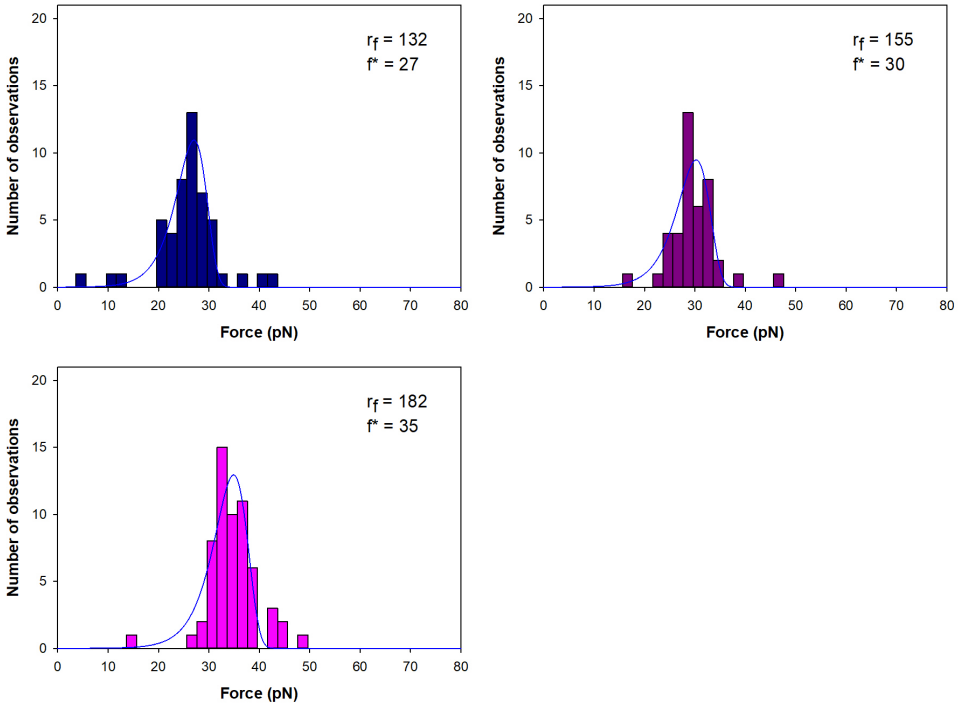

Figure 53: Histograms obtained for forces in sub-distributions of loading rate, for interactions between TR-PSM-H8 with itself

5.7 Polyacrylamide-GalNAc

Polyacrylamide (PAA) 450K (450 KDa) polymer with GalNAc groups was used to investigate whether it is the GalNAc-groups that are responsible for the characteristics of the MUC1-Tn interactions, and that the interactions are not dependent on a peptide backbone. This polymer was also used to try to obtain information on whether a polymer with GalNAc groups would result in interactions similar, but more-or-less multiple than those for the MUC1-Tn glycoprotein.

A 30 KDa PAA polymers, with Gal/GalNAc/Glc/GlcNAc were also used to study the self-interactions of th mentioned groups. These polymers were investigated to gain more insight of the role of the N-acetyl group andf the C4-OH group of GalNAc, and to investigate whether it was actually possible for the Gal to have self-interactions, as was, seemingly, observed for MUC1-T.

5.7.1 PAA-450K

Two PAA-450K polymers were investigated: PAA-450K-40 and PAA-450K-80, where the last number represents the percentage of GalNAc attached onto the polymer. The 450 KDa PAA polymer was found to be challenging to work with, as it fre-

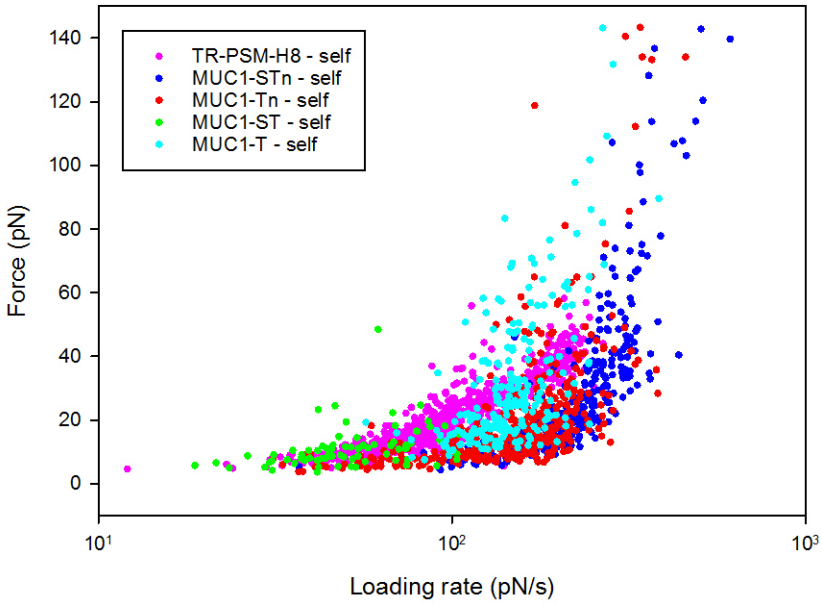

Figure 54: A comparison of some of the data gathered for self-interactions between the different mucins studied. As seen, data for MUC1-ST - self and MUC1-T - self is only available for a small part of the loading rate spectrum. This is due to gathering the data on beads of different sizes: 3.36 μm and 2.01 μm, respectively. The data for MUC1-STn was also gathered using 2.01 μm beads only. Interactions between TR-PSM H8 - self were gathered using both sizes of beads.

quently had very strong interactions, which lead to the beads being pulled out of the traps. This is not considered to be well represented in the dynamic force spectrum and the histogram of interactions.

A dynamic force spectrum (Figure 57) shows a comparison between MUC1-Tn - self (531 datapoints), PAA-450K-40 - self (94 data points) and PAA-450K-80 (292 data points). The histogram (Figure 58) shows that much higher forces were obtained for the PAA-450K-80 polymer against itself than for MUC1-Tn - self, where the most common forces for PAA-450K-80 is twice as high as for MUC1-Tn - self. Examples of interactions between the PAA-450K polymers can be observed in Figure 59:

5.7.2 Glycosylated PAA for investigation of the N-acetyl group of GalNAc

A short study was done to investigate whether it was possible to infer something about what groups on the GalNAc could be important for the interactions that have

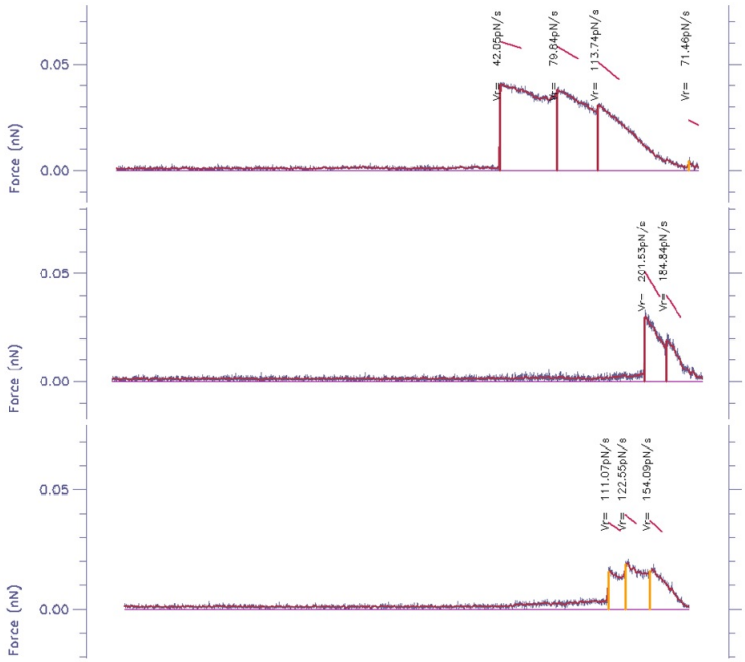

Figure 55: Double and tripple interactions was a common occurence while studying the interactions between the MGL-protein and MUC1-Tn. This might be due to the dimerization and trimerizations of the protein, which causes two or three carbohydrate-binding sites to be located in close proximity

been observed so far. For this, biotinylated PAA-polymer from lectinity was used. Four different polymers were investigated: PAA-βGalNAc, PAA-βGlcNAc, PAA-βGal and PAA-βGlc. It was suspected that the N-acetyl group could be involved in the interactions between the GalNAc groups. If this was the case, both PAA-GalNAc and -GlcNAc should be able to self-interact, but not PAA-Gal and -Glc. Additionally, it was of interest to find out whether the PAA-Gal polymer would have interactions.

The interactions were not analysed, but the frequency of interactions was investigated. As a control experiment, beads with PAA without glycosylation were tested against each other. It was found that PAA did not appear to exhibit any self-interactions (0/366). No control experiments were conducted to test whether glycosylated PAA did or did not have interactions with unglycosylated PAA, due to unavailability of different sizes of beads for these experiments. Working with a shorter PAA-polymer than the PAA-450K polymer was much easier. From the summary of the frequency on interactions (Table 7) it is possible to see that all of the investigated polymers exhibited interactions.

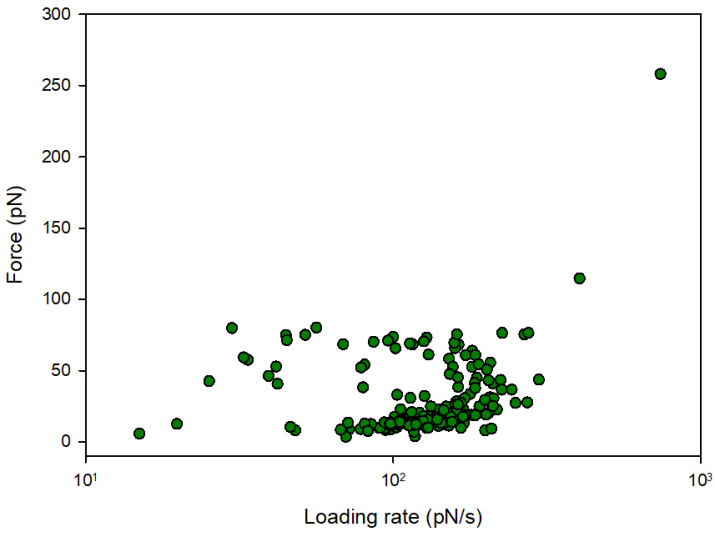

Figure 56: The dynamic power spectrum of interactions between MUC1-Tn and the protein MGL. The distribution is based on 230 interactions.

5.8 Fumonisin

The work done on the interactions between fumonisin is not related to cancer glycans. These experiments have still been useful in the investigation of glycans and their binding partners, and they have contributed to the broadening of the knowledge about such interactions.

5.8.1 Interactions between fumonisin and yeast

As a control experiment, NH_2-functionalized polystyrene beads were alowed to interact with wild type (WT) yeast cells. It was found that only 3/199 curves contained interactions, and that we could proceed with the experiments where fumonisin would be immobilized onto the surface of NH_2-functionalize beads. Fumonisin was tested against intact WT yeast cells, and also genetically modified cells (mnn9-Δ FB1 yeast). The genetically modified cells have a disruption in one of the subunits of α-1,6 mannosyltransferase, which causes aberrations in the cell wall structure and deficiency in mannosylation of the surface proteins. This should result in increased exposure of cell wall proteins and β glucan-layer below the mannan layer.

WT and mnn9 mutant cells were allowed to react with densely fumonisin-coated polystyrene beads. Even when the bead was pushed strongly against the cell, observed as deformation of the cell, there were very few interactions registered between the bead and the cell. Dwell times up to 10 seconds were used in these experiments,

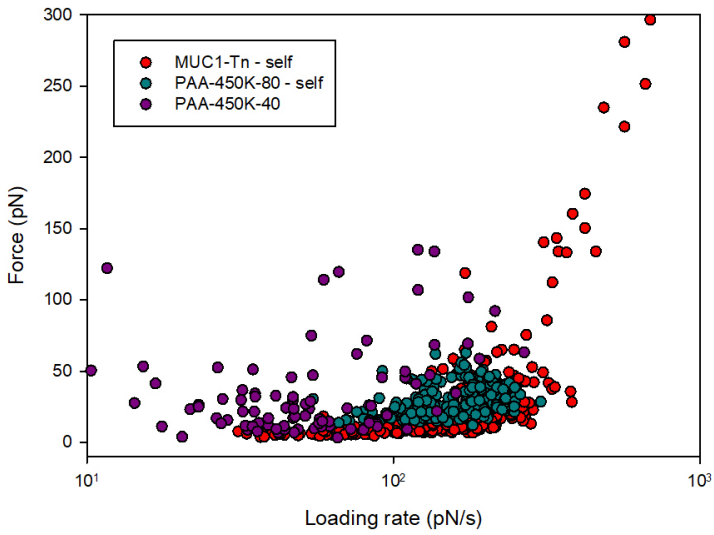

Figure 57: The dynamic power spectrum of interactions between MUC1-Tn - self, PAA-450K-40 - self and PAA-450K-80 - self.

with no success in obtaining interactions. For WT yeast, interactions were observed in 39/504 curves. For mnn9 mutants, 0/103 curves showed interactions.

5.8.2 Interactions between mannan-coated beads

It was attempted to measure interactions between mannan-coated beads. It was found that mannan is highly inert, with interactions happening under 1% of the time, even when pressing the beads together strongly (15-20 pN) and having a hold-time (1 s). In addition, many of the mannan-mannan interactions did not seem to be specific, where many were due to entanglement of molecules (Figure 27, lower left frame).

5.8.3 Interactions between fumonisin and laminarin

As β glucan is an insoluble polymer, laminarin, which is hydrolyzed β-glucan from algae was instead chosen to test the interactions between fumonisin and β-glucan. Fumonisin was shown to have strong interactions with laminarin-coated beads. Laminarin was found to bind fumonisin with a high frequency with little force required to initiate the interactions; 1620/3464 curves showed interactions. However, the control experiments showed that when a laminarin-coated bead was let to interact with an NH_2-functionalized bead, 21/180 curves showed interactions.

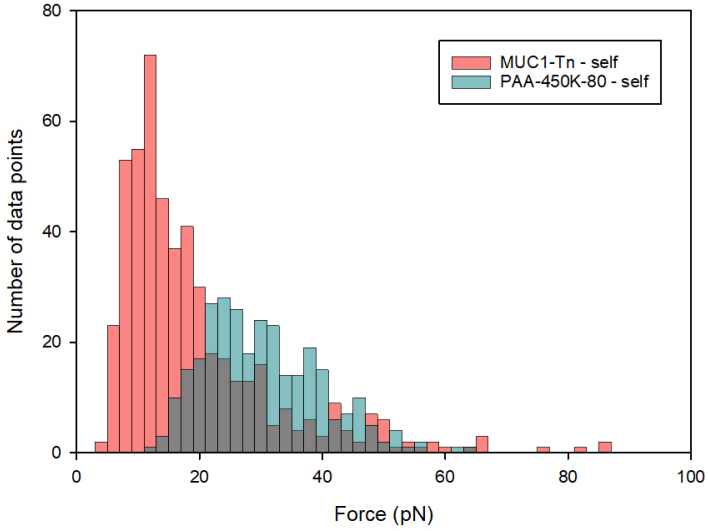

Figure 58: The dynamic power spectrum of interactions between MUC1-Tn - self, PAA-450K-40 - self and PAA-450K-80 - self. The PAA polymer was found to often exhibit multiplicity of interactions.

A dynamic force spectrum (Figure 60) and and a histogram of the distribution of unbinding forces (Figure 61) was made based on on the data gathered in November 2016 - January 2017. Althought there is around 950 intreactions between fumonisin and laminarin, a very good Bell-Evans analysis of the dataset could not be done due to the way the dataset looked (Figure 62), where data gathered in September and November - January did not show complete overlap.

5.8.4 Interactions between fumonisin and chitosan

Because chitin (component of yeast cell wall) too is highly insoluble, chitosan was used instead. It was impossible to immobilize chitin onto beads for use with optical tweezers due to its gelling properties. Chitosan-coated beads were found to have very strong interactions with fumonisin-coated beads when binding was achieved; 75/423 curves showed interactions. However, the control experiments showed that 14/112 curves showed interactions when a chitosan-coated bead was let to interact wit a NH_2-functionalized bead.

Very few interactions were obtained for fumonisin and chitosan (Figure 63) due to the high strength of the interactions. Both high concentration of chitosan and a concentration ten times lower resulted in interactions so strong that the beads were pulled out of the traps before a reasonable amount of interactions could be

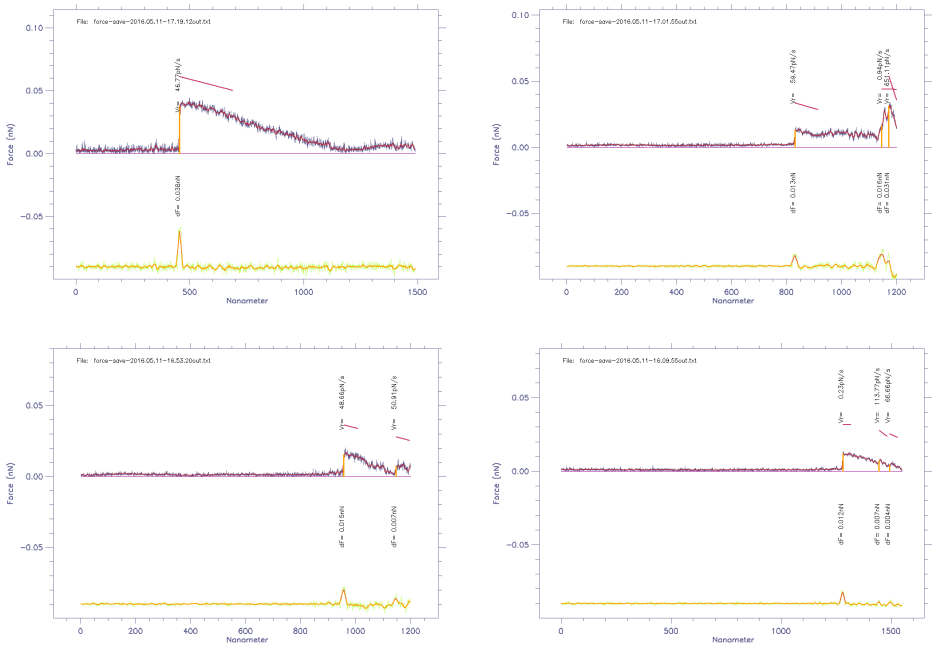

Figure 59: Examples of some unspecific unbinding events for PAA-450K-80. Many unspecific and multiple interactions were observed for this system. The poor quality of the figure is due to the limited export options of the analysis program.

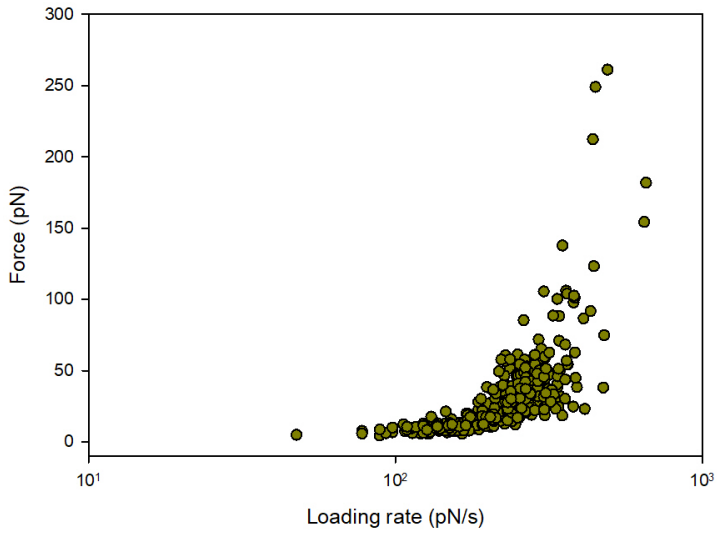

Figure 60: A dynamic force spectrum showing the distribution of unbinding forces between fumonisin B1 and laminarin.

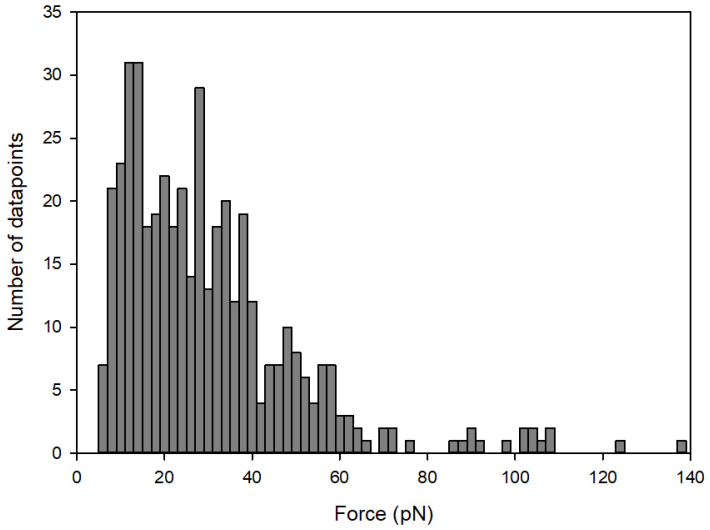

Figure 61: The distribution of unbinding forces between fumonisin B1 and laminarin.

Table 7: An overview of self-interactions between 30 kDa PAA-polymer with different glycosyl groups. The interactions were gathered from multiple pairs of beads.

Polymer	**Interactions**	**Total number of curves**	**Percentage (%)**
PAA-GalNAc - self	319	698	46
PAA-GlcNAc - self	101	561	18
PAA-Gal - self	52	392	13
PAA-Glc - self	153	831	18

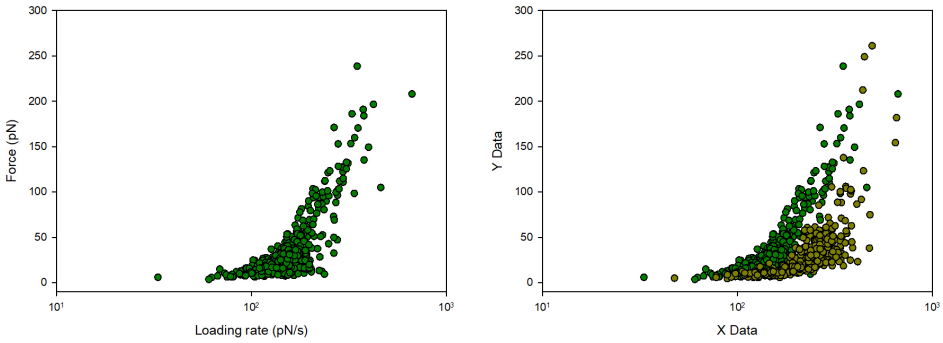

Figure 62: Dynamic force spectrums of interactions between fumonisin B1 and laminarin. The spectrum to the left shows interactions gathered in september 2016, while the right one shows a comparison of interactions gathered in September and those gathered in November - January. It is suspected that there is much more multiplicity of interactions from September due to the EDC being completely new.

obtained. As chitosan-coated beads also stuck to the surface of the liquid chamber a short time after measurements began, new liquid chambers had to be prepared frequently.

5.8.5 Summary of fumonisin-experiments

A summary of the fumonisin experiments together with some previously known data [5] can be seen in Table 8 and 9, which should give a better overview of all of the data, including the control experiments. As seen, neither the wild-type FB1 *S. cereviciae* nor the mannose-deficient mutant mnn9 Δ FB1 were found to bind the fumonisin. Mannan did not bind fumonisin, while laminarin (algeal β-glucan) and chitosan (deacetylated yeast chitin) did.

[5] Vuković, Renata, and Vladimir Mrša. "Structure of the Saccharomyces cerevisiae cell wall." Croatica Chemica Acta 68.3 (1995): 597-605.

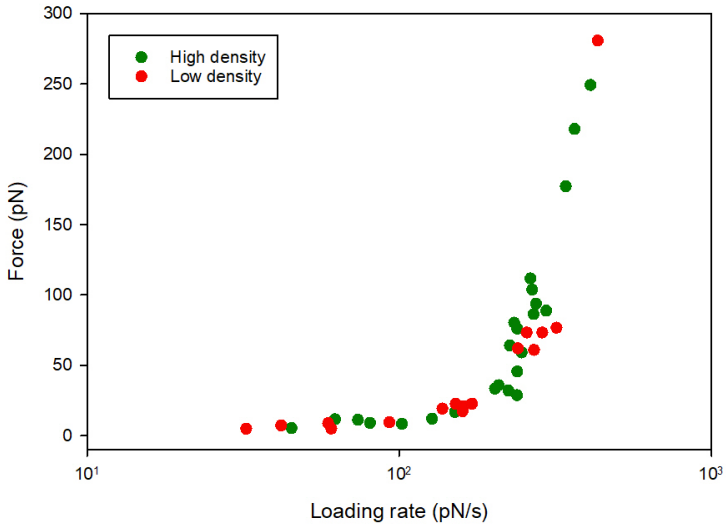

Figure 63: The histogram shows the distribution of the few unbinding forces obtained between fumonisin B1 and chitosan.

Table 8: A summary of all of the fumonisin-related experiments.

Interacting pairs	**Curves with interactions**	**Total number of curves**
WT yeast - amino bead	3	189
WT yeast - fumonisin	39	504
Mnn9 FB1 yeast - fumonisin	0	103
Fumonisin - amino bead	7	164
Fumonisin - carboxyl bead	4	320
Mannan - mannan	70	1195
Laminarin - amino bead	21	180
Laminarin - carboxyl bead	9	331
Chitosan - amino bead	14	112
Chitosan - carboxyl bead	17	55
Fumonisin - mannan	23	282
Fumonisin - laminarin	1620	3464
Fumonisin - chitosan	75	423

Table 9: The interactions found in crossing-experiments, to elucidate the parts of the yeast cell wall that were able to bind to fumonicin. *From conference paper, footnote 5. ** Binds rarely, see Table 8. A (?) means that it has not been tested whether the molecules interacted.

	COOH beads	**NH_2 beads**	**Laminarin**	**Chitosan**	**Mannan**
COOH beads	NO	NO	Rarely	YES	?
NH_2 beads	NO	NO	Sometimes	YES	?
Laminarin	Rarely	Sometimes	YES*	YES*	NO*
Chitosan	YES	YES	YES*	YES*	NO*
Mannan	?	?	NO*	NO*	NO*
Fumonisin	NO	NO	YES	YES	NO

6 Discussion

Being able to study different systems of molecules that interact has been very useful to gain understanding about important aspects of doing such experiments. Working with such a system has also been challenging. As it is not possible to observe directly what is interacting, it is important to be confident in the set-up and execution of the experiments, and in that the analysis has been conducted correctly.

In theory, it should be simple to determine whether molecules immobilized on two beads do interact or not. As a first step, the control experiments are carried out, and if they are negative, it is likely safe to assume that one can proceed with the experiments. However, as it is not possible to observe in any way what is actually bound to the beads, clever control experiments should be carried out continuously and large amounts of data is needed to rule out outliers. A lot of time went into figuring out how to prepare the samples and perform the experiments in such a way that the result would be reproducible and credible. This has made it possible to gain understanding of factors that might influence the results, and has lead to a few suggestions that can, hopefully, improve future measurements and analysis.

6.1 Experimental challenges and potential solutions

6.1.1 Avoiding contamination

It was found that neither amino-functionalized beads not carboxyl-functionalized beads interacted in MilliQ water (pH 5.5 - 5.7). There should not be any change in neither the alkyl arm or the primary amino group in HEPES-buffer of pH 7.2, and thus, the surface of the beads should continue to be inert. The beads should also not exhibit any interactions during the control experiments, where beads experience the same treatment as beads with immobilized polymer, but where no polymer is added. During the control experiments it was found that some contamination had gotten into the samples and was immobilized on the surface of the beads. Whatever this contamination was, it was able to cause some interactions between the beads. Many steps were taken to reduce this contamination to a minimal level - this too is described in the results-part. It is recommended that the same measures are taken when preparing future samples for experiments with optical tweezers.

As a first step in these experiments it is important to be able to identify observations that indicate that something might have gone wrong during the sample preparation. One of the main problems in the beginning of the experiments was seeing foreign objects float around in the sample, stuck to the bottom of the liquid chamber or the beads. At other times, polymer behaviour was observed in control experiments, where there was no polymer added. This is a sign of poor hygiene. If the inside of the liquid chamber appears to be contaminated, measurements in such an environment might not be reliable. As the concentration of polymers in solution for immobilization on the beads is about 0,2 mg/ml, it is understandable that even a small speck of dust that makes its way into the sample can make a difference in the surface decoration of the beads.

It was found that the most basic step in discovering such impurities was to begin the experiment by examining the surface of the liquid chamber. During these experiments, the impurities in the samples have been found to originate from various sources: buffers, glasses used, dust that gathered on the Eppendorf tube rack, and possibly unknown sources that may have contaminated the stock solution of the biopolymers. This showed that it is very important to work in an environment that is as clean as possible when preparing samples for experiments with optical tweezers. Samples of high purity are important in such experiments because contaminants can both result in interactions, but also be pulled up into the traps during measurements, if they have a refractive index higher than that of the liquid around.

Even after taking all of the measures mentioned earlier, some interactions were still observed in the control experiments. It is unknown what type of molecules these interactions could originate from. Most, but not all of the interactions had an abnormal shape that resembled peeling, which indicates that some kind of polymer is attached to the surface of the beads. As glasses and glassware seemed to be the biggest source of contamination in these experiemnts, it was suggested that cleaning glasses with plasma might reduce the interactions even further, to below 5%. This could be done if 5% interactions from contaminants is unacceptable, but might make beads stick to the glass surface strongly, which was why BSA-coating of glasses were performed.

It was found that beads in boric acid, boric acid and EDC, HEPES, and beads treated with all of the aforementioned solutions exhibited a few interactions. At the same time, interactions were not found between beads in MilliQ water. The interactions here might originate from the surface of the bead itself, or from something getting stuck to the bead. The most surprising finding here is that there was some interactions in boric acid, but not in MilliQ water. As these have the approximately same pH - 5.8 and 5.5, respectively, it would be interesting to test whether there is some kind of contamination in the boric acid that is not present in MilliQ water. The boric acid was filtered using a 0.2 μm syringe filter, while the MilliQ water is much cleaner. It is possible that the filter cannot manage to filter out the smallest contaminants from the boric acid, or that it is the filter itself that is the cause of the contaminants. This can be tested out by suspending beads in MilliQ water that has been filtered using a syringe filter.

6.1.2 Avoiding interactions between bead and polymer

The ideal way the molecules would be bound to the surface is by one of the ends, while the rest of the polymer is free. When using EDC as crosslinking agent to immobilize the protein onto the beads, there is a possibility for any primary amine group to be linked to any carboxylic acid group. On the MUC1-protein there is only one amino acid per tandem repeat of the VNTR sequence that can be immobilized onto amino- or carboxylic acid-functionalized beads: threonine, which has a carboxylic acid group and asparagine that has two primary amino groups. The MUC1-molecule will also be able to bind the beads by its amino- or carboxylic acid-end. As the MUC1-molecules used here have 16-31 VNTR-repeats, there are

many points at which it can potentially be bound to the bead - some possibly more available than others. The molecules can also be arbitrarily oriented.

It is desirable that there should be free polymer ends protruding from the bead surface. However, experiments indicate the molecules are associated quite closely with the surface of the beads, as interactions far away from the contact point of the beads have been observed rarely. When the biopolymer does not have interactions with the bead surface, all interactions between two beads with polymers are assumed to be specific.

It was found that some of the mucins (MUC1-Tn, MUC1-ST) could have unspecific interactions with the bead surface. When the polymer is shown to interact with the surface of the bead, it is important to be able to distinguish interactions due to inter-polymer contact from those interactions arising between the polymer and the surface of the bead. One way to solve this is to have a very dense layer of mucin on the bead surface, but this would also lead to more multiple interactions, which is undesirable. This can be illustrated with what was found for the fumonisin-laminarin system earlier (Figure 62).

Another solution is to try to make the surface between the target mucin inert. There are possibly several ways of doing this. In these experiments, it was found that MUC1 did not interact with any of the mucins other than MUC1-STn, and it should also not be able to interact with the macrophage C-type galactose-type lectin (MGL), as it has no sugar groups. This mucin could possibly be used to coat the surface of the bead instead of having a very dense layer of interacting molecules. In other cases, MUC1-T seems to be a possibility, but this is discussed later. Hopefully, this will allow for a relatively low amount of mucins on the surface while reducing the frequency of interactions between mucins and the bead surface.

Another possible way to deal with interactions between bead and surface is to attach the polymer of interest to an inert linker polymer. It could then be possible to modify the analysis program to show at what distance from the surface the bond breaks. The additional criterion for identifying a specific interaction would, with this addition, be that the distance where the bond breaks should be greater than the length of the polymer with the linker. This is likely to decrease the amount of interactions that are accepted as specific, if there is a high possibility that the molecule of interest might bind the surface of the bead at more than one point. If it is desirable that the biopolymer is bound to the bead surface the least points along the chain, high-affinity binding sites must be used on the linker. An example of such can be biotin and streptavidin, which forms a highly stable complex through non-covalent bonds.

6.1.3 Identifying issues by sorting the data

It is strongly recommended to save all gathered data, and to save force-measurements for each pair of beads separately, as some pairs may behave differently than others. Looking back at such information can be useful for detecting atypical behaviour. This was useful in these experiments to exclude pairs of beads that were calibrated incorrectly or not at all, to identify the difference between data gathered using small

and big beads, to identify the change in the activity of EDC, and to identify and quantify the highly variable coating of beads. When data gathered from different days was examined, it was found that there was more spread in the data gathered in the morning, which can be attributed to that the power of the lasers had not stabilized. By saving data from different pairs of beads separately, it was later possible to evaluate the results: did all of the interaction originate from a single pair of beads?

Data must always be gathered using several different pairs of beads. As the size of the beads varies slightly, there will be slight variation in the placement of the data points in the dynamic power spectrum. If all of the data originates from a single pair of beads, the spread of the data can be unnaturally small. Because the polystyrene beads have some variety in size it is also useful to measure interactions between several different pairs of beads to include this variation. It is also always important to establish the normal interaction behaviour in a sample, which is only possible by assessing the behaviour of several pairs of beads. In these experiments, it was found that at least 6 beads should be tested before anything could be said about their behaviour. If a behaviour is observed where half of the beads experience interactions and the other half does not, it is important to increase the concentration of polymer in the immobilization reaction.

6.2 Challenges with quantifying frequency of interactions

One of the ways it would be highly desirable to be able to reliably compare different systems is to measure not only the strength of interactions, but also their frequency, which might say something about the availability of the binding groups. This has not been possible during these experiments. This is due to several factors, discussed below. Thus, the interaction frequencies presented in this work should not be considered a good measure of actual degree of interaction between the polymers.

6.2.1 Variation in the efficiency of the immobilization procedure

It was noted during the experiments that MUC1-Tn interacted in the early stages of the measurements. With time, the frequency of interactions decreased, until there were almost none. Sometimes the lack of interactions can be blamed on an inefficient immobilization procedure. This was later shown to be due to the degradation of EDC, the crosslinking agent used for immobilizing molecules onto the beads. Later, this was experienced again, and the solution was for a short time to add more EDC to the reaction mix. Soon after, the concentration needed to be further increased, until it was decided that it would be best to buy a new batch. In total, EDC had to be purchased three times during these experiments.

When comparing data gathered from time points about two months apart, there was a systematic change in the force measured at a given loading rate. It was difficult to say with certainty what this is caused by. It would be easy to eliminate temperature differences as a factor if there was a record of this available. However, as the tempetarure in the equation for calibrating the spring constant is in Kelvin

and not Celcius, even if there was a relatively big difference in temperature - for example of 7 °, this would still not be able to change the results much. It is from this clear that it is beneficial to not lump all of data together, or these effects would not have been apparent.

It is known that EDC loses its activity due to degradation because of absorbtion of moisture from the air [154] [155]. It is important to be aware of this. If degradation of EDC occurs during experiments where work is done using a polymer that has not previously been investigated, it is possible to conclude that there are no interactions. The solution to this was to prepare a single mixture of EDC and boric acid. Positive and negative control samples were prepared together with the samples that were to be investigated. The positive sampler was one that was known to exhibit interactions (MUC1-STn), while the negative one was beads with no polymers attached. While the positive sample should confirm a successful immobilization, the negative control tested the purity of the samples. If the positive control did not result in interactions, the immobilization procedure was believed to not have worked. If the negative control exhibited interactions, the other samples were not used further. As the same batched of solutions (EDC in boric acid, HEPES-buffer) were used to prepare all of the samples, interactions in a negative control could mean that the solution were contaminated. This is more time-consuming and leads to a higher sample consumption, but has proven to be useful to reduce error.

6.2.2 Inter-bead differences in density of immobilized polymer

During the early stages of the experiments it was found that there could be a big difference in the amount of molecules immobilized on the polystyrene beads. This was performed by choosing 10 pairs of beads and performing 200 approach-retract-cycles using beads covered with a molecule that is known to have self-interactions: MUC1-Tn. The result was that 0-22.5 % of the curves had interactions; 3 of these bead pairs contained no interactions.

The ideal case after immobilization would be that the polymer is bound to the bead at a single end, with the rest of the polymer protruding away from the bead surface. Ideally, the polystyrene beads should be covered with a fluffy layer of molecules, pointing outwards from the bead. In reality, it is not known how the surface of the bead looks. There is a high probability that many of the molecules are stuck to each other on the surface of the bead, creating some kind of unordered network; some might extend far from the surface of the bead, while others lie flat along the bead surface. Some molecules might have the tendency to clump together, or organize themselves into small bundles and create islands on the beads.

This can be due to factors like interactions or entanglement of the polymers, sedimentation of the beads during immobilization, uneven coating of the beads with reactive groups, or random variation. During the experiments with fumonisin, it was found that fumonisin and chitosan had a tendency to clump together in solution and also to make beads aggregate. This was solved by using sonification during the immobilization procedure. Sonification is a mild method of dispersing particles in solution and should not lead to denaturation of proteins, as long as it

is not done for a prolonged time.

If the difference in distribution on molecules on beads is combined with the variation in the immobilization efficiency in different samples, it's not possible to easily compare two samples. Constant mixing during the immobilization might even out the distribution of molecules. Several pairs of beads should be used from each sample to compare both the inter- and intra-sample variation.

6.2.3 Importance of the applied inter-bead force

During the experiments it was noticed that the amount of interactions could be strongly increased in two ways: by pressing the beads stronger together and by increasing the time the beads were held in contact. To increase the contact time of beads has been shown to efficiently increase the frequency of interactions. While the contact time can be controlled with high precision through the software, the amount of force the beads are pressed together with is a parameter that is difficult to control. Even though one bead approaches the other along a single axis, if the beads are not perfectly aligned, the beads will experience forces in all three directions.

It was found during the experiments that if two beads are pressed together with the high force, about anything is able to have interactions. If beads are pressed together strongly, some intermolecular bonds will at some point be created; an example is between NH_2-functionalized beads dissolved in MilliQ water. If even beads that are not covered with biopolymer have the ability to sometimes form interactions, it is likely not a good idea to press polymer-functionalized beads together strongly, as that they might exhibit unspecific interactions.

6.3 Analytical challenges

6.3.1 Descriminating between specific and non-specific interactions

It is important to know how the shape of force curves of specific interactions look before beginning the analysis. Normally, an elastic polymer will, when being stretched, give rise to a force vs. distance curve, where the rise in force prior to the bond rupture reflects the elasticity of the polymer. When multiple polymers are stretched, the shape of the curves can become more straight.

Some atypical interactions are easy to identify, such as peeling and entanglement. Another potential source of unspecific interactions is contaminants. It was believed that the interactions found for MUC1-T and MUC1-ST might originate from something else, as the curves had, what looked like, a linear increase in force from the baseline to the bond rupture, consistently. However, this was an incorrect assumption. As mentioned, curves with linearly increasing force can arise from multiple bonds. Some of these might stretch and rupture simultaneously, or almost simultaneously, which would result in a more linearly increasing force. These interactions should not be analyzed when it is known that the elasticity of the polymer does not correspond to what the force curves show. Instead, the amount of polymer on the surface should be decreased. If multiplicity is the problem, the curves should change shape when less molecules are available for interaction.

It was attempted to reduce the multiplicity of interactions between MUC1-ST - self by reducing the amount of mucin on the beads to 1/3 of the amount used normally. This did not result in a change in the shape of curves. This might have to do with that the majority of forces measured for this system are so weak that the force curves would not change significantly in the way it looks anyway, according to the worm-like chain model model.

6.3.2 Lifetime analysis

Lifetime analysis was performed for some of the interacting systems, where bond dissociation rate (k_0) and thermally averaged distance from the bound complex to the transition state (x_β) was estimated. A lot of datapoints is required for a good lifetime analysis. It is important to have enough data to be able to achieve a good fit of histograms for the sub-distributions of the dynamic force spectrum of interactions, and subsequently: a close to linear relation between average $f*$ and r_f for each of the subdistributions.

The only dataset that had enough data to perform a potentially good analysis was interactions between fumonisin and laminarin. However, after the analysis it was shown to be unsuitable because of high multiplicity (Figure 62) of the interactions of half of the dataset. The dataset for TR-PSM H8 - self interactions could potentially have a good fit of parameters, as the multiplicity of interactions seemed to be quite low, compared to the other systems. However, it seems that using two different sizes of beads resulted in a small break in the dataset, which made it difficult to achieve a good fit.

As many different systems were investigated, there was not enough time to collect and analyze enough data for many of them. During the analysis, many of the curves can exhibit features that make them unsuitable for analysis, such as noise, multiplicity and erroneous estimation of force (Figure 26). This can easily reduce the amount of available data to 25-30% of the amount of curves that contained interactions.

For most of the systems, interactions of high strength were included in the analysis. Some of the datapoints are likely to be due to multiple interactions, as the exhibited force is so high that is it unlikely to originate from a single interaction. The software that fit the histograms can handle a small amount of this kind of data, but the fit will be affected when there is a significant amount of data. This made it necessary to exclude even more of the data that could otherwise have been used for the lifetime analysis.

The remaining datasets were small, and even though many of the sub-distributions have a nice curve fit to the histograms, it is possible to see that there is a strong variation in the estimated parameters between sub-distributions (Table 3, 4, 5. To be able to obtain a good fit of these parameters using the Bell-Evans method, the data set must be much larger.

6.4 Interactions between different mucins

6.4.1 Interactions between naked MUC1 and different glycosylated MUC1-proteins

It was found that beads decorated with naked MUC1 did not have any self-interactions. When such beads were probed with beads with different glycosylated MUC1, again, no interactions were found, except for with MUC1-STn. The glycosylated MUC1-protein has an extended conformation due to steric hindrance of hydrophobic interactions. However, when the sugar groups are removed, the protein collapses into a globular shape, and thus does not have the same conformation as the glycosylated peptide [72]. It can be concluded that the protein, when it looks this way, has no self-interactions and no interactions with the sugar residues, but it can not be stated with absolute certainty that the the glycosyl groups do not interact with the protein core in any way when it is in its normal, extended conformation.

6.4.2 Association of Tn-self- and STn-self

By usingsing optical tweezers it was found that MUC1-Tn does self-interact. This was as expected, as it has previously been investigated [153, 132]. MUC1-Tn - self interactions have previously been measured using atomic force microscopy, which is less sensitive than optical tweezers. It was thus of interest to use a more sensitive method for investigating the strength of these interactions. From the spread of the data points for the MUC1-Tn - self-interactions, it seems that the analysis could be done better, which might result in a more narrow distribution. This was not performed due to time constrains.

MUC1-STn was also found to interact, which too was found in earlier studies [153]. An additional finding during this work was that MUC1-STn seemed to exhibit more frequent self-interactions than MUC1-Tn. Thus, the the sialic acid-group might actually contribute to the GalNAc-group being more available. The sialic acid might possibly affect the conformation of the glycan, as it affects the overall charge. Even though the sialic acid is deprotenated at the pH of the buffer used in these experiments, which gives the polymer a net negative charge, this charge does not appear to prevent interactions between MUC1-STn.

There is no signifficant differences between the dynamic force spectra of MUC1-Tn - self and MUC1-STn - self, and the estimated x_β are not very different: 0.39 nm for MUC1-Tn - self and 0.33 for MUC1-STn - self. The values are comparable to those found earlier for Tn - self and STn - self: 0.38 nm and 0.41 nm, respectively. The k_{off} values differ more though. This might mean that the interacting groups of the molecule are still the same, but that the sialic acid somehow affects the molecule in such a way that they come in close contact. As described in the theory, this should also result in a stronger bond. Biologically, this could mean that MUC1-STn might have a higher ability to aggregate proteins, and possibly lipids, with the same glycan epitope.

It might seem like there is a slight difference in the strength of most probable interactions, but this is not believed to be a reliable parameter, as it is affected

by the multiplicity of interactions, the spectrum of the accessed loading rates, and possibly other factors.

6.4.3 Association of MUC1-ST - self and MUC1-T - self

From the results, it seems that the bonds arising between MUC1-ST - self and MUC1-T - self are pecific, and thus arise from binding of sugars. In earlier studies it was found that MUC1-T mucins did not interact [153]. In this study, many self-interactions between these mucins were observed. This became evident especially when beads coated with these mucins were found to have interactions even when the beads were barely brought in contact.

It was found that MUC1-ST could interact with the surface of the bead. This is worrisome, as this can mean that some of the interactions found could actually originate be between the mucin and the bead surface. However, this is not very likely, as the shape of the force curves differed from that found in curves believed to originate between MUC1-ST - self (Appendix A). The strength of the interactions was also much higher than that found between MUC1-ST - self. It is thus believed that the majority of the interactions recorded for beads with MUC1-ST are due to the binding of mucins to each other. MUC1-T was not found to have interactions against the surface of the beads, and the data recorded for this system is thus believe to all originate from the binding between mucins.

The confusion about these interactions originated from the strange force curves for these systems, which displayed a linear increase in force as the polymer was pulled at. At high pulling speeds it is expected that there will be less energy for the mucins to disassociate on their own. It was difficult to understand why MUC1-ST - self interactions were only observed at lower loading rates, but not at higher, as the opposite should be the case. It was also strange that MUC1-T interactions were only observed at higher loading rates, but not at lower.

The understanding of this phenomenon came about after seeing the combined dynamic spectra for many of the systems investigated during this work. The smaller available beads (2.01 μm) were chosen for many of the experiments of association between the same kinds of mucins because they sedimented more slowly to the bottom of the liquid chamber. This was an advantage because many of the mucins bound strongly and rapidly to the glass surface - most beads of 3.36 μm could be completely immobilized after only 2-3 minutes on the glass surface. It was observed that immobilization often happened immediately upon contact with the glass. The smaller beads sedimented much more slowly.

The realization that the loading rate distributions followed a trend that was dependent on the size of the beads used to conduct the experiments gave clarity to the results. Thus, it is expected that the stronger forces and higher loading rates of the dynamic spectrum of interactions between MUC1-ST can be probed by using smaller beads (2.01 μm), and the lower forces and loading rates of MUC1-T - self will be accessible by using bigger beads (3.36 μm). The utilization of different size beads is suspected to also be the cause of the difference in the histograms that show the most probable force: the most probable force will likely be lower when bigger

beads are used.

Linear increase in force of the stretching curves of MUC1-T - self an MUC1-ST - self was hypothesized to possibly be due to several reasons. It was believed that the polymer could be less elastic than that with MUC1-Tn and -STn, but this is unlikely. The unglycosylated MUC1-molecule has a globular shape. Upon addition of a single saccharide to the glycosylation sited, the molecule is linearized. Upon the addition of a second saccharide, the rigidity increases, but it had not been found to be strongly affected by further elongation of the glycans. The increased rigidity is not expected to affect the elasticity of the molecule. The higher rigidity might affect how the molecule is immobilized on the surface of the bead, but this is just speculation. Furthermore, it would then be expected that the proteins with longer glycans (MUC1-ST and MUC1-STn) might show more linear force curves as well.

It was first believed that the bonds could be unspecific interactions between other things stuck to the bead surface. This was investigated, and it was possible to see from the galleries made for the two different systems (Appendix A) that the MUC1-Tn interactions were quite different from the interactions between some kind of contaminants on the surface (Figure 66 vs 68. In any case, it should be due to a lesser degree of elasticity of the molecules being stretched. This can be achieved by stretching more than one molecule at a time. However, when more than one molecule is stretched, it is not very likely that all of the bonds will be broken simultaneously, consistently throughout the measurements. However, this is believed to be the case. The shapes of the force curves might change with less molecule on the surface.

As it was shown that the surface of the beads would always have a small amount of contaminant immobilized to it, using a low amount of target molecule was not desirable without making the rest of the surface inert. Also, having a low amount of polymer on the surface does not seem like a good idea with polymers that can exhibit interactions to the surface, as MUC1-ST was found to do.

There is plenty of unanalyzed data available for experiments between MUC1-T - self and MUC1-ST - self. It might be of interest to analyse some this data at a later point, as it might be possible that more interaction curves with correct stretching profiles actually exist.

6.4.4 Interactions between the different mucins

The results from these experiments indicate little difference in self-association between mucins with different different tumor-associated cancer antigens. There seems to be a difference in the degree of interactions of some on the mucins: MUC1-STn seems to interact more easily than MUC1-Tn. As long as this is not because of some kind of difference in the concentration of the stock-solutions, or something about the glycosylation that affects he efficiency of the immobilization procedure, this difference indicates that the sialyl-group does not act as a steric hindrance, but instead makes the interacting groups more available for binding.

More work needs to be done in the investigation of interactions between MUC1-ST/-T self-interactions and interactions with other mucins. As the results have been

conflicting during this study due to what is likely to be the degradation of EDC and issues with setting up the optical tweezers correctly. After finding a satisfactory way of conducting the experiments, most of the experiments have been attempted repeated, but there has not been enough time to repeat them all.

It seems possible that MUC1-T and MUC1-ST might have self-interactions. Likewise, it is plausible that MUC1-ST has interactions with MUC1-Tn and MUC1-STn, as have been seen. If GalNAc is the interacting group, and it is not hindered from interacting by the sialic acid, this would be a logical result. However, it seems strange that MUC1-T has not been found to interact with any of the other mucins other than itself. As found during the investigation of vaccines against the T-antigen, GalNAc-Gal bond is highly flexible, and thus should not create considerable sterical hindrance of the GalNAc- GalNAc interaction. It could be possible that the Gal was bound to an important interacting group (C3) of the GalNAc, but it is then strange that MUC1-T and MUC1-ST self-interact. If the sialic acid does not hinder MUC1-ST from interacting with itself, it is also strange that MUC1-ST and MUC1-T do not seem to have interactions. It is possible that the new method for preparing and working with the samples could lead to a different result if the mucin crossing-experiments were repeated.

Even though clear conclusions are lacking for the interactions between MUC1 with cancer-associated glycans, a difference has been found in the interactions between MUC1-with such mucins and the fully glycosylated mucin TR-PSM H8 - self. From the dynamic force spectrum of the mucins (Figure 50) it is possible to observe almost no overlap between the data from the cancer-associated MUC1-Tn/-STn self-interactions and TR-PSM H8 - self interactions. The x_β value found for the interactions between TR-PSM H8 is 0.22 nm, which is quite lower than 0.33 and 0.39 - Tn-self and STn-self, respectively. However, TR-PSM H8 has a more complex glycosylation, including the presence of 40% NeuNGl (not present of human proteins), so there is a posibility that the interacting groups are different to MUC1-Tn and MUC1-STn. In short, these mucins thus seem to behave differently. It was found that the TR-PSM-H8 mucin had frequent, interactions, but they were not as multiple as those obtained for crossings between cancer-associated mucins. It might indicate that the interacting groups on TR-PSM H8 are spaced further apart than those on MUC1-Tn/MUC1-STn.

From the findings, it is still unknown whether the difference in self-association of mucins would grant cancer cells the metastatic characteristics they have.

6.4.5 The significance of MUC1-O-glycosylation in a biological context

It is difficult to say only from the mucin-crossing experiments what function the different cancer-associated antigens might equip cells with. A lot is known about lectins and their specificity for different types of sugar moieties. The binding of ligand can induce various different changes in the cell, activation of different signalling cascades, anti-apoptotic behaviour, migration, transcription and much more. It is likely that frequency of such events can be affected by glycoproteins by making certain types of cells associate more-or-less tightly. It was desirable to test this

using force spectroscopy. At his point, not much is known about any difference in self-association of the MUC1-protein decorated with cancer-associated glycans, as it seems like most of them might be able to self-associate, and the frequency of interactions is difficult to determine. From the frequency of MUC1-STn interactions vs MUC1-Tn - self, MUC1-STn might have a higher ability to aggregate membrane molecules posessing the STn-epitope.

From these experiments, no conclusions can be drawn for most of the systems. It was noticed that MUC1-STn seemed to exhibit more interactions than MUC1-Tn, but no certain difference was found between MUC1-T and MUC1-ST. The non-cancer-accosiated glycan differed from the cancer-associated glycan, but it is different from human glycans. Unfortunately, no conclusions can be drawn about the structures bound mucins might assume on the cell surface, whether they might create patches of aggregated glyco-protein, or whether certain mucins can inhibit the contact between cells.

The investigation of the interactions between TACAs is still considered to be an important topic, as the dysregulation of glycosylation in a cell does not only affect MUC1, but many different proteins and lipids that are either O- or N-glycosylated. This can change both their antigenicity and possibly also their conformation, as it has been found for MUC1 that the first three sugar moieties attached to a glycosylation site can result in a signifficant change in the conformation of the protein.

6.5 Interactions of the MGL-protein with MUC1-Tn and PAA-Tn

6.5.1 MGL - MUC1-Tn

Interactions between MUC1-Tn-coated beads and beads coated with MGL were studied. It was found that MGL appeared to not require the presence of calcium ions to be able to bind to mucins. This has been observed in earlier studies [132]. The MGL protein looks like a stalk with a globular head domain, and has the ability to create dimers and trimers. The globular domains of dimers and trimers are in close proximity and contain the carbohydrate-binding site. The interactions obtained were believed to originate from the binding between MUC1-Tn and MGL due to the high abundance of double and tripple bond ruptures, which would correspond to the three CRD-domains of MGL when it trimerizes. At the same time, curves with multiple ruptures were rarely obtained for MUC1-Tn - self, or any other systems. Thus double and triple interactions would be consistent with a dimerization or trimerization og MGL.

This is considered as strange, as MGL is categorized as a C-type lecting, which is a type of lectin that exhibits rearrangement of its carbohydrate-binding site upon binding of calcium. This calcium binding is believed to be essential for rearangement of the hydroxyl-groups of some sugars into positions that lead to binding. However, chrystallographic studies showed that different ligands have different orientations in the ligand-binding site og MGL [156]. Other studies have used inhibition assays, where calcium ions are chelated, which reduced the binding of GalNAc, but did

not extinguish it completely [157]. MGL has been found to bind its ligand even at calcium concentrations as low as 0.1-0.001 mM [157].

Even though binding in the absence of calcium was observed, it is not unthinkable that the strength of bonds created might be different from those in presence of calcium, or the lifetime of the complex can differ. It is possible that the Ca^{2+} ions are more important in stabilizing the complex than for the binding itself. Biologically, it is possible that signal transduction would not be possible without calcium.

Rupture-force data from MGL - MUC1-Tn in the absence of Ca^{2+} was not available, but it would be of high interest to see how the data would compare. If MGL indeed has the ability to bind GalNAc in the absense of Ca^{2+}, there is likely to be a difference in the xβ and k_{off} values for the two situations.

(Burde her ha en sammenligning om mulig)

It was found that the Macrophage Galactose Lectin (MGL) protein had frequent and strong interactions with the MUC1-Tn-protein, only glycosylated with GalNAc. The dynamic power spectrum showed a much greater spread of these interactions than those between MUC1-Tn - self. The data was subjected to analysis both early on during this thesis and also at a later point, to ensure that the spread of the data was not due to the change in quality of analysis. The result was not significantly different, with only a lowered frequency of multiple interactions included in the data. It might be that the spread of the data, as with the early MUC1-Tn - self, is the result of not letting the laser stabilize before calibrating the traps and conducting the measurements.

Because it contradicted data from other studies that MGL should be able to bind GalNAc in the absence of Ca^{2+}, the chemical reagents for the preparation of samples were thoroughly investigated for the presence of calcium as an additive. No mentions of calcium was found on the webpages of the producers of the chemicals used in these experiments. However, it is not unthinkable that trace amounts of it can have been present of some of the equipment that has been in contact with the sample.

6.5.2 MGL - PAA-450K-40

MGL was tested against PAA-450K-40. Previous studies have found that MGL binds specifically to GalNAc, and that increased density of the sugar on a synthetic peptide backbone results in increasing affinity of MGL. The increase in density was also suggested to promote trimerization of MGL [158]. A study was conducted, where GalNAc was bound to a polyacrylic acid backbone. Mouse bone marrow-derived dendritic immune cells were tested for binding and internalization of the PAA-GalNAc polymer, and were found to bind and internalize it through mMGL2 [159]. Humans only have one type of MGL: hMGL, while mice have two different types of MGL: mMGL1 and mMGL2 [160], which differes in their carbohydrate specificity. The hMGL and mMGL2 both bind GalNAc and Gal [82, 161]. Thus, this study demonstrated not only the internalization mechanism, but also that the binding og MGL does not require a protein backbone.

The PAA-450K-40 polymer was expected to have interactions with MGL, as

it had been demonstrated before that such binding happens [132]. Surprisingly, PAA-450K-40 was found to have plenty self-interactions, but was not found to interact with MGL. It was hypothesized that the GalNAc subunits might have been spaced out in an unfavourable way, so that steric hindrance might have prevented interactions. However, due to problems with chemicals and with the optical tweezers early during this study, it is believed that technical problems might be the cause of the results.

6.6 The interactions of glycosylated PAA-polymers

6.6.1 PAA-450K

The dynamic force spectrum for PAA-450K-80 suggests that there is likely high multiplicity of interactions, as the data points have quite a large spread instead forces at a given loading rate. From Figure 57 it is difficult to conclude about whether PAA-450K-80 behaves in a signifficantly different way than MUC1-Tn. It is possible to see that the dynamic power spectra are mostly overlapping, but the multiplicity of interactions makes the comparison difficult. It is not known whether the spread of the data would be different if the analysis was done again, as the presented analysis was performed relativel early in this work.

When the histrograms for PAA-450K-80 and MUC1-Tn are compared, it is obvious that the synthetic polymer clearly has many more strong interactions. This is as expected, if the GalNAc is the interacting group on both of the polymers, and the density og GalNAc is higher on the PAA. It was also of interest to test how PAA-450 with 40% and 10% GalNAc would behave, and whether the frequency of interactions decreased with the amount of GalNAc on the polymer. This would confirm that it is the GalNAc that is the interacting group. No control experiments were done with this polymer to ensure that the PAA backbone did not interact with PAA-GalNAc due to unavailability of unglycosylated PAA. This means it cannot be concluded that the GalNAc does not bind to the PAA.

6.6.2 PAA-Gal/GalNAc/Glc/GlcNAc

It was much easier to work with this, shorter (30 kDa) PAA-polymer than the PAA-450K polymer (450 kDa). The longer PAA-450K polymer had very strong self-interactions, which often caused one of the beads to be pulled out of the trap. It is not unthinkable that this might also have happened due to entanglement of molecules. The shorter PAA did not cause such experimental challenges, and also exhibited much fewer very strong interactions. When the goal of the experiments is to measure forces accurately, it is desirable to have a low multiplicity of interactions. The shorter PAA polymer would thus be the recommended polymer of choice in the future. Control experiments showed that the PAA-polymers did not exhibit any self-interactions.

If the interactions frequency is any indication of what the interacting groups on the GalNAc might be, it may seem like the N-acetyl group indeed seems to matter for the GalNac. The percentage of interactions between PAA-βGalNAc was 46%, while

it was only 13% for PAA-βGal. However, it is seemingly not the only important interacting group on this sugar, as PAA-Gal did exhibit some interactions.

What is additionally interesting about this result is that MUC1-T (Gal bound to GalNAc) was previously found to not interact. The finding during the work with MUC1-T work indicated otherwise, as ca. 1750 out of 8127 curves contained interactions. It was then hypothesized that the Gal-group might actually have interactions either against GalNAc or against itself. Due to the unavailability of suitably sized streptavidin-coated beads, PAA-Gal was not tested against PAA-GalNAc. That PAA-Gal did exhibit interactions, supports the findings of MUC1-T interacting with itself as plausible. Note that the Gal is not only an anomer of GalNAc, but also bound to the PAA by the same group it would be bound by to the GalNac of the Tn-antigen. However, it should be noted that GalNAc is bound to Ser/Thr by an α- and not a β-glycosdic linkage. Thus, it would be adviseable to also look at PAA-αGalNAc-binding; it is not known how much the conformation of the sugar would change its reactivity.

The presence or absence of the N-acetyl group did not seem to matter in the case of GlcNac, as both PAA-Glc and PAA-GlaNAc were found to have interactions in 18% of the curves. This might indicate that this sugar might have a different set of interacting groups. Glucose and galactose are epimers; in glucose, the C4-OH group is in the axial position, while it is in the equatorial position in galactose. From the data, it is unclear whether the position of the OH-group on the sugars has any effect, as the difference between 13% and 18% interactions is small.

No control experiments were done to test whether PAA exhibited interactions against glycosylated PAA, but it is not known how useful such experiments would be. Like the unglycosylated MUC1-protein, PAA assumes a very different conformation when it is not glycosylated [162]. However, even when bunched-up, the PAA polymer has a repeating structure, all of which might still be available.

6.7 The fumonisin-experiments

Yeast cells are normally found floating around as single-cells in solution. Their outer layer has a high abundance on mannoproteins. From the experiments performed during this work, the outer layer of mannan seemed to be responsible for much of the reason that yeast do not stick together, as close to no interactions were found when working with beads coated with an abundant amount of mannan. Only when pressing beads strongly together, a few interactions were obtained. When fumonisin-coated beads were used to probe mannan-covered beads it was found that interactions were rare. It was speculated that the mannan layer might contribute to the inertness of the surface to fumonisin. The few interactions that were found could well be due to interactions between fumonisin and the surface of the other bead.

Both laminarin and chitosan were shown to interact strongly with the fumonisin. Quite a lot of data was obtained for the fumonisin-laminarin experiments, which showed that the laminarin was able to bind the fumonisin strongly, without the need to apply almost any force for the interactions to happen. Laminarin is an

algeal β-glucan, but equivalent to that found in yeast.

A much smaller amount of data was gathered from the fumonisin-chitosan experiments, as chitosan was a molecule that proved difficult to work with as it created quite thick and uneven coatings on the beads, which resulted in very strong interactions happening frequently, and lead to the beads being pulled out of the traps. Even thought this molecule resulted in binding of fumonisin, it is of less interest because of its ability to bind a big variety of biological molecules, unlike laminarin.

It is difficult to compare laminarin and chitosan polymers as they behave quite differently - both when in solution and when bound to beads. According to the approach-retract- curves, laminarin seemed to be located quite close to the surface of the beads and created a relatively thin layer of molecules, compared to chitosan. As β-glucan organizes the yeast cell wall, this might not be a strange phenomenon. Chitosan seemed to rather create some kind of very fluffy network around the beads, which extended quite far from their surface. As this network seamed to cause very little repulsion of the fumonisin bead, it seemed to be of low density. It is noteworthy that the fumonisin-covered beads did not often bind as soon as they encountered this network, but bound when the bead surfaces were much closer. This may also result from chitosan binding the bead surface, which was shown to be the case during the control experiments.

The wild-type FB1 yeast only had a few interactions with the fumonisin-coated bead. No beta-glucan is accessible at a normal yeast cell, but some chitin is. The chitin can be found where a new cell wall is being built, and some chitin will remain at the budding scar of the yeast. This can be visualized by staining of the chitin with the fluorescent dye calcofluor white, which binds strongly to chitin [163]. mnn9Δ knockout yeast has only half the amount of mannan on the surface of the cell as a wild type (WT) yeast. When testing fumonisin against this mannan-deficient yeast mutant, interactions were not obtained even when pressing the fumonisin-functionalized bead and yeast together with high forces for a prolonged time (10 s). This might have several reasons. It was hypothesized that a mutation that would result in a lower degree of mannosylation of the yeast cell surface might contribute to increased interactions with the glycan layers beneath the mannan. However, it seems as if the glucan layer beneath the mannan layer was still inaccessible. This can be due to the remaining mannans, or the tight organization of the β-glucan layer.

7 Conclusion

Optical tweezers are a good tool to reveal interactions that other methods might not be sensitive enough to detect, like the calcium-independency of the binding of MGL to GalNAC of MUC1. However, this method was not a reliable way to estimate the frequency of interactions of two complexes. During these experiments it was found that there are several parameters that are difficult to control: the amount of molecules bound to the beads, affected by the efficiency of the crosslinking agent and random variation, the amount of force molecules were pushed together with, alignment of the traps.

It is important to have experimental methods of high quality to ensure reproducibility of the results. During these experiments this was an issue that resulted in qualitatively conflicting results: a variation in whether a pair of molecules seemed to exhibit interactions or not, where datasets of hundreds of interactions could suggest the opposite. Measures that were found to achieve reliable results was a set of steps to prevent contamination of the sample, making sure that beads are properly aligned in one plane during measurements, as well as a positive and negative control for the experiment of interest. The positive control will ensure the efficiency of the crosslinking agent used to attach biomolecules to the beads, while the negative sample will be work as a test for contamination.

It was found that MUC1-Tn and MUC1-STn could bind with themselves and each other. MUC1-STn seemed to exhibit interactions more frequently, which might mean that the sialic acid created a favourable conformation of the glycan-groups, which aids in interactions. MUC1-ST was found to bind with itself and to the previously mentioned mucins. MUC1-T was found to have self interactions. When MUC1-Tn, MUC1-STn, MUC1-T and MUC1-ST were crossed with each other, the rest of the results of the crossing experiments were determined to be inconclusive due to experimental difficulties. It is adviceable to repeat the experiments using the suggestions described for improving the experimental method.

MGL was found to bind MUC1-Tn, in the absence of calcium, but this experiment might need to be repeated with a chelating agent present in the medium. Polyacrylamide-Tn was not observed to be bound by MGL. This result is different from what was found previously, and could be due to experimental error.

The *Saccharomyces cerevisiae* yeast cell wall consists of an outer layer on mannan, middle layer of β-glucan and inner layer of chitosan. Fumonisin B1 is a fungal toxin. Fumonisin coated beads were found to not bind mannan-coated beads, but bound beads with laminarin (hydrolyzed β-glucan) and chitin (deacetylated chitosan) strongly. Fumonisin-coated beads were found to not bind to wild type (WT) FB1 yeast cells nor mnn9Δ FB1, which has about 50% as much mannan on the cell wall as the WT. This is believed to be due to the unavailability of the interacting parts of the cell wall at the surface of the yeast cells.

8 Future work

8.0.1 Improvement of the experiment set up

Issues with contamination was encountered during this work, but several measures were taken to reduce this. It was found that washing the components of the liquid chamber immediately before use, filtering the solutions frequently (at least one every other week), washing the beads before use to remove unwanted additives, keeping the working surfaces clean, and keeping all equipment sealed when not in use was necessary (described further in "Materials and Methods", and quantified in "Results"). It is recommended that positive and negative controls would be used for each of the experiments. The positive control should be a molecule known to self-interact, to ensure that the immobilization procedure has worked, while the negative control should be beads without immobilized molecules. The negtive control should not exhibit interactions, as it should serve to detect contamination.

It was early on noticed that the immobilizing agent used to attach polymers to the surface of the beads seemed to degrade over time - sometimes rapidly. To test whether EDC really is the problem could be possible in several ways. One of these ways can perhaps be to immobilize fluorescent molecules onto the beads and observe the fluorescence after the washing steps. It could also be possible to quantify the degradation by using some of the batch of EDC and boric acid to perform a crosslinking reaction between other types of molecules (no beads) and then quantify the amount of reactants and products using chromatographic methods such as HPLC. In any case, EDC is likely to affect the amount of immobilized polymers strongly, and will thus affect the frequency of interactions. According to these findings, it would be highly practical if ECD used for the experiments could be packaged in smaller batches.

To estimate the force the beads are pressed together with from the NanoTracker GUI can be challenging, as the evaluation is based on observed force curves. For an estimate of total force, three curves (X, Y, Z) for the two beeds must be evaluated. A way that this could possibly be overcome is by implementing a force-feedback loop in NanoTracker. When the approaching bead reaches a pre-set repulsive force, it will retract. It might be possible to continue the experiments without this loop when the appropriate distance between the beads has been established. At the moment, it is possible to have a loop that controls the bead separation by maintaining a set tension. It could be very useful to have a similar loop that controls the force beads are pressed together with. This would also be useful for comparing different systems of interacting molecules in terms of interaction frequency.

It was found that the coating of beads is highly variable. Sonification could possibly be used to create a more even distribution of molecules in solution and prevent them from aggregating by disrupting weak intermolecular. This might result in a more even coating of the beads. Constant mixing during the immobilization might work similarly. This can be achieved by constant turning or shaking of the Eppendorf tubes samples are kept in during the immobilization reaction.

Several pairs of beads should be used from each sample to compare both the

inter- and intra-sample variation. In any case, a more even coating of beads would be beneficial to experiments like these, as the results would likely be more consistent.

It was found that beads of size 3.36 μm, sedimented to the bottom of the liquid chamber in only 2-3 minutes. If the molecules on the bead are able to bind the surface on the liquid chamber, most beads get permanently stuck fast, and prolonged measurements using the same sample can be challenging. However, beads of 2.01 μm sedimented much more slowly. It can be possible to continue using the smaller beads for these experiments while still getting access to the lower loading rates by adjusting the strength of the laser to a lower power. In this way, it should be possible to increase the sensitivity and thus measure the weaker forces.

Some interactions, such as those between MUC1-T - self and MUC1-ST - self were found to exhibit high multiplicity of binding, which resulted in many force curves tht could not be analyzed. Multiplicity can often be reduced by reducing the density of molecules bound to the surface. However, for MUC1-ST interactions were found between the mucin and the surface of the bead. Such interactions are highly undesirable, as they can be difficult to sort out during analysis, and can affect the estimtion of parameters of the investigated bonds. It was found that unglycosylated MUC1-protein did not exhibit self-interactions, was not found to interact with the bead surface, and did not seem to bind to any of the glycosylated mucins, except MUC1-STn. Unglycosylated MUC1 can possibly be used to coat the surface between glycosylated MUC1.

8.1 Improvement of analytical set up

During this work, it was found that much bigger dataset were required to get a good estimation of parameters of he energy landscape of intermolecular bonds. Atop of the lack of data, manually fitting the loading rate is a slow process that requires good knowledge about the correct appearance of a single bond for a given system. The analysis might be improved by a adapting a worm-like chain-model to the polymer at hand. This can possibly make the data analysis semi-automatic, and reduce human error in the interpretation of data.

8.2 Future work with mucins

The work that has been done on mucins and cancer-associated glycans is still limited, and much is still not known. Conflicting results were found for the interactions between some of the mucins - some times pairs of mucins seemed to be able to bind each other, and sometimes not, depending on the sample studied. This is believed to be due to problems with the experimental setup, improvements of which are suggested in the above section. It is recommended to repeat the mucin experiments where consensus was not reached, using the abovementioned improvements.

While MUC1 with cancer-associated glycans was provided for this study, no fully glycosylated human mucin was available. It could be on interest, from a biological standpoint, to study how cancer-associated mucin interacts with normally-glycosylated mucin. TR-PSM H8 is a fully glycosylated mucin that was available for

investigation, but it contains 40% glycosylation with NeuNGl, which is a non-human sugar. It is not known how this sugar might affect the result of interaction-studies.

8.3 Future work with MGL

MGL was found to bind MUC1-Tn in the absense of added calcium in the sample. This contradicts NMR-studies on these interactions. Even though the MGL - GalNAc-binding might be possible even without Ca^{2+}, it would be of interest to see whether binding would occur if a chelating agent was added to the sample. It is not unthinkable that the samples might have been contaminated with low amounts of calcium, from an unknown sourse. If this is so, a chelator of divalent cations can make these unavailable for the MGL.

It would be interesting to study the binding of MGL in samples with added calcium vs. samples without, as it can provide data about whether the lifetime of the bond and the binding interaction length, as well as other parameters of the bond, differ in the two cases.

MGL has previously been found to bind GalNAc attached to different types of backbones. However, it was not found to bind PAA with 80% GalNAc substitution. This is thought to be due to problems with the set up of the experiment, and thus, this experiment should be repeated using the improved set up, described in Section 8.0.1. This would be of interest to investigate to make sure that the absence of binding is not due to steric hindrance because of the tightly spaced GalNAc groups.

For the investigation of vaccine development, it would be interesting to add another step to these experiments. MGL is a protein that is internalized after it binds to its ligand, and then preceeds though the endosomal-lysosomal pathway [88] through the cell. During this pathway, the changing pH gradient in the different cellular compartments leads to the release of the ligand from the MGL. As the tumor environment often is acidic due to the high lactic acid content produced by the cancer cells, it can be of interest to know whether the interaction of MGL with its ligand is possible and lasting also in an environment of low pH.

Polyelectrolytes have in previous studies been shown to be well suited to activate immune cells. It could be interesting to study the interactions between cancer-associated antigens bound on such molecules, and MGL, or other lectins.

8.4 Future studies with PAA

PAA appears to be a promising polymer for the studies of interactions between sugar moieties. It might be desirable to use it in further studies, to map the possible interactions of β-GalNAc and α-Gal, and a variety of other sugars present on proteins and lipids of humans. It was found that the shorter PAA polymer of 30 kDa was much easier to work with that the longer PAA, of 450 kDa, so it is advised to use shorter PAA-polmers for such studies. Studies on the effects of density can also be done using this polymer.

8.5 Further tests on yeast and fumonisin B1

Fumonisin B1 was not found to bind to whole cells of *Saccharomyces cereviciae*, probably due to its protective mannan-layer on the cell wall. A mutant yeast with 50% of the normal amount of mannosylation of the cell wall was also not found to bind fumonisin. It seems as if the glucan layer beneath the mannan layer was still inaccessible. It was hypothesized that there might still be enough mannan on the surface of the yeast to be able to shield it from fumonisin. It is believed that the removal of mannans might be insufficient to cause β-glucans to be available for binding. β-glucans of yeast are tightly associated [164] and thus, this layer might need to be less organized in order for interactions to be possible. It would be of interest to investigate the interactions between fumonisin-coated bead and a yeast with a poorly organized β-glucan part of the cell wall.

That the yeast does not bind fumonisin on beads might not mean that it would not do so if the fumonisin was free in solution. It could be interesting to investigate whether yeast incubated with fumonisin could be able to absorb or adsorb it, by incubating yeast in a fumonisin-solution and then remove the yeast and measure the concentration of fumonisin in the solution. Again, if a mutant with a loosely organized cell wall is available, testing it with the same procedure could give the answer to whether it is the tight cell wall organization of yeast that causes the hindrance.

Another way to achieve a lesser degree of organization of yeast cell walls is to dry the yeast (yeast ghost). It has been found that the surface of dried yeast cells is not smooth, as that of live yeast cells. Some of the β-glucan is exposed; it would be of interest to see whether fumonisin could be able to interact with these yeast ghosts. It would then also be an advantage to test whether such yeast would be able to bind more fumonisin in solution.

Yeast has been found useful to remove mycotoxins from animal feed. This is done by mixin the yeast with the feed that animals eat. As the food passes through the digestive tract of the animal, the yeast bind the mycotoxins and is passed through the digestive tract without being digested. As the different parts of digestive tract has varying pH, it would be desirable to ensure that the fumonisin is able to be bound by yeast cells in conditions of varying acidity.

As laminarin seems to bind fumonisin, this might be useful for other applications than detoxification of animal feed. The binding of these molecules can be further confirmed by studying it with other methods.

References

[1] Keir C Neuman and Attila Nagy. Single-molecule force spectroscopy: optical tweezers, magnetic tweezers and atomic force microscopy. *Nature methods*, 5(6):491, 2008.

[2] Peter B Armstrong. Cell sorting out: the self-assembly of tissues in vitro. *Critical Reviews in Biochemistry and Molecular Biology*, 24(2):119–149, 1989.

[3] Malcolm S Steinberg. Reconstruction of tissues by dissociated cells. *Science*, 141(3579):401–408, 1963.

[4] Duke Duguay, Ramsey A Foty, and Malcolm S Steinberg. Cadherin-mediated cell adhesion and tissue segregation: qualitative and quantitative determinants. *Developmental biology*, 253(2):309–323, 2003.

[5] Melissa D Pope and Anand R Asthagiri. Short-lived, transitory cell-cell interactions foster migration-dependent aggregation. *PloS one*, 7(8):e43237, 2012.

[6] Robert A Copeland. The drug-target residence time model: a 10-year retrospective. *Nature Reviews Drug Discovery*, 2015.

[7] George P Anderson, Vasudha A Kowtha, and Chris R Taitt. Detection of fumonisin b1 and ochratoxin a in grain products using microsphere-based fluid array immunoassays. *Toxins*, 2(2):297–309, 2010.

[8] WCA Gelderblom, NPJ Kriek, WFO Marasas, and PG Thiel. Toxicity and carcinogenicity of the fusanum monilzforine metabolite, fumonisin b1, in rats. *Carcinogenesis*, 12(7):1247–1251, 1991.

[9] Walter Friedrich Otto Marasas, T Stephanus Kellerman, WCA Gelderblom, PG Thiel, and Jaco J Van der Lugt. Leukoencephalomalacia in a horse induced by fumonisin b1 isolated from fusarium moniliforme. 1988.

[10] Lenn R Harrison, Billy M Colvin, J Todd Greene, Louis E Newman, and John R Cole Jr. Pulmonary edema and hydrothorax in swine produced by fumonisin b1, a toxic metabolite of fusarium moniliforme. *Journal of Veterinary Diagnostic Investigation*, 2(3):217–221, 1990.

[11] Fun S Chu and Guo Y Li. Simultaneous occurrence of fumonisin b1 and other mycotoxins in moldy corn collected from the people's republic of china in regions with high incidences of esophageal cancer. *Applied and environmental microbiology*, 60(3):847–852, 1994.

[12] WC Gelderblom, K Jaskiewicz, WF Marasas, PG Thiel, RM Horak, R Vleggaar, and NP Kriek. Fumonisins–novel mycotoxins with cancer-promoting activity produced by fusarium moniliforme. *Applied and environmental microbiology*, 54(7):1806–1811, 1988.

[13] Árpád Bata and Radomir Lásztity. Detoxification of mycotoxin-contaminated food and feed by microorganisms. *Trends in Food Science & Technology*, 10(6):223–228, 1999.

[14] A Dean Howes and Kyle E Newman. Compositions and methods for removal of mycotoxins from animal feed, April 4 2000. US Patent 6,045,834.

[15] Stefan Freimund, Martin Sauter, and Paul Rys. Efficient adsorption of the mycotoxins zearalenone and t-2 toxin on a modified yeast glucan. *Journal of Environmental Science and Health, Part B*, 38(3):243–255, 2003.

[16] Danielle H Dube and Carolyn R Bertozzi. Glycans in cancer and inflammation—potential for therapeutics and diagnostics. *Nature reviews Drug discovery*, 4(6):477–488, 2005.

[17] Anne Dell and Howard R Morris. Glycoprotein structure determination by mass spectrometry. *Science*, 291(5512):2351–2356, 2001.

[18] Daniel J Moloney and Robert S Haltiwanger. The o-linked fucose glycosylation pathway: identification and characterization of a uridine diphosphoglucose: fucose-β1, 3-glucosyltransferase activity from chinese hamster ovary cells. *Glycobiology*, 9(7):679–687, 1999.

[19] Dapeng Zhou. Why are glycoproteins modified by poly-n-acetyllactosamine glycoconjugates? *Current Protein and Peptide Science*, 4(1):1–9, 2003.

[20] Ajit Varki and John B Lowe. Biological roles of glycans. 2009.

[21] Robert G Spiro. Protein glycosylation: nature, distribution, enzymatic formation, and disease implications of glycopeptide bonds. *Glycobiology*, 12(4):43R–56R, 2002.

[22] Trent R Gemmill and Robert B Trimble. Overview of n-and o-linked oligosaccharide structures found in various yeast species. *Biochimica et Biophysica Acta (BBA)-General Subjects*, 1426(2):227–237, 1999.

[23] Perry G Wang and Weixuan He. *Hydrophilic interaction liquid chromatography (HILIC) and advanced applications*. CRC press, 2011.

[24] Inka Brockhausen, Harry Schachter, and Pamela Stanley. O-galnac glycans. 2009.

[25] Elias Meezan, Henry C Wu, Paul H Black, and Phillips W Robbins. Comparative studies on the carbohydrate-containing membrane components of normal and virus-transformed mouse fibroblasts. ii. separation of glycoproteins and glycopeptides by sephadex chromatography. *Biochemistry*, 8(6):2518–2524, 1969.

[26] Sen-itiroh Hakomori. Tumor-associated carbohydrate antigens. *Annual review of immunology*, 2(1):103–126, 1984.

[27] David J Gill, Joanne Chia, Jamie Senewiratne, and Frederic Bard. Regulation of o-glycosylation through golgi-to-er relocation of initiation enzymes. *The Journal of cell biology*, pages jcb–201003055, 2010.

[28] Robert Sewell, Malin Bäckström, Martin Dalziel, Steven Gschmeissner, Hasse Karlsson, Thomas Noll, Jochem Gätgens, Henrik Clausen, Gunnar C Hansson, Joy Burchell, et al. The st6galnac-i sialyltransferase localizes throughout the golgi and is responsible for the synthesis of the tumor-associated sialyl-tn o-glycan in human breast cancer. *Journal of Biological Chemistry*, 281(6):3586–3594, 2006.

[29] Teresa M Horm and Joyce A Schroeder. Muc1 and metastatic cancer: expression, function and therapeutic targeting. *Cell adhesion & migration*, 7(2):187–198, 2013.

[30] Michael A Hollingsworth and Benjamin J Swanson. Mucins in cancer: protection and control of the cell surface. *Nature Reviews Cancer*, 4(1):45–60, 2004.

[31] M Madhan, M Venkataraman, Zachriah Bobby, and PH Ananthanarayanan. T-antigen (gal β3 gainac α-) containing glycoproteins of human reace. *Indian Journal of Clinical Biochemistry*, 14(2):159–167, 1999.

[32] Richard Beatson, Virginia Tajadura-Ortega, Daniela Achkova, Gianfranco Picco, Theodora-Dorita Tsourouktsoglou, Sandra Klausing, Matthew Hillier, John Maher, Thomas Noll, Paul R Crocker, et al. The mucin muc1 modulates the tumor immunological microenvironment through engagement of the lectin siglec-9. *Nature immunology*, 17(11):1273–1281, 2016.

[33] Lenneke AM Cornelissen and Sandra J Van Vliet. A bitter sweet symphony: Immune responses to altered o-glycan epitopes in cancer. *Biomolecules*, 6(2):26, 2016.

[34] Sean K Lau, Peiguo G Chu, and Lawrence M Weiss. Cd163a specific marker of macrophages in paraffin-embedded tissue samples. *American journal of clinical pathology*, 122(5):794–801, 2004.

[35] J Sakurai, N Hattori, M Nakajima, T Moriya, T Suzuki, A Yokoyama, and N Kohno. Differential expression of the glycosylated forms of muc1 during lung development. *European journal of histochemistry: EJH*, 51(2):95, 2007.

[36] Gherman Wiederschain. Introduction to glycobiology and human diseases. *Glycobiology and Human Diseases*, page 1, 2016.

[37] Sukhwinder Kaur, Sushil Kumar, Navneet Momi, Aaron R Sasson, and Surinder K Batra. Mucins in pancreatic cancer and its microenvironment. *Nature Reviews Gastroenterology and Hepatology*, 10(10):607–620, 2013.

[38] Tongzhong Ju, Grainger S Lanneau, Tripti Gautam, Yingchun Wang, Baoyun Xia, Sean R Stowell, Margaret T Willard, Wenyi Wang, Jonathan Y Xia, Rosemary E Zuna, et al. Human tumor antigens tn and sialyl tn arise from mutations in cosmc. *Cancer research*, 68(6):1636–1646, 2008.

[39] Tongzhong Ju, Yingchun Wang, Rajindra P Aryal, Sylvain D Lehoux, Xiaokun Ding, Matthew R Kudelka, Christopher Cutler, Junwei Zeng, Jianmei Wang, Xiaodong Sun, et al. Tn and sialyl-tn antigens, aberrant o-glycomics as human disease markers. *PROTEOMICS-Clinical Applications*, 7(9-10):618–631, 2013.

[40] Miao Wang, Shiuan Wey, Yi Zhang, Risheng Ye, and Amy S Lee. Role of the unfolded protein response regulator grp78/bip in development, cancer, and neurological disorders. *Antioxidants & redox signaling*, 11(9):2307–2316, 2009.

[41] Richard Beatson, Gjertrud Maurstad, Gianfranco Picco, Appitha Arulappu, Julia Coleman, Hans H Wandell, Henrik Clausen, Ulla Mandel, Joyce Taylor-Papadimitriou, Marit Sletmoen, et al. The breast cancer-associated glycoforms of muc1, muc1-tn and sialyl-tn, are expressed in cosmc wild-type cells and bind the c-type lectin mgl. *PLoS One*, 10(5):e0125994, 2015.

[42] Yuzuru Ikehara, Naoya Kojima, Nobuyuki Kurosawa, Takashi Kudo, Mari Kono, Shoko Nishihara, Soichiro Issiki, Kyoei Morozumi, Steven Itzkowitz, Tetsuro Tsuda, et al. Cloning and expression of a human gene encoding an n-acetylgalactosamine-α2, 6-sialyltransferase (st6galnac i): a candidate for synthesis of cancer-associated sialyl-tn antigens. *Glycobiology*, 9(11):1213–1224, 1999.

[43] GF Springer, PR Desai, WA Fry, RL Goodale, JG Shearen, and EF Scanlon. T antigen, a tumor marker against which breast, lung and pancreas carcinoma patients mount immune responses. *Cancer detection and prevention*, 6(1-2):111, 1983.

[44] Paulina Sindrewicz, Lu-Yun Lian, and Lu-Gang Yu. Interaction of the oncofetal thomsen–friedenreich antigen with galectins in cancer progression and metastasis. *Frontiers in oncology*, 6, 2016.

[45] Jack L Summers, John S Coon, Rose M Ward, William H Falor, Alexander W Miller, and Ronald S Weinstein. Prognosis in carcinoma of the urinary bladder based upon tissue blood group abh and thomsen-friedenreich antigen status and karyotype of the initial tumor. *Cancer research*, 43(2):934, 1983.

[46] Stephan E Baldus, Franz-Georg Hanisch, Georg M Kotlarek, Thomas K Zirbes, Juergen Thiele, Joerg Isenberg, Uwe R Karsten, Peter L Devine, and Hans P Dienes. Coexpression of muc1 mucin peptide core and the thomsen-friedenreich antigen in colorectal neoplasms. *Cancer*, 82(6):1019–1027, 1998.

[47] John Sotiriadis, Soon-Cheon Shin, Daesong Yim, David Sieber, and Yoon Berm Kim. Thomsen-friedenreich (t) antigen expression increases sensitivity of natural killer cell lysis of cancer cells. *International journal of cancer*, 111(3):388–397, 2004.

[48] Salomé S Pinho and Celso A Reis. Glycosylation in cancer: mechanisms and clinical implications. *Nature Reviews Cancer*, 15(9):540–555, 2015.

[49] JF Codington and DM Frim. Cell-surface macromolecular and morphological changes related to allotransplantability in the ta3 tumor. *Biomembranes*, 11:207, 1983.

[50] Harry G Rittenhouse, George L Manderino, and G Michael Hass. Mucin-type glycoproteins as tumor markers. *Laboratory Medicine*, 16(9):556–560, 1985.

[51] KERMIT L CARRAWAY, NEVIS FREGIEN, and CORALIE A CAROTHERS CARRAWAY. Tumor sialomucin complexes as tumor antigens and modulators of cellular interactions and proliferation. *Journal of Cell Science*, 103(2):299–307, 1992.

[52] Mina Fogel, Peter Altevogt, and Volker Schirrmacher. Metastatic potential severely altered by changes in tumor cell adhesiveness and cell-surface sialylation. *Journal of Experimental Medicine*, 157(1):371–376, 1983.

[53] Lu-Gang Yu, Nigel Andrews, Qicheng Zhao, Daniel McKean, Jennifer F Williams, Lucy J Connor, Oleg V Gerasimenko, John Hilkens, Jun Hirabayashi, Kenichi Kasai, et al. Galectin-3 interaction with thomsen-friedenreich disaccharide on cancer-associated muc1 causes increased cancer cell endothelial adhesion. *Journal of Biological Chemistry*, 282(1):773–781, 2007.

[54] Charles J Dimitroff. Galectin-binding o-glycosylations as regulators of malignancy. *Cancer research*, 75(16):3195–3202, 2015.

[55] Herbert Hildebrandt, Martina Mühlenhoff, Birgit Weinhold, and Rita Gerardy-Schahn. Dissecting polysialic acid and ncam functions in brain development. *Journal of neurochemistry*, 103(s1):56–64, 2007.

[56] Marjolijn JL Ligtenberg, Femke Buijs, Hans L Vos, and John Hilkens. Suppression of cellular aggregation by high levels of episialin. *Cancer Research*, 52(8):2318–2324, 1992.

[57] Jelle Wesseling, Sylvia W Van Der Valk, Hans L Vos, Arnoud Sonnenberg, and John Hilkens. Episialin (muc1) overexpression inhibits integrin-mediated cell adhesion to extracellular matrix components. *The Journal of cell biology*, 129(1):255–265, 1995.

[58] Richard K Assoian. Anchorage-dependent cell cycle progression. *The Journal of cell biology*, 136(1):1–4, 1997.

[59] Nigel Peat, Sandra J Gendler, El-Nasir Lalani, Trevor Duhig, and Joyce Taylor-Papadimitriou. Tissue-specific expression of a human polymorphic epithelial mucin (muc1) in transgenic mice. *Cancer research*, 52(7):1954–1960, 1992.

[60] Franz-Georg Hanisch and Stefan Müller. Muc1: the polymorphic appearance of a human mucin. *Glycobiology*, 10(5):439–449, 2000.

[61] Joy Burchell, Sandra Gendler, Joyce Taylor-Papadimitriou, Anne Girling, Angela Lewis, Rosemary Millis, and Derek Lamport. Development and characterization of breast cancer reactive monoclonal antibodies directed to the core protein of the human milk mucin. *Cancer research*, 47(20):5476–5482, 1987.

[62] Celso A Reis, Leonor David, Mario Seixas, Joy Burchell, and Manuel Sobrinho-Simoes. Expression of fully and under-glycosylated forms of muc 1 mucin in gastric carcinoma. *International journal of cancer*, 79(4):402–410, 1998.

[63] Yaron Niv. Muc1 and colorectal cancer pathophysiology considerations. *World Journal of Gastroenterology: WJG*, 14(14):2139, 2008.

[64] John Hilkens, Marjolÿn JL Ligtenberg, Hans L Vos, and Sergey V Litvinov. Cell membrane-associated mucins and their adhesion-modulating property. *Trends in biochemical sciences*, 17(9):359–363, 1992.

[65] Sandra Gendler, Joyce Taylor-Papadimitriou, Trevor Duhig, Jonathan Rothbard, and Joy Burchell. A highly immunogenic region of a human polymorphic epithelial mucin expressed by carcinomas is made up of tandem repeats. *Journal of Biological Chemistry*, 263(26):12820–12823, 1988.

[66] Sandra J Gendler, Carole A Lancaster, Joyce Taylor-Papadimitriou, Trevor Duhig, Nigel Peat, Joy Burchell, Lucy Pemberton, El Nasir Lalani, and David Wilson. Molecular cloning and expression of human tumor-associated polymorphic epithelial mucin. *Journal of Biological Chemistry*, 265(25):15286–15293, 1990.

[67] J Taylor-Papadimitriou, J Burchell, D.W Miles, and M Dalziel. {MUC1} and cancer. *Biochimica et Biophysica Acta (BBA) - Molecular Basis of Disease*, 1455(2–3):301 – 313, 1999.

[68] J Darrell Fontenot, SV Santhana Mariappan, Paolo Catasti, Neives Domenech, Olivera J Finn, and Goutam Gupta. Structure of a tumor associated antigen containing a tandemly repeated immunodominant epitope. *Journal of Biomolecular Structure and Dynamics*, 13(2):245–260, 1995.

[69] Neil Jentoft. Why are proteins o-glycosylated? *Trends in biochemical sciences*, 15(8):291–294, 1990.

[70] Thomas A Gerken. The solution structure of mucous glycoproteins: proton nmr studies of native and modified ovine submaxillary mucin. *Archives of biochemistry and biophysics*, 247(2):239–253, 1986.

[71] Thomas A Gerken and Neil Jentoft. Structure and dynamics of porcine submaxillary mucin as determined by natural abundance carbon-13 nmr spectroscopy. *Biochemistry*, 26(15):4689–4699, 1987.

[72] Randal Shogren, Thomas A Gerken, and Neil Jentoft. Role of glycosylation on the conformation and chain dimensions of o-linked glycoproteins: light-scattering studies of ovine submaxillary mucin. *Biochemistry*, 28(13):5525–5536, 1989.

[73] AN Round, M Berry, TJ McMaster, S Stoll, Darren Gowers, AP Corfield, and MJ Miles. Heterogeneity and persistence length in human ocular mucins. *Biophysical Journal*, 83(3):1661–1670, 2002.

[74] Silvia von Mensdorff-Pouilly, Maria Moreno, and René HM Verheijen. Natural and induced humoral responses to muc1. *Cancers*, 3(3):3073–3103, 2011.

[75] Caroline Gronnier, Emilie Bruyère, Fatima Lahdaoui, Nicolas Jonckheere, Michaël Perrais, Emmanuelle Leteurtre, Guillaume Piessen, Christophe Mariette, and Isabelle Van Seuningen. The {MUC1} mucin regulates the tumorigenic properties of human esophageal adenocarcinomatous cells. *Biochimica et Biophysica Acta (BBA) - Molecular Cell Research*, 1843(11):2432 – 2437, 2014.

[76] Subrata K Ghosh, Pamela Pantazopoulos, Zdravka Medarova, and Anna Moore. Expression of underglycosylated muc1 antigen in cancerous and adjacent normal breast tissues. *Clinical breast cancer*, 13(2):109–118, 2013.

[77] Li Wang, Jie Ma, FengHua Liu, QingKai Yu, GuangMin Chu, Alan C Perkins, and Yong Li. Expression of muc1 in primary and metastatic human epithelial ovarian cancer and its therapeutic significance. *Gynecologic oncology*, 105(3):695–702, 2007.

[78] Keiji Matsuda, Tadahiko Masaki, Toshiaki Watanabe, Joji Kitayama, Hirokazu Nagawa, Tetsuichiro Muto, and Yoichi Ajioka. Clinical significance of muc1 and muc2 mucin and p53 protein expression in colorectal carcinoma. *Japanese journal of clinical oncology*, 30(2):89–94, 2000.

[79] Prakash Radhakrishnan, Sally Dabelsteen, Frey Brus Madsen, Chiara Francavilla, Katharina L Kopp, Catharina Steentoft, Sergey Y Vakhrushev, Jesper V Olsen, Lars Hansen, Eric P Bennett, et al. Immature truncated o-glycophenotype of cancer directly induces oncogenic features. *Proceedings of the National Academy of Sciences*, 111(39):E4066–E4075, 2014.

[80] Noriko Suzuki, Kazuo Yamamoto, Satoshi Toyoshima, Toshiaki Osawa, and Tatsuro Irimura. Molecular cloning and expression of cdna encoding human macrophage c-type lectin. its unique carbohydrate binding specificity for tn antigen. *The Journal of Immunology*, 156(1):128–135, 1996.

[81] Jeremy M Berg, John L Tymoczko, and Lubert Stryer. Biochemistry. 5th. *New York: WH Freeman*.

[82] Nobuaki Higashi, Kouki Fujioka, Kaori Denda-Nagai, Shin-ichi Hashimoto, Shigenori Nagai, Taku Sato, Yuko Fujita, Akiko Morikawa, Makoto Tsuiji, Megumi Miyata-Takeuchi, et al. The macrophage c-type lectin specific for galactose/n-acetylgalactosamine is an endocytic receptor expressed on monocyte-derived immature dendritic cells. *Journal of Biological Chemistry*, 277(23):20686–20693, 2002.

[83] Sho Yamasaki. *C-type Lectin Receptors in Immunity*.

[84] Sabine AF Jégouzo, Adrián Quintero-Martínez, Xiangyu Ouyang, Ália dos Santos, Maureen E Taylor, and Kurt Drickamer. Organization of the extracellular portion of the macrophage galactose receptor: A trimeric cluster of simple binding sites for n-acetylgalactosamine. *Glycobiology*, 23(7):853–864, 2013.

[85] Ilaria Grazia Zizzari, Chiara Napoletano, Federico Battisti, Hassan Rahimi, Salvatore Caponnetto, Luca Pierelli, Marianna Nuti, and Aurelia Rughetti. Mgl receptor and immunity: when the ligand can make the difference. *Journal of immunology research*, 2015, 2015.

[86] Filipa Marcelo, Fayna Garcia-Martin, Takahiko Matsushita, João Sardinha, Helena Coelho, Anneloes Oude-Vrielink, Christiane Koller, Sabine André, Eurico J Cabrita, Hans-Joachim Gabius, et al. Delineating binding modes of gal/galnac and structural elements of the molecular recognition of tumor-associated mucin glycopeptides by the human macrophage galactose-type lectin. *Chemistry-a European Journal*, 20(49):16147–16155, 2014.

[87] Sandra J van Vliet, Sonja I Gringhuis, Teunis BH Geijtenbeek, and Yvette van Kooyk. Regulation of effector t cells by antigen-presenting cells via interaction of the c-type lectin mgl with cd45. *Nature immunology*, 7(11):1200–1208, 2006.

[88] Sandra J van Vliet, Corlien A Aarnoudse, Venice Broks-van den Berg, Martine Boks, Teunis BH Geijtenbeek, and Yvette van Kooyk. Mgl-mediated internalization and antigen presentation by dendritic cells: A role for tyrosine-5. *European journal of immunology*, 37(8):2075–2081, 2007.

[89] Davide Serruto and Rino Rappuoli. Post-genomic vaccine development. *FEBS letters*, 580(12):2985–2992, 2006.

[90] E Lacunza, M Baudis, AG Colussi, A Segal-Eiras, MV Croce, and MC Abba. Muc1 oncogene amplification correlates with protein overexpression in invasive breast carcinoma cells. *Cancer genetics and cytogenetics*, 201(2):102–110, 2010.

[91] Susan F Slovin, Stacy J Keding, and Govind Ragupathi. Carbohydrate vaccines as immunotherapy for cancer. *Immunology and cell biology*, 83(4):418–428, 2005.

[92] Yan Hu, Jinhong Duan, Qimin Zhan, Fengdan Wang, Xin Lu, and Xian-Da Yang. Novel muc1 aptamer selectively delivers cytotoxic agent to cancer cells in vitro. *PLoS One*, 7(2):e31970, 2012.

[93] J Gong, V Apostolopoulos, D Chen, H Chen, S Koido, Sandra J Gendler, IF McKenzie, and D Kufe. Selection and characterization of muc1-specific cd8+ t cells from muc1 transgenic mice immunized with dendritic-carcinoma fusion cells. *Immunology*, 101(3):316–324, 2000.

[94] VA Kabanov. From synthetic polyelectrolytes to polymer-subunit vaccines. review. *Polymer science. Series A, Chemistry, physics*, 46(5):451–470, 2004.

[95] VA Kabanov, MI Mustafaev, AV Nekrasov, ASh Norimov, and RV Petrov. Critical nature of the effect of the degree of polyelectrolyte polymerization on immunostimulating properties. *Doklady Akademii Nauk SSSR*, 274(4):998, 1984.

[96] RV Petrov, VA Kabanov, RM Khaitov, MI Mustafaev, ASh Norimov, TV Abramenko, and ER Eivazova. Effect of heparin on the immunogenicity of electrostatic covalent albumin complexes with synthetic polyions. immunogenicity of the triple covalent complex polyelectrolyte-protein-heparin. *Molekuliarnaia genetika, mikrobiologiia i virusologiia*, (6):30–35, 1986.

[97] Murat Topuzogullari, Rabia Cakir Koc, Sevil Dincer Isoglu, Melahat Bagirova, Zeynep Akdeste, Serhat Elcicek, Olga N Oztel, Serap Yesilkir Baydar, Sezen Canim Ates, and Adil M Allahverdiyev. Conjugation, characterization and toxicity of lipophosphoglycan-polyacrylic acid conjugate for vaccination against leishmaniasis. *Journal of biomedical science*, 20(1):35, 2013.

[98] Gilbert S Banker, Juergen Siepmann, and Christopher Rhodes. *Modern pharmaceutics*. CRC Press, 2002.

[99] Suttipun Sungsuwan, Zhaojun Yin, and Xuefei Huang. Lipopeptide-coated iron oxide nanoparticles as potential glycoconjugate-based synthetic anticancer vaccines. *ACS applied materials & interfaces*, 7(31):17535–17544, 2015.

[100] Zhaojun Yin, Sudipa Chowdhury, Craig McKay, Claire Baniel, W Shea Wright, Philip Bentley, Katarzyna Kaczanowska, Jeffrey C Gildersleeve, MG Finn, Lbachir BenMohamed, et al. Significant impact of immunogen design on the diversity of antibodies generated by carbohydrate-based anticancer vaccine. *ACS chemical biology*, 10(10):2364–2372, 2015.

[101] Zhaojun Yin, Steven Dulaney, Craig S McKay, Claire Baniel, Katarzyna Kaczanowska, Sherif Ramadan, MG Finn, and Xuefei Huang. Chemical synthesis of gm2 glycans, bioconjugation with bacteriophage qβ, and the induction of anticancer antibodies. *Chembiochem*, 17(2):174–180, 2016.

[102] Fernando J Irazoqui, Victor G Sendra, Ricardo D Lardone, and Gustavo A Nores. Immune response to thomsen–friedenreich disaccharide and glycan engineering. *Immunology and cell biology*, 83(4):405–412, 2005.

[103] Victor G Sendra, Natacha Zlocowski, Yanina Ditamo, Silvina Copioli, Mads P Tarp, Eric P Bennett, Henrik Clausen, German A Roth, Gustavo A Nores, and Fernando J Irazoqui. Glycan bioengineering in immunogen design for tumor t antigen immunotargeting. *Molecular immunology*, 46(16):3445–3453, 2009.

[104] Adel Almogren, Julia Abdullah, Kshipra Ghapure, Kimiko Ferguson, Vladislav V Glinsky, and Kate Rittenhouse-Olson. [frontiers in bioscience s4, 840-863, january 1, 2012] anti-thomsen-friedenreich-ag (anti-tf-ag) potential for cancer therapy. *Frontiers in bioscience*, 4:840–863, 2012.

[105] MG Nair. Fumonisins and human health. *Annals of tropical paediatrics*, 18(sup1):S47–S52, 1998.

[106] KRN Reddy, B Salleh, B Saad, HK Abbas, CA Abel, and WT Shier. An overview of mycotoxin contamination in foods and its implications for human health. *Toxin reviews*, 29(1):3–26, 2010.

[107] Patimaporn Plodpai, Vasun Petcharat, Samerchai Chuenchit, Suda Chakthong, Nantiya Joycharat, and Supayang P Voravuthikunchai. Desmos chinensis: A new candidate as natural antifungicide to control rice diseases. *Industrial crops and products*, 42:324–331, 2013.

[108] Eric W Sydenham, Wentzel CA Gelderblom, Pieter G Thiel, and Walter FO Marasas. Evidence for the natural occurrence of fumonisin b1, a mycotoxin produced by fusarium moniliforme, in corn. *Journal of Agricultural and Food Chemistry*, 38(1):285–290, 1990.

[109] JPF D'mello, CM Placinta, and AMC Macdonald. Fusarium mycotoxins: a review of global implications for animal health, welfare and productivity. *Animal feed science and technology*, 80(3):183–205, 1999.

[110] TH Nguyen, GH Fleet, and PL Rogers. Composition of the cell walls of several yeast species. *Applied microbiology and biotechnology*, 50(2):206–212, 1998.

[111] Jan Kocourek and Clinton E Ballou. Method for fingerprinting yeast cell wall mannans. *Journal of bacteriology*, 100(3):1175–1181, 1969.

[112] Elena Kiseleva, Terry D Allen, Sandra A Rutherford, Steve Murray, Ksenia Morozova, Fiona Gardiner, Martin W Goldberg, and Sheona P Drummond.

A protocol for isolation and visualization of yeast nuclei by scanning electron microscopy (sem). *Nature protocols*, 2(8):1943–1953, 2007.

[113] Margaret A Johnson and David R Bundle. Designing a new antifungal glycoconjugate vaccine. *Chemical Society Reviews*, 42(10):4327–4344, 2013.

[114] Frans M Klis, Pieternella Mol, Klaas Hellingwerf, and Stanley Brul. Dynamics of cell wall structure in saccharomyces cerevisiae. *FEMS microbiology reviews*, 26(3):239–256, 2002.

[115] Enrico Cabib and Blair Bowers. Chitin and yeast budding localization of chitin in yeast bud scars. *Journal of Biological Chemistry*, 246(1):152–159, 1971.

[116] Diego Carlström. The crystal structure of α-chitin (poly-n-acetyl-d-glucosamine). *The Journal of Cell Biology*, 3(5):669–683, 1957.

[117] Antoinette C O'sullivan. Cellulose: the structure slowly unravels. *Cellulose*, 4(3):173–207, 1997.

[118] David L Kaplan. Introduction to biopolymers from renewable resources. In *Biopolymers from renewable resources*, page 102. Springer, 1998.

[119] Tsunenori Kameda, Mitsuhiro Miyazawa, Hiroshi Ono, and Mitsuru Yoshida. Hydrogen bonding structure and stability of α-chitin studied by 13c solid-state nmr. *Macromolecular bioscience*, 5(2):103–106, 2005.

[120] Olga E Philippova, Evgeniya V Korchagina, Evgeny V Volkov, Valery A Smirnov, Alexei R Khokhlov, and Marguerite Rinaudo. Aggregation of some water-soluble derivatives of chitin in aqueous solutions: Role of the degree of acetylation and effect of hydrogen bond breaker. *Carbohydrate polymers*, 87(1):687–694, 2012.

[121] Renata Vuković and Vladimir Mrša. Structure of the saccharomyces cerevisiae cell wall. *Croatica Chemica Acta*, 68(3):597–605, 1995.

[122] Rudolf Merkel, Pierre Nassoy, Andrew Leung, Ken Ritchie, and Evan Evans. Energy landscapes of receptor–ligand bonds explored with dynamic force spectroscopy. *Nature*, 397(6714):50–53, 1999.

[123] JM Berg, JL Tymoczko, and L Stryer. Chemical bonds in biochemistry. *Biochemistry*, 2002.

[124] Amy M Clobes and William H Guilford. Ionic strength influences the mechanical force regulation of myosin's unbinding rate. *Biophysical Journal*, 100(3):11a, 2011.

[125] Nicholas Keller, Shelley Grimes, Paul J Jardine, and Douglas E Smith. Single dna molecule jamming and history-dependent dynamics during motor-driven viral packaging. *Nature physics*, 12(8):757–761, 2016.

[126] Shu-ou Shan and Daniel Herschlag. The change in hydrogen bond strength accompanying charge rearrangement: Implications for enzymatic catalysis. *Proceedings of the National Academy of Sciences*, 93(25):14474–14479, 1996.

[127] Gerrit Sitters, Douwe Kamsma, Gregor Thalhammer, Monika Ritsch-Marte, Erwin JG Peterman, and Gijs JL Wuite. Acoustic force spectroscopy. *Nature methods*, 12(1):47–50, 2015.

[128] Evan Evans. Probing the relation between force—lifetime—and chemistry in single molecular bonds. *Annual review of biophysics and biomolecular structure*, 30(1):105–128, 2001.

[129] Alexei Valiaev, Stefan Zauscher, and Scott C Schmidler. Statistical analysis of single-molecule afm force spectroscopy curves. *Department of Statistical Science, Duke University, Durham, NC*, 36.

[130] Sebastian Getfert and Peter Reimann. Hidden multiple bond effects in dynamic force spectroscopy. *Biophysical journal*, 102(5):1184–1193, 2012.

[131] Thorsten Erdmann, Sébastien Pierrat, Pierre Nassoy, and US Schwarz. Dynamic force spectroscopy on multiple bonds: Experiments and model. *EPL (Europhysics Letters)*, 81(4):48001, 2008.

[132] Soosan Hadjialirezaei, Gianfranco Picco, Richard Beatson, Joy Burchell, Bjørn Torger Stokke, and Marit Sletmoen. Interactions between the breast cancer-associated muc1 mucins and c-type lectin characterized by optical tweezers. *PloS one*, 12(4):e0175323, 2017.

[133] Arthur Ashkin. Acceleration and trapping of particles by radiation pressure. *Physical review letters*, 24(4):156, 1970.

[134] Arthur Ashkin, James M Dziedzic, JE Bjorkholm, and Steven Chu. Observation of a single-beam gradient force optical trap for dielectric particles. *Optics letters*, 11(5):288–290, 1986.

[135] A. Ashkin. Acceleration and trapping of particles by radiation pressure. *Phys. Rev. Lett.*, 24:156–159, Jan 1970.

[136] Keir C Neuman and Steven M Block. Optical trapping. *Review of scientific instruments*, 75(9):2787–2809, 2004.

[137] Robert M Simmons, Jeffrey T Finer, Steven Chu, and James A Spudich. Quantitative measurements of force and displacement using an optical trap. *Biophysical Journal*, 70(4):1813, 1996.

[138] Sylvie Henon, Guillaume Lenormand, Alain Richert, and Francois Gallet. A new determination of the shear modulus of the human erythrocyte membrane using optical tweezers. *Biophysical journal*, 76(2):1145–1151, 1999.

[139] Ulrich Bockelmann, Ph Thomen, B Essevaz-Roulet, Virgile Viasnoff, and Francois Heslot. Unzipping dna with optical tweezers: high sequence sensitivity and force flips. *Biophysical journal*, 82(3):1537–1553, 2002.

[140] Arthur Ashkin and JM Dziedzic. Optical trapping and manipulation of viruses and bacteria. *Science*, 235(4795):1517–1520, 1987.

[141] L Tskhovrebova, J Trinick, JA Sleep, and RM Simmons. Elasticity and unfolding of single molecules of the giant muscle protein titin. *Nature*, 387(6630):308–312, 1997.

[142] Frederick Gittes and Christoph F Schmidt. Interference model for back-focal-plane displacement detection in optical tweezers. *Optics letters*, 23(1):7–9, 1998.

[143] Kirstine Berg-Sørensen and Henrik Flyvbjerg. Power spectrum analysis for optical tweezers. *Review of Scientific Instruments*, 75(3):594–612, 2004.

[144] A Wozniak, J Van Mameren, and S Ragona. Single-molecule force spectroscopy using the nanotracker^{TM} optical tweezers platform: from design to application. *Current pharmaceutical biotechnology*, 10(5):467–473, 2009.

[145] Kristin E Haugstad, Bjørn T Stokke, C Fred Brewer, Thomas A Gerken, and Marit Sletmoen. Single molecule study of heterotypic interactions between mucins possessing the tn cancer antigen. *Glycobiology*, 25(5):524–534, 2014.

[146] Thomas Link, Malin Bäckström, Ros Graham, R Essers, K Zörner, Jochem Gätgens, J Burchell, Joyce Taylor-Papadimitriou, Gunnar C Hansson, and Thomas Noll. Bioprocess development for the production of a recombinant muc1 fusion protein expressed by cho-k1 cells in protein-free medium. *Journal of biotechnology*, 110(1):51–62, 2004.

[147] Malin Bäckström, LINK Thomas, Fredrik J Olson, Hasse Karlsson, Rosalind Graham, Gianfranco Picco, Joy Burchell, Joyce Taylor-Papadimitriou, NOLL Thomas, and Gunnar C Hansson. Recombinant muc1 mucin with a breast cancer-like o-glycosylation produced in large amounts in chinese-hamster ovary cells. *Biochemical Journal*, 376(3):677–686, 2003.

[148] Thomas A Gerken, Cheryl L Owens, and Murali Pasumarthy. Determination of the site-specific o-glycosylation pattern of the porcine submaxillary mucin tandem repeat glycopeptide model proposed for the polypeptide: Galnac transferase peptide binding site. *Journal of Biological Chemistry*, 272(15):9709–9719, 1997.

[149] Thermo Scientific Pierce. Crosslinking technical handbook. *Thermo Fisher Scientific, Rockford, IL, USA*, 2009.

[150] William J Cooper, Rod G Zika, Robert G Petasne, and John MC Plane. Photochemical formation of hydrogen peroxide in natural waters exposed to sunlight. *Environmental science & technology*, 22(10):1156–1160, 1988.

[151] J Jeffrey Morris and Erik R Zinser. Continuous hydrogen peroxide production by organic buffers in phytoplankton culture media. *Journal of phycology*, 49(6):1223–1228, 2013.

[152] JS Zigler, JL Lepe-Zuniga, B Vistica, and I Gery. Analysis of the cytotoxic effects of light-exposed hepes-containing culture medium. *In Vitro Cellular & Developmental Biology*, 21(5):282–287, 1985.

[153] Kristin E Haugstad, Soosan Hadjialirezaei, Bjørn T Stokke, C Fred Brewer, Thomas A Gerken, Joy Burchell, Gianfranco Picco, and Marit Sletmoen. Interactions of mucins with the tn or sialyl tn cancer antigens including muc1 are due to galnac–galnac interactions. *Glycobiology*, 26(12):1338–1350, 2016.

[154] Marcel JE Fischer. Amine coupling through edc/nhs: a practical approach. *Surface plasmon resonance: methods and protocols*, pages 55–73, 2010.

[155] Maxime A Gilles, Antoine Q Hudson, and CL Borders. Stability of water-soluble carbodiimides in aqueous solution. *Analytical biochemistry*, 184(2):244–248, 1990.

[156] Anand R Kolatkar and William I Weis. Structural basis of galactose recognition by c-type animal lectins. *Journal of Biological Chemistry*, 271(12):6679–6685, 1996.

[157] Takeshi Hosoi, Yasuyuki Imai, and Tatsuro Irimura. Coordinated binding of sugar, calcium, and antibody to macrophage c-type lectin. *Glycobiology*, 8(8):791–798, 1998.

[158] Shin-ichiro Iida, Kazuo Yamamoto, and Tatsuro Irimura. Interaction of human macrophage c-type lectin witho-linked n-acetylgalactosamine residues on mucin glycopeptides. *Journal of Biological Chemistry*, 274(16):10697–10705, 1999.

[159] Kaori Denda-Nagai, Satoshi Aida, Kengo Saba, Kiwamu Suzuki, Saya Moriyama, Sarawut Oo-puthinan, Makoto Tsuiji, Akiko Morikawa, Yosuke Kumamoto, Daisuke Sugiura, et al. Distribution and function of macrophage galactose-type c-type lectin 2 (mgl2/cd301b) efficient uptake and presentation of glycosylated antigens by dendritic cells. *Journal of Biological Chemistry*, 285(25):19193–19204, 2010.

[160] Makoto Tsuiji, Mayuko Fujimori, Yoshimi Ohashi, Nobuaki Higashi, Thandi M Onami, Stephen M Hedrick, and Tatsuro Irimura. Molecular cloning and characterization of a novel mouse macrophage c-type lectin, mmgl2, which has a distinct carbohydrate specificity from mmgl1. *Journal of Biological Chemistry*, 277(32):28892–28901, 2002.

[161] Satwinder Kaur Singh, Ingeborg Streng-Ouwehand, Manja Litjens, Danny R Weelij, Juan Jesús García-Vallejo, Sandra J van Vliet, Eirikur Saeland, and Yvette van Kooyk. Characterization of murine mgl1 and mgl2 c-type lectins:

distinct glycan specificities and tumor binding properties. *Molecular immunology*, 46(6):1240–1249, 2009.

[162] Shuhui Wu and Robert A Shanks. Conformation of polyacrylamide in aqueous solution with interactive additives and cosolvents. *Journal of applied polymer science*, 89(11):3122–3129, 2003.

[163] Li Ni and Michael Snyder. A genomic study of the bipolar bud site selection pattern insaccharomyces cerevisiae. *Molecular biology of the cell*, 12(7):2147–2170, 2001.

[164] Enrico Cabib and Javier Arroyo. How carbohydrates sculpt cells: chemical control of morphogenesis in the yeast cell wall. *Nature reviews Microbiology*, 11(9):648–655, 2013.

9 Appendix A: Galleries for different systems

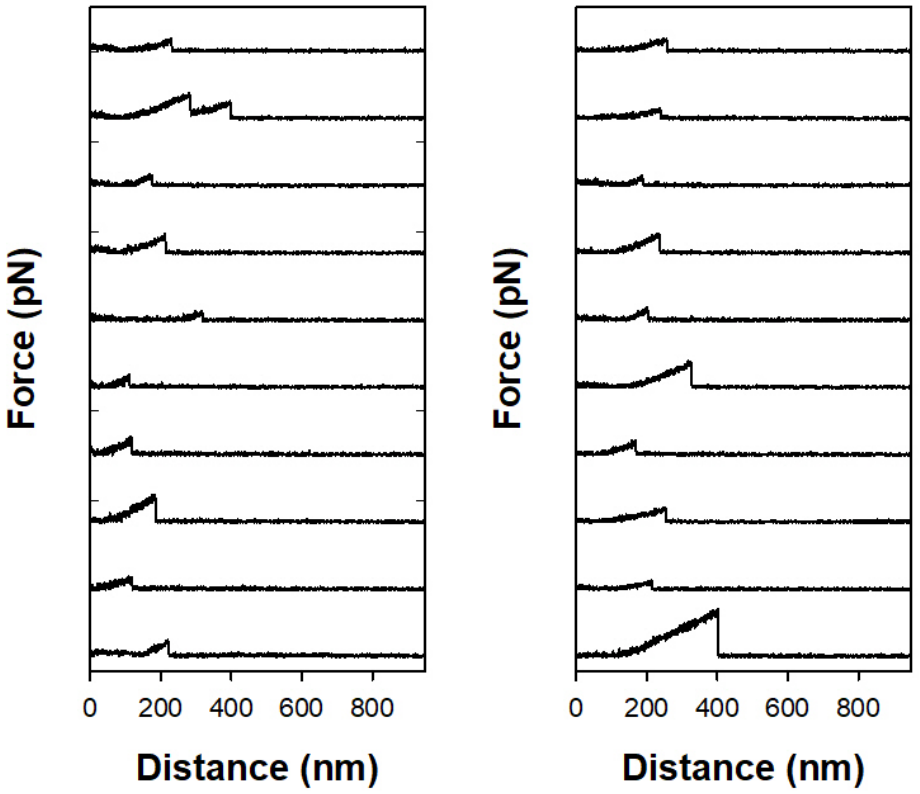

Figure 64: The left frame shows a gallery for MUC1-Tn - self, while the right one shows the Gallery for MUC1-STn - self.

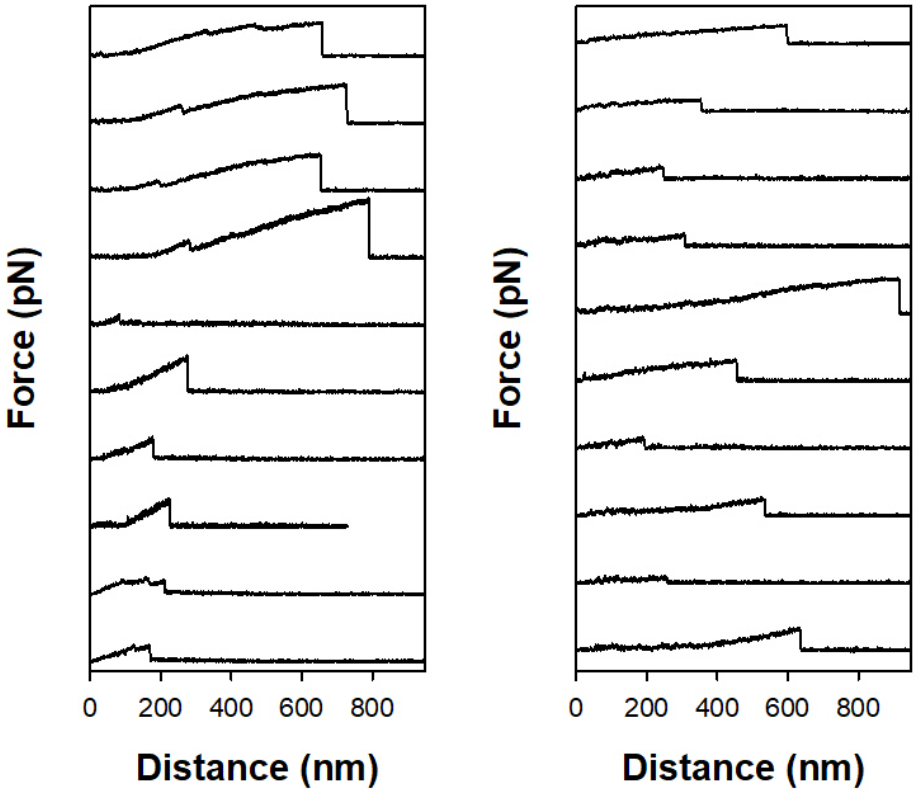

Figure 65: The left frame shows a gallery for MUC1-Tn - MGL, while the right one shows the Gallery for PAA-450K-80 - self.

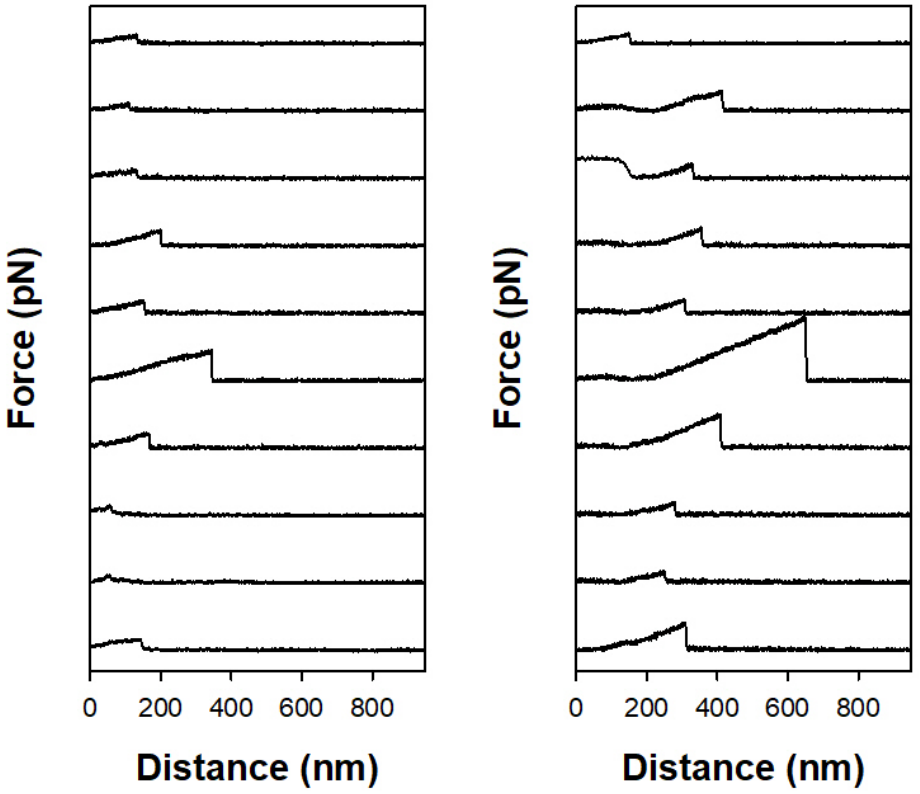

Figure 66: The left frame shows a gallery for MUC1-ST - self, while the right one shows the Gallery for MUC1-T - self.

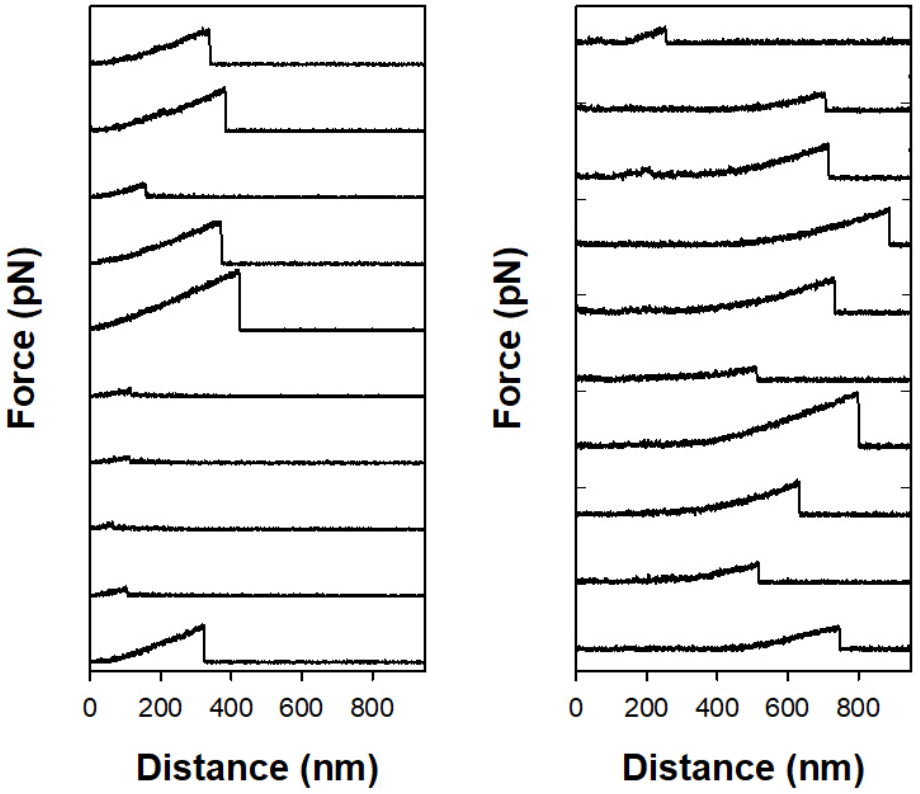

Figure 67: The left frame shows a gallery for fumonisin - laminarin, while the right one shows interactions commonly observed between the fully glycosylated MUC1-protein TR-PSM-H8 - self.

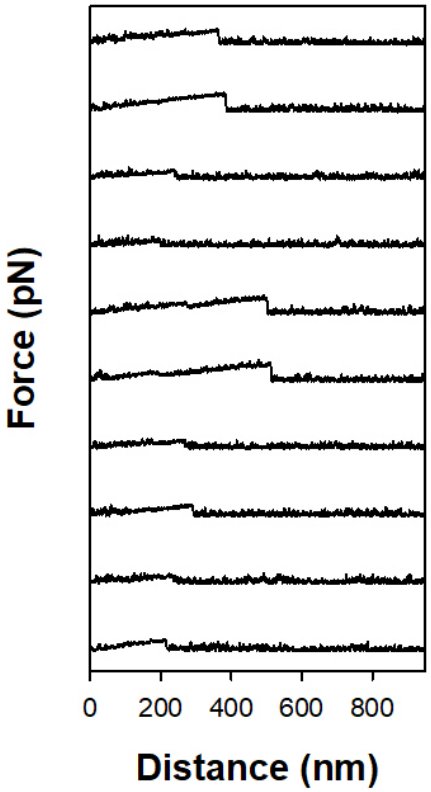

Figure 68: Gallery for the control experiments, where beads underwent the same treatment as beads in the actual experiments (EDC in aqueous boric acid, then washed with HEPES), but no polymer was added to be immobilized.